Biophysical and biochemical characterization of human tRNA nucleotidyltransferase variants

Michael Chung

A Thesis in

The Department of

Biology

Presented in Partial Fulfillment of the Requirements for

The Degree of Master of Science (Biology)

At Concordia University

Montreal, Quebec, Canada

July 2019

CONCORDIA UNIVERSITY

School of Graduate Studies

This is to certify that the thesis prepared

By: Michael Chung

Entitled: Biophysical and biochemical characterization of human tRNA nucleotidyltransferase variants

and submitted in partial fulfillment of the requirements for the degree of

Master of Science (Biology)

complies with the regulations of the University and meets the accepted standards with respect to originality and quality.

Signed by the final Examining Committee:

Dr. David Kwan	_____	Chair & Examiner
Dr. Peter Pawelek	_____	Examiner
Dr. Paul Joyce	_____	Supervisor

Approved by: Dr. Robert Weladji _____ Graduate Program Director

Dr. André Roy _____ Dean of Arts & Science

Date: July 2019

ABSTRACT

Biophysical and biochemical characterization of human tRNA nucleotidyltransferase variants

Michael Chung

The enzyme ATP(CTP):tRNA nucleotidyltransferase (tRNA-NT) is required for tRNA maturation and repair. This enzyme adds to tRNAs the universally conserved 3'-cytidine-cytidine-adenosine (CCA) sequence required for aminoacylation. Given the essential role of this enzyme in protein synthesis, human disease phenotypes have been linked to mutations in the gene encoding this protein (Aksentijevich *et al.* 2014; Chakraborty *et al.* 2014; Sasarman *et al.* 2015; DeLuca *et al.* 2016; Hull *et al.* 2016; Wedatilake *et al.* 2016; Frans *et al.* 2017; Lougaris *et al.* 2018; Giannelou *et al.* 2018; Bader-Meunier *et al.* 2018; Gorodetsky *et al.* 2018; Kumaki *et al.* 2019; Abdulhadi *et al.* 2019). The variant proteins characterized to date have shown reduced thermostability relative to the native enzyme (Leibovitch *et al.* 2018, 2019), suggesting that reduced stability of tRNA-NT may lead to the phenotypes observed.

Here, we looked at additional variant proteins to see if these disease-linked variants also show reduced thermostability. The variant proteins characterized here were E43Δ which had a glutamate residue deleted near the N-terminus of the protein, R99W which contained an arginine-to-tryptophan substitution near the active site of the enzyme, and A[8] with a frame shift that truncated the protein by nine amino acids and altered the new C-terminal eight amino acids.

Interestingly, biophysical and biochemical characterization of these variants showed no major decrease in thermostability relative to the native enzyme. However, all three variants showed a reduced ability to incorporate AMP into a specific tRNA template *in vitro*. This suggests that, in addition to reduced thermostability, effects in AMP incorporation may also be linked to a disease phenotype. Interestingly, the E43Δ, R99W and A[8] variants all affected different aspects of AMP incorporation, reflecting their different locations in the protein and suggesting that AMP incorporation may be mediated by different domains and substructures spanning the entire enzyme and not confined simply to the active site.

ACKNOWLEGDMENTS

I would like to thank Dr. Joyce for his judgment, kindness, patience, knowledge and wisdom throughout my three years at Concordia University. His continuous support and that of his research team have brought the best out of me in terms of scientific rigour – and these have been invaluable to me.

I would like to thank Pam for her assistance and expertise in molecular genetics, and for all the idle yet very pleasant conversations during the long hours of the lab; Dr. Turnbull for her critical assessment and guidance in the area of enzymology; Matthew for the initial training in the context of tRNA and enzyme biochemistry; and my labmates Sami and Nathalie for their continuous enthusiasm, camaraderie and support.

Moreover, I would also like to thank my parents for their unceasing love and support throughout the highs and lows of my academic journey. Last but not least, a huge shout-out goes to my ex, Kif, whom I've shared genuine tender moments with and a summer that lasted forever.

TABLE OF CONTENTS

LIST OF FIGURES

LIST OF TABLES

LIST OF ABBREVIATIONS

A-addition	AMP addition
Amp	Ampicillin
AMP	Adenosine monophosphate
APS	Ammonium persulfate
ATP	Adenosine triphosphate
C-addition	CMP addition
CCA	Cytidine-cytidine-adenosine
CD	Circular dichroism
CMP	Cytidine monophosphate
CTP	Cytidine triphosphate
dH_2O	Distilled water
DNA	Deoxyribonucleic acid
dNTP	Deoxynucleoside triphosphate
EDTA	Ethylenediaminetetraacetic acid
Gdn-HCl	Guanidine-hydrochoride
GTP	Guanosine triphosphate
His	Histidine
iPSC	Induced pluripotent stem cell
IPTG	Isopropyl-β-D-thiogalactopyranoside
k_{cat}	Turnover number
$k_{cat}/K_{M,Apparent}$	Specificity constant
K_D	Dissociation constant
K_M	Michaelis constant
$K_{M,Apparent}$	Apparent Michaelis constant
LOF	Loss-of-function
mRNA	Messenger ribonucleic acid
MRW	Mean residue ellipticity
MS	Mass spectrometry
MTS	Mitochondrial targeting signal
MW	Molecular weight

MWCO	Molecular weight cut-off
n	Hill coefficient
Ni-NTA	Nickel-nitrilotriacetic acid
NTP	Nucleoside triphosphate
OD	Optical density
PAGE	Polyacrylamide gel electrophoresis
PBS	Phosphate-buffered saline
PDB	Protein Data Bank
RNA	Ribonucleic acid
SDS	Sodium dodecyl sulfate
SEM	Standard error of the mean
SIFD	Sideroblastic anemia associated with B-cell immunodeficiency, periodic fevers and developmental delay
siRNA	Small interfering ribonucleic acid
TBE	Tris/Borate/EDTA
TEMED	Tetraethylmethlenediamine
T_m	Melting temperature
tRNA	Transfer ribonucleic acid
tRNAdb	Transfer RNA Database
tRNA-NT	ATP(CTP):tRNA nucleotidyltransferase
ts	Temperature-sensitive
UTP	Uridine triphosphate
UV-Vis	Ultraviolet-visible
V_{max}	Maximum reaction rate
v_o	Initial velocity
YT	Yeast extract, tryptone

1.0 INTRODUCTION

1.1 tRNA Structure, Function and Maturation

In protein synthesis, transfer ribonucleic acids (tRNAs) serve as essential intermediaries in the information flow between messenger ribonucleic acids (mRNAs) and the amino acid sequence of the encoded proteins. During translation, tRNAs function as adaptor molecules within the cell, "ferrying" specific amino acids to the ribosome where protein synthesis, defined by the mRNA transcript, occurs (Jakubowski 2012). In eukaryotic cells, genes encoding tRNAs are found in the nuclear, mitochondrial and chloroplast genomes, and tRNAs are found in all of these locations and in the cytosol where they are maintained and active.

In general, tRNAs consist of 70 to 85 nucleotides which typically fold into the cloverleaf-like secondary structure first proposed by Kim *et al.* (1973) (Fig. 1-1A). Crystallographic analysis also revealed an L-shaped tertiary structure (Kim *et al.* 1973), due to interactions between individual residues and the stacking of helical regions (Phizicky and Hopper 2010; Giegé *et al.* 2012) (Fig. 1-1B). The key parts of the tRNA structure (Juhling *et al.* 2009; Giegé *et al.* 2012) (Fig. 1-1A) include the acceptor stem (where the cognate amino acid attaches), the anticodon arm (which interacts with the complementary codon in the mRNA), the D arm (which is recognized by appropriate aminoacyl-tRNA synthetases) (Hendrickson 2001), the TΨC arm (with a role in stabilizing the tRNA tertiary structure by facilitating long-range interactions) (Chan *et al.* 2013), the variable loop (which may function in recognition by the appropriate aminoacyl-tRNA synthetase) (Wu and Gross 1993) and the discriminator base. Importantly, the protruding 3'-end of the acceptor stem contains an invariant cytidine-cytidine-adenosine (CCA) trinucleotide sequence required for attachment of the cognate amino acid by the appropriate aminoacyl-tRNA synthetase (Sprinzl and Cramer 1979; Tamura and Hasegawa 1997; Jakubowski 2012).

The CCA sequence is vital for an assortment of functions, including the ability of the tRNA to attach to its cognate amino acid, efficient export of mature tRNAs from the nucleus (Kutay *et al.* 1998; Arts *et al.* 1998; Lipowsky *et al.* 1999), proper positioning of the transported amino acid in the ribosomal A site (Green and Noller 1997; Liu *et al.* 1998), assistance in peptide bond formation at the ribosomal P site (Kim and Green 1999; Nissen *et al.* 2000; Weinger *et al.* 2004) and reordering of water molecules leading to translation termination by hydrolysis at the peptidyl-tRNA (Simonovic and Steitz 2008).

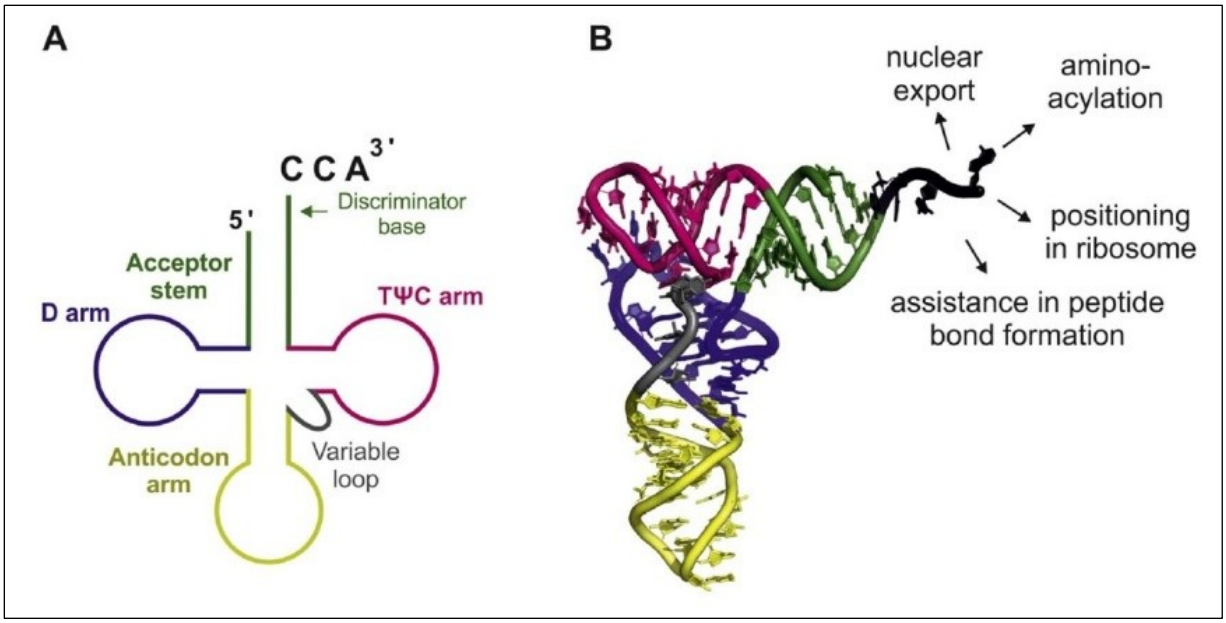

Figure 1-1: Secondary and Tertiary Structure of tRNA (Wellner *et al.* 2018). (A) Secondary structure displaying all key parts, including the discriminator base and the CCA sequence. **(B)** Tertiary structure with diverse functions ascribed to the CCA sequence. Shown here is the cytosolic $tRNA^{Phe}$ from *Saccharomyces cerevisiae* (PDB ID: 1TN1), with an equivalent colour scheme to **(A)**.

1.2 Class II tRNA Nucleotidyltransferase Function and Structure

In eukaryotes, this 3'-CCA sequence is not encoded in the tRNA genes (Sprinzl and Cramer 1979) and is post-transcriptionally added to the 3'-end of the tRNA by a specialized nucleic-acid-template-independent RNA polymerase, ATP(CTP):tRNA nucleotidyltransferase (tRNA-NT) (Deutscher 1983). This enzyme belongs to the polymerase β superfamily which is characterized by an amino acid signature element near the N-terminus of the protein (Holm and Sander 1995) and is divided into two distinct groups – Class I and Class II (Yue *et al.* 1996; Aravind and Koonin 1999; Martin and Keller 2007). Of note, in addition to catalyzing CCA addition during tRNA maturation, Class II tRNA-NTs also possess a repair function, where partially degraded or truncated CCA-ends are readily restored by incorporation of the missing nucleotides (Rosset and Monier 1963; Zhu and Deutscher 1987; Deutscher 1990; Weiner 2004). Furthermore, Class II tRNA-NTs also play a role in quality control of tRNAs, as those that have mismatching and destabilizing base-pairs at the acceptor stem undergo a second round of CCA addition, by which they are effectively tagged for degradation via 3'-5' exonucleases (Wilusz *et al.* 2011; Kuhn *et al.* 2015; Betat and Mörl 2015).

The resolved crystal structures of several Class II tRNA-NTs (Li et *al.* 2002; Augustin *et al.* 2003; Tomita *et al.* 2004; Toh *et al.* 2009) suggest a seahorse-shaped protein, which contains four domains – designated head, neck, body and tail (Li *et al.* 2002) – that are primarily composed of α-helical elements with the exception of a single antiparallel β-sheet in the head domain (Fig. 1-2). The head and neck domains of Class II tRNA-NTs contain five conserved motifs, designated A to E (Li *et al.* 2002) (Fig. 1-3). These motifs

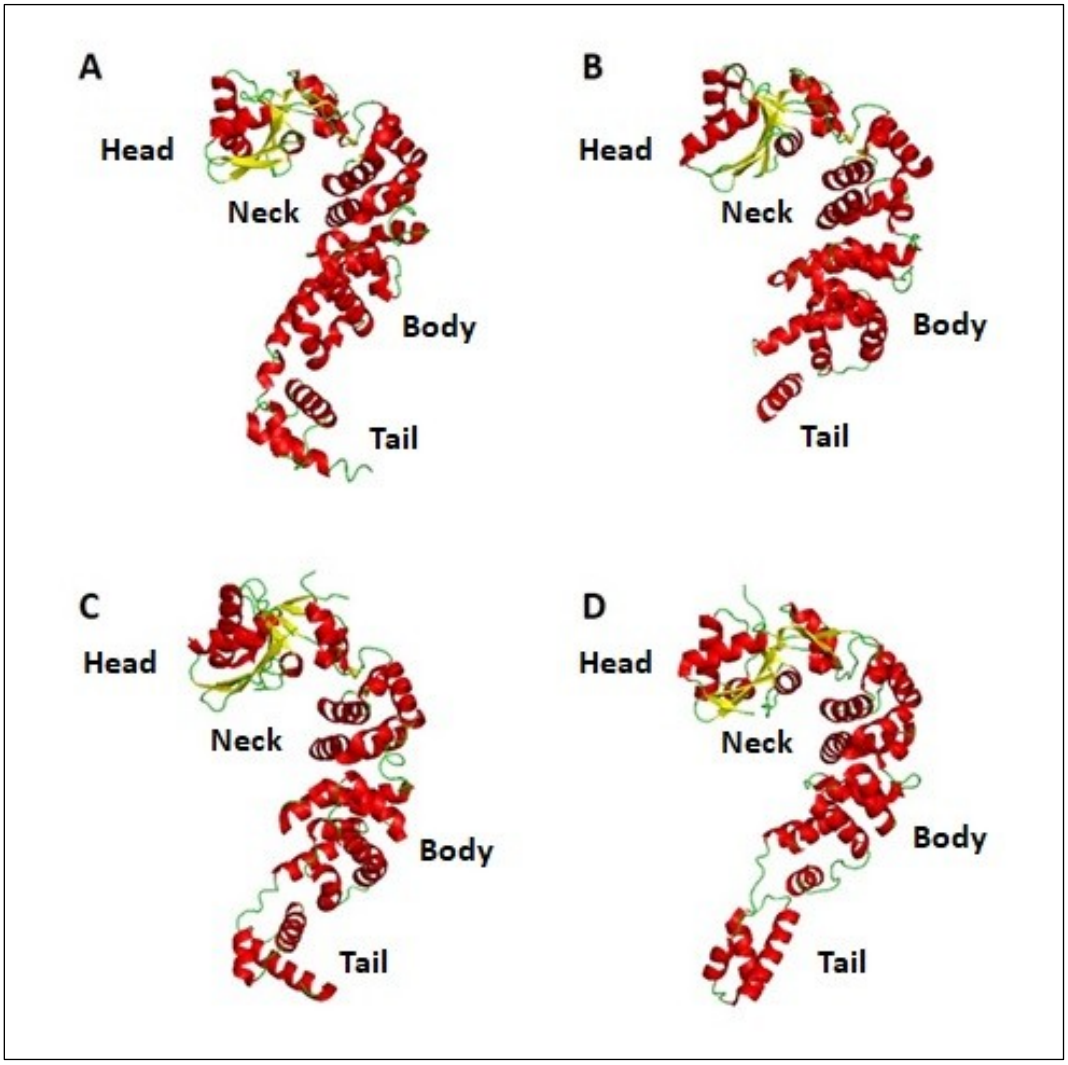

Figure 1-2: Crystal Structures of Class II tRNA-NTs. Shown are the solved Class II tRNA-NT crystal structures from **(A)** *Bacillus stearothermophilus* (PDB ID: 1MIV) (Li *et al.* 2002), **(B)** *Aquifex aeolicus* (PDB ID: 1VFG) (Tomita *et al.* 2004), **(C)** *Thermotoga maritima* (PDB ID: 3H37) *(Toh et al.* 2009) and **(D)** human (PDB ID: 4X4W) (Kuhn *et al.* 2015). Each structure consists of α-helices (red), β-strands (yellow) and loops/β-turns (green). The head, neck, body and tail domains are also labeled. All structures are visualized by PyMOL *(v.1.7.4.5)* (Schrödinger 2018).

define the catalytic residues and nucleotide binding site (Li *et al.* 2002; Augustin *et al.* 2003; Tomita *et al.* 2004; Toh *et al.* 2009) in the positively charged cleft in the head and neck region that serves as the

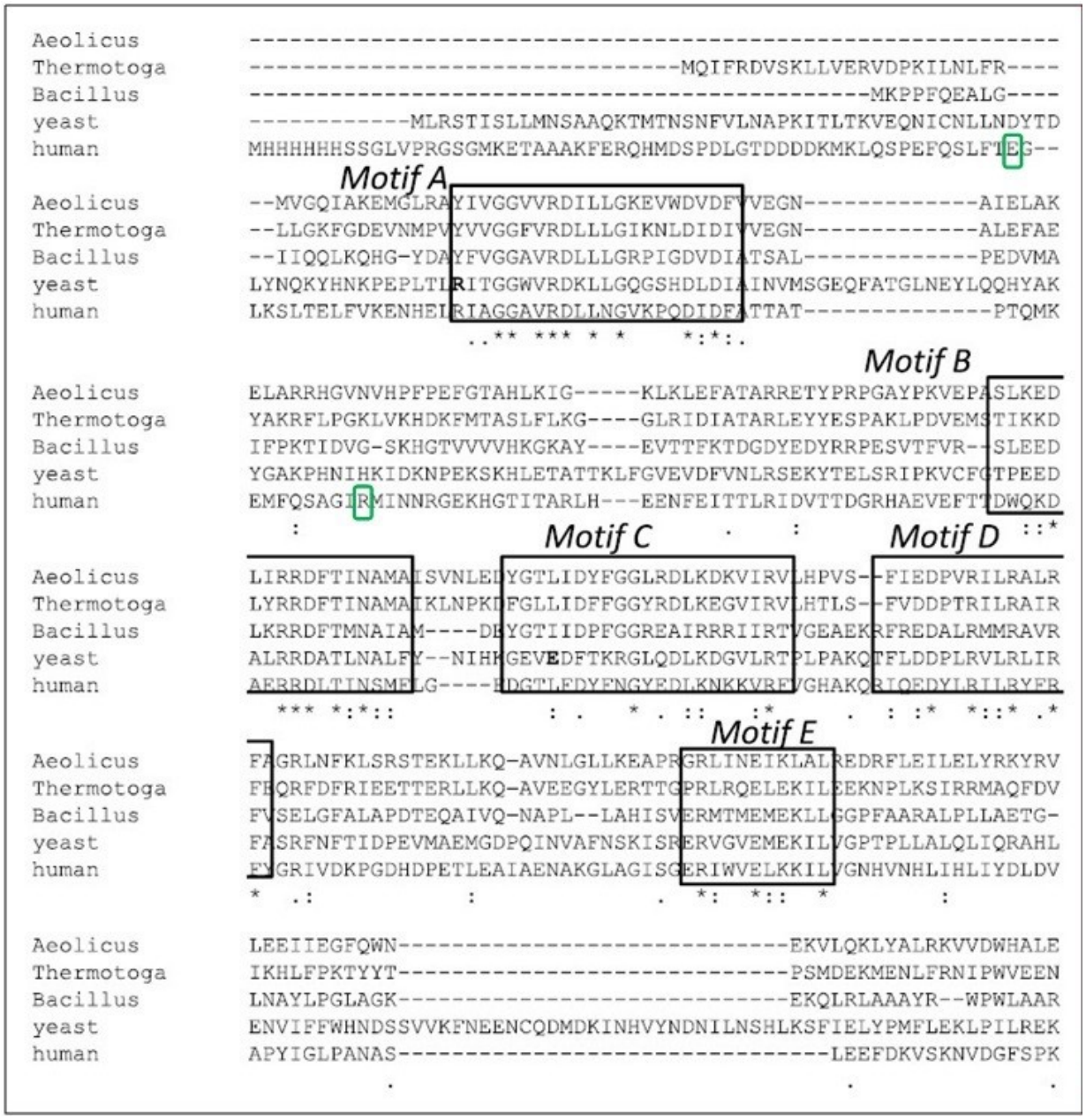

Figure 1-3: ClustalW Alignment of Motifs A to E in the Head and Neck Domains of Class II tRNA-NTs (Goring *et al.* 2013). Shown are the amino acid sequences of Class II tRNA-NTs from *Aquifex aeolicus*, *Thermotoga maritima*, *Bacillus stearothermophilus*, *Saccharomyces cerevisiae* (yeast) and human. Motifs A to E are boxed and labeled. Amino acid alterations in the N-terminus, discussed in this thesis, are shown in green boxes. (*) amino acid identity, (:) strongly conserved amino acid, (.) weakly conserved amino acid.

binding region for the incoming nucleotide – cytidine triphosphate (CTP) or adenosine triphosphate (ATP) – and the 3'-end of the tRNA (Li *et al.* 2002; Tomita *et al.* 2004; Toh *et al.* 2009). The body and tail domains, on the other hand, interact nearly exclusively with the sugar-phosphate backbone of the top half of the tRNA, namely with the acceptor stem, the D loop and the TΨC loop; while the anticodon arm is left exposed (Tomita *et al.* 2004; Xiong and Steitz 2004; Toh *et al.* 2009). The tail domain, in particular, acts as an "anchor" for the tRNA, where it binds the TΨC loop and prevents the tRNA from "slipping" (Tomita *et al.* 2004; Betat *et al.* 2004; Kuhn *et al.* 2015) (Fig. 1-4).

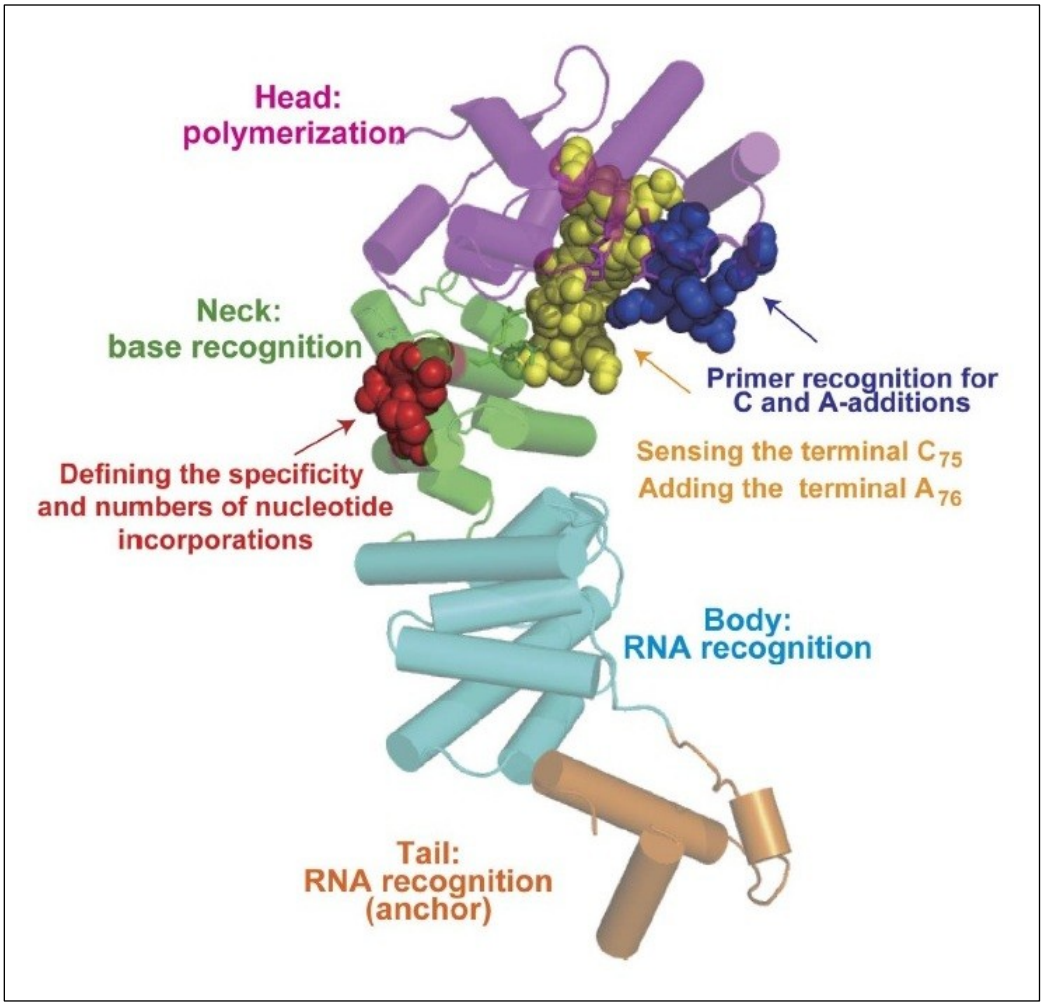

Figure 1-4: Signature Elements of the Class II tRNA-NT and Their Associated Roles (Toh *et al.* 2009). In the *T. maritima* Class II tRNA-NT structure (PDB ID: 3H37), shown here as an example, the head, neck, body and tail domains are coloured magenta, green, cyan and orange, respectively. Additional signature elements – the β-turn, flexible loop and α-helical spring – are represented by spheres (coloured blue, yellow and red, respectively). The function(s) of each signature element is/are shown.

1.2.1 C-Terminal Body and Tail Domains

While the roles of motifs A (Steitz *et al.* 1994; Yue *et al.* 1996; Steitz 1998), B (Li *et al.* 2002; Cho *et al.* 2007), C (Li *et al.* 2002; Shan *et al.* 2008; Goring *et al.* 2013; Ernst *et al.* 2015), D (Shi *et al.* 1998; Yue *et al.* 1998; Li *et al.* 2002; Cho *et al.* 2007) and E (Li *et al.* 2002) in the N-terminal portion of the protein (Fig. 1-3) have been well characterized over the last approximately 20 years, less is known about the body and tail domains of the Class II tRNA-NT due to a lack of sequence conservation in this portion of the protein (Betat *et al.* 2010).

It has been shown that swapping the C-terminal region of an *Escherichia coli* Class II tRNA-NT with the corresponding region of a related poly(A) polymerase resulted in chimeric enzymes that generate multiple CCA triplets on tRNAs – revealing that the anchoring nature of the tail domain is directly linked to a single round of CCA addition (Betat *et al.* 2004). The HD domain in the C-terminus of the *E. coli* Class II tRNA-NT can act as a metal-dependent phosphohydrolase, removing the 2'-3' cyclic phosphate group from hydrolytically damaged tRNAs and regenerating the 3'-OH group, allowing for repair of the CCA-end by the same enzyme to proceed (Thompson *et al.* 1994; Aravind and Koonin 1998; Soukup and Breaker 1999; Yakunin *et al.* 2004; Lizano *et al.* 2008). The C-terminal region of tRNA-NT can also block entry of tRNAs lacking a CC sequence, for the specific case of an enzyme that catalyses only addition of adenosine monophosphate (AMP) (Tretbar *et al.* 2011). The removal of 124 amino acids from the C-terminus of the *Drosophila melanogaster* tRNA-NT does not completely eliminate the activity of the enzyme, suggesting that the tail portion of the protein carries out its functions without interacting directly with the catalytic region of the enzyme (Yang 2008). Furthermore, removal of nine amino acids from the C-terminus of the Arabidopsis tRNA-NT has resulted in small changes in the kinetic parameters (K_M and k_{cat}) of this enzyme (Leibovitch *et al.* 2013). Moreover, if a green fluorescent protein is attached to the C-terminus of tRNA-NT, the enzyme retains activity *in vivo* (Leibovitch *et al.* 2013). Much work remains to understand fully the role of the C-terminus of the tRNA-NT.

1.3 *TRNT1* Mutations and Diseases

Given the central role of tRNA-NT in protein synthesis, it seems likely that this protein would be encoded by an essential gene and this is the case in *Saccharomyces cerevisiae* (Aebi *et al.* 1990; Giaever *et al.* 2002). Moreover, this is likely also the case in most eukaryotes, as in the majority of eukaryotic organisms characterized to date, there is a single gene encoding tRNA-NT (Leibovitch *et al.* 2013; Betat *et al.* 2015). Previously, a temperature-sensitive (*ts*) mutation has been identified in the yeast *CCA1*

gene, encoding tRNA-NT (Aebi *et al.* 1990). The *ts* defect in *S. cerevisiae* has been shown to be a hypomorphic effect, and can be overcome by overexpressing the variant protein (Goring *et al.* 2013). This observation suggests that the *ts* phenotype may result because the defective enzyme cannot generate functional tRNAs at a sufficient rate for protein synthesis at the restrictive temperature, but can do so at the permissive temperature (Goring *et al.* 2013). Based on these observations and given the essentiality of tRNA-NT, it seemed reasonable that partial loss-of-function (LOF) mutations may be found in other organisms.

This has proven to be the case, as a number of these LOF mutations have been found in the *TRNT1* gene encoding human tRNA-NT (TRNT1). This enzyme has been shown to be required for the maturation of both human cytosolic and mitochondrial tRNAs (Lizano *et al.* 2008). Partial LOF mutations have been found in, to date, 27 patients presenting a wide range of phenotypes with differing clinical severities (Aksentijevich *et al.* 2014; Chakraborty *et al.* 2014; Sasarman *et al.* 2015; DeLuca *et al.* 2016; Hull *et al.* 2016; Wedatilake *et al.* 2016; Frans *et al.* 2017; Lougaris *et al.* 2018; Giannelou *et al.* 2018; Bader-Meunier *et al.* 2018; Gorodetsky *et al.* 2018; Kumaki *et al.* 2019; Abdulhadi *et al.* 2019). These mutations encompass various combinations of missense mutations, nonsense mutations, deletions, frame shifts and splicing mutations (Table 1-1). Thus far, there have been eighteen, one, one, four and five of these types of mutations, respectively, reported alone or in combination in patients.

Table 1-1: Genotypes and Manifestations of Known *TRNT1* Mutations

	Genotype(s)	Symptom(s) Manifested
E43Δ	Compound heterozygous with **c.1246A[6]** (DeLuca *et al.* 2016)	○ Retinitis pigmentosa with erythrocytic microcytosis and anisocytosis with mild anemia (DeLuca *et al.* 2016)
R99W	Compound heterozygous with **D163V** (Aksentijevich *et al.* 2014) Compound heterozygous with **R412X** (Kumaki *et al.* 2019) Homozygous recessive (Hull *et al.* 2016; Frans *et al.* 2017)	○ Anemia, fever, gastrointestinal symptoms, B-cell immunodeficiency, autoinflammation (Aksentijevich *et al.* 2014) ○ Atypical SIFD[α] (B-cell deficiency, periodic fever and developmental delay without sideroblastic anemia), iron deficiency anemia, leukopenia and thrombocytopenia, cataracts, pneumonia, partial albinism, short stature, abnormal gonadal development (Kumaki *et al.* 2019) ○ Childhood cataract, inner retinal dysfunction, immunodeficiency, hypogammaglobulinemia, short stature with microcephaly, poor balance, sensorineural hearing loss, primary ovarian failure (Hull *et al.* 2016) ○ Progressive B-cell immunodeficiency, bilateral

		congenital cataracts, dysmorphic features, inflammatory bowel disease, psychomotor retardation, severe dermatitis, bilateral sensorineural hearing loss, Crohn's disease (Frans *et al.* 2017)
K107R	Compound heterozygous with frame shift mutation	○ *n / a*
T110I	Compound heterozygous with **D128G** (Giannelou *et al.* 2018)	○ Sideroblastic anemia, fever, hereditary pyropoikilocytosis, hypogammaglobulinemia, common variable immunodeficiency, combined B- and T-cell immunodeficiency, mild developmental delay, attention deficit disorder, nausea, vomiting, diarrhea, hepatosplenomegaly, nodular regenerative hyperplasia and hemosiderosis, retinitis pigmentosa, decreased night time vision, hyperopic astigmatism, asymmetric erythema and swelling of digits of the hands and feet, septal panniculitis, superficial and deep lymphocytic dermatitis, asthma, recurrent otitis media, upper respiratory infections, sinusitis, pneumonia, undetermined hypercoagulable syndrome, deep venous thrombosis (Giannelou *et al.* 2018)
D128G	Compound heterozygous with **T110I** (Giannelou *et al.* 2018) Compound heterozygous with **Y173F** (Sasarman *et al.* 2015)	○ Sideroblastic anemia, fever, hereditary pyropoikilocytosis, hypogammaglobulinemia, common variable immunodeficiency, combined B- and T-cell immunodeficiency, mild developmental delay, attention deficit disorder, nausea, vomiting, diarrhea, hepatosplenomegaly, nodular regenerative hyperplasia and hemosiderosis, retinitis pigmentosa, decreased night time vision, hyperopic astigmatism, asymmetric erythema and swelling of digits of the hands and feet, septal panniculitis, superficial and deep lymphocytic dermatitis, asthma, recurrent otitis media, upper respiratory infections, sinusitis, pneumonia, undetermined hypercoagulable syndrome, deep venous thrombosis (Giannelou *et al.* 2018) ○ Gait ataxia, dysarthria, gross motor regression, hypotonia, ptosis, horizontal ophthalmoplegia, abnormal signals in brainstem and dentate nucleus (Sasarman *et al.* 2015)
A148V	Homozygous recessive (Sasarman *et al.* 2015)	○ Acute lactic acidosis, severe developmental delay, hypotonia, microcephaly, seizures, central apnea, progressive cortical atrophy, neurosensorial deafness, sideroblastic anemia, renal Fanconi syndrome, fever (Sasarman *et al.* 2015)
T154I	Compound heterozygous with **L166S** and **c.608+1G>T** (Chakraborty *et al.* 2014)	○ SIFD [a] (Chakraborty *et al.* 2014)
I155T	Compound heterozygous with **R203K** (Lougaris *et al.* 2018)	○ Fever, recurrent infections, respiratory and gastrointestinal symptoms, hypertrophic cardiomyopathy, hypogammaglobulinemia,

		developmental delay, microcytic/sideroblastic anemia, combined B- and T-cell defects (Lougaris *et al.* 2018)
M158V	Compound heterozygous with **I326T** (Chakraborty *et al.* 2014)	○ SIFD [a] (Chakraborty *et al.* 2014)
D163V	Compound heterozygous with **R99W** and **I223T** (Aksentijevich *et al.* 2014)	○ Anemia, fever, gastrointestinal symptoms, B-cell immunodeficiency, autoinflammation (Aksentijevich *et al.* 2014)
L166S	Compound heterozygous with **T154I** (Chakraborty *et al.* 2014)	○ SIFD[a] (Chakraborty *et al.* 2014)
Y173F	Compound heterozygous with **D128G** (Sasarman *et al.* 2015)	○ Gait ataxia, dysarthria, gross motor regression, hypotonia, ptosis, horizontal ophthalmoplegia, abnormal signals in brainstem and dentate nucleus (Sasarman *et al.* 2015)
R190I	Homozygous recessive (Chakraborty *et al.* 2014; Wedatilake *et al.* 2016)	○ SIFD[a] (Chakraborty *et al.* 2014) ○ Retinitis pigmentosa, bilateral sensorineural deafness, hearing loss, retinopathy (Wedatilake *et al.* 2016)
R203K	Compound heterozygous with **I155T** (Lougaris *et al.* 2018)	○ Fever, recurrent infections, respiratory and gastrointestinal symptoms, hypertrophic cardiomyopathy, hypogammaglobulinemia, developmental delay, microcytic/sideroblastic anemia, combined B- and T-cell defects (Lougaris *et al.* 2018)
H215R	Homozygous recessive (Aksentijevich *et al.* 2014)	○ Anemia, fever, gastrointestinal symptoms, B-cell immunodeficiency, autoinflammation (Aksentijevich *et al.* 2014)
I223T	Compound heterozygous with **D163V** (Aksentijevich *et al.* 2014) Compound heterozygous with **W381fs**, **c.218_219ins22** and **c.1246A[8]** (Chakraborty *et al.* 2014) Compound heterozygous with **c.1057-7C>G** (Chakraborty *et al.* 2014; Abdulhadi *et al.* 2019) Compound heterozygous with **c.342+5G>T** (Wedatilake *et al.* 2016) Homozygous recessive (Chakraborty *et al.* 2014; Gorodetsky *et al.* 2018)	○ Anemia, fever, gastrointestinal symptoms, B-cell immunodeficiency, autoinflammation (Aksentijevich *et al.* 2014) ○ SIFD [a] (Chakraborty *et al.* 2014) ○ SIFD [a], skin autoimmune phenomena (lichen sclerosus and morphea), hypogammaglobulinemia, sensorineural hearing loss, retinitis pigmentosa, hypothyroidism, osteoporosis (Abdulhadi *et al.* 2019) ○ Fever, diarrhea, vomiting, metabolic acidosis, electrolyte imbalance, hypogammaglobulinaemia, sideroblastic anaemia, encephalopathy, developmental delay, retinal dystrophy, progressive cerebellar atrophy, bacterial infections, gastrointestinal symptoms, dyserythropoeisis, central hypotonia, retinal pigmentation, hepatosplenomegaly, exocrine pancreatic insufficiency, seizures (Wedatilake *et al.* 2016) ○ Leigh syndrome (Gorodetsky *et al.* 2018)
I326T	Compound heterozygous with **M158V** (Chakraborty *et al.* 2014)	○ SIFD [a] (Chakraborty *et al.* 2014)
G405R	Compound heterozygous with **c.1057-7C>G** (Bader-Meunier *et al.* 2018)	○ Aseptic panniculitis associated with inherited immunodeficiency, fever, failure to thrive, septicemias, aseptic febrile manifestations, lobular

		and septal neutrophilic panniculitis, chronic microcytic anemia (Bader-Meunier *et al.* 2018)
R412X	Compound heterozygous with **R99W** (Kumaki *et al.* 2019)	○ Atypical SIFD [a] (B-cell deficiency, periodic fever and developmental delay without sideroblastic anemia), iron deficiency anemia, leukopenia and thrombocytopenia, cataracts, pneumonia, partial albinism, short stature, abnormal gonadal development (Kumaki *et al.* 2019)
K416E	Compound heterozygous with **c.del1054_1056+10** (Chakraborty *et al.* 2014) Compound heterozygous with **c.1246A[8]** (Giannelou *et al.* 2018)	○ SIFD[a] (Chakraborty *et al.* 2014) ○ Fever, sideroblastic anemia, hypogammaglobulinemia, developmental delay, bilateral sensorineural hearing loss, bilateral cataracts, swelling of digits of the hands and knee, recurrent cough, rotavirus gastroenteritis (Giannelou *et al.* 2018)
c.1246A[6]	Compound heterozygous with **E43Δ** (DeLuca *et al.* 2016)	○ Retinitis pigmentosa with erythrocytic microcytosis and anisocytosis with anemia (DeLuca *et al.* 2016)
c.1246A[8]	Compound heterozygous with **I223T** (Chakraborty *et al.* 2014; Giannelou *et al.* 2018) Compound heterozygous with **c.609-26T>C** (DeLuca *et al.* 2016) Compound heterozygous with **K416E** (Giannelou *et al.* 2018)	○ SIFD[a] (Chakraborty *et al.* 2014) ○ Fever, sideroblastic anemia, combined B- and T-cell immunodeficiency, developmental delay, protein-losing enteropathy, feeding intolerance, pancreatic insufficiency, hypoglycemia, retinitis pigmentosa, bilateral sensorineural hearing loss, CMV viremia, CMV pneumonitis, *Pseudomonas* necrotizing perianal colitis (Giannelou *et al.* 2018) ○ Retinitis pigmentosa with erythrocytic microcytosis and anisocytosis with mild anemia (DeLuca *et al.* 2016) ○ Fever, sideroblastic anemia, hypogammaglobulinemia, developmental delay, bilateral sensorineural hearing loss, bilateral cataracts, swelling of digits of the hands and knee, recurrent cough, rotavirus gastroenteritis (Giannelou *et al.* 2018)

Note: TRNT1 *mutations, emphasized in this study, are in green boxes.*
[a]*SIFD, sideroblastic anemia associated with B-cell immunodeficiency, periodic fevers and developmental delay.*

Although congenital sideroblastic anemia associated with B-cell immunodeficiency, periodic fevers and developmental delay (SIFD) ranks as the most clinically severe phenotype with childhood onset, a multitude of other symptoms is associated with *TRNT1* mutations. These symptoms include sensorineural hearing loss, cardiomyopathy and central nervous system abnormalities (Wiseman *et al.* 2013) (Table 1-1). While most of these phenotypes are systemic and affect multiple organs, some are restricted to specific areas of the body. One instance of the latter is retinitis pigmentosa, where degeneration of light-sensing photoreceptor cells gradually take place within the outer neural retina,

leading to progressive loss of vision (Sharma *et al.* 2017). This condition is typically accompanied by asymptomatic erythrocytic microcytosis, anisocytosis and mild anemia. In general, certain *TRNT1* mutations are linked to a homozygous recessive mode of inheritance, while others are associated with a compound heterozygous mode. For patients with SIFD, unfortunately, many do not survive past their first decade of life, due to multiple systemic dysfunctions (Wiseman *et al.* 2013).

This essential nature of tRNA-NT is underscored by the finding that small interfering RNA (siRNA) knockdown of *TRNT1* in wild-type human fibroblasts causes cytotoxicity and apoptosis – demonstrating immediate lethality when TRNT1 function is reduced (Chakraborty *et al.* 2014). This observation is as expected, given the central role of this enzyme in tRNA maturation and function. When the amino acid changes resulting from these mutations are mapped onto the higher-order structure of the human tRNA-NT, it is, perhaps, not surprising that most map to the head and neck region of the protein where catalysis occurs (Fig. 1-5).

Recently, *in vitro* characterization (Leibovitch *et al.* 2018, 2019) of six amino acid substitutions (T154I, M158V, L166S, R190I, I223T and I326T) linked to mutations found in SIFD patients (Chakraborty *et al.* 2014) has shown that these amino acid substitutions reduce the stability and catalytic activity of the enzyme. The T154I and M158V amino acid substitutions map to conserved motif B which contains residues required to discriminate against deoxyribonucleotides during substrate binding and catalysis (Li *et al.* 2002). The L166S substitution maps to motif C, thought to function as a spring to allow rearrangement of the catalytic region of the protein during catalysis (Ernst *et al.* 2015). The R190I substitution maps to motif D, which has been implicated in the specific binding of CTP and ATP substrates (Shi *et al.* 1998; Yue *et al.* 1998; Li *et al.* 2002). The I223T substitution maps between motifs D and E with the latter motif potentially playing a role in tRNA binding. The I326T substitution maps to the body domain, about which relatively less is known (Fig. 1-5).

All six of these amino acid substitutions have resulted in TRNT1 variants with decreased thermal stability (Leibovitch *et al.* 2018, 2019). In particular, thermal denaturation studies have revealed melting temperatures of these substitution variants to be 5-7°C lower than that of the native protein. Furthermore, the M158V and I223T variants also have revealed affinities for CTP 20-fold lower than that

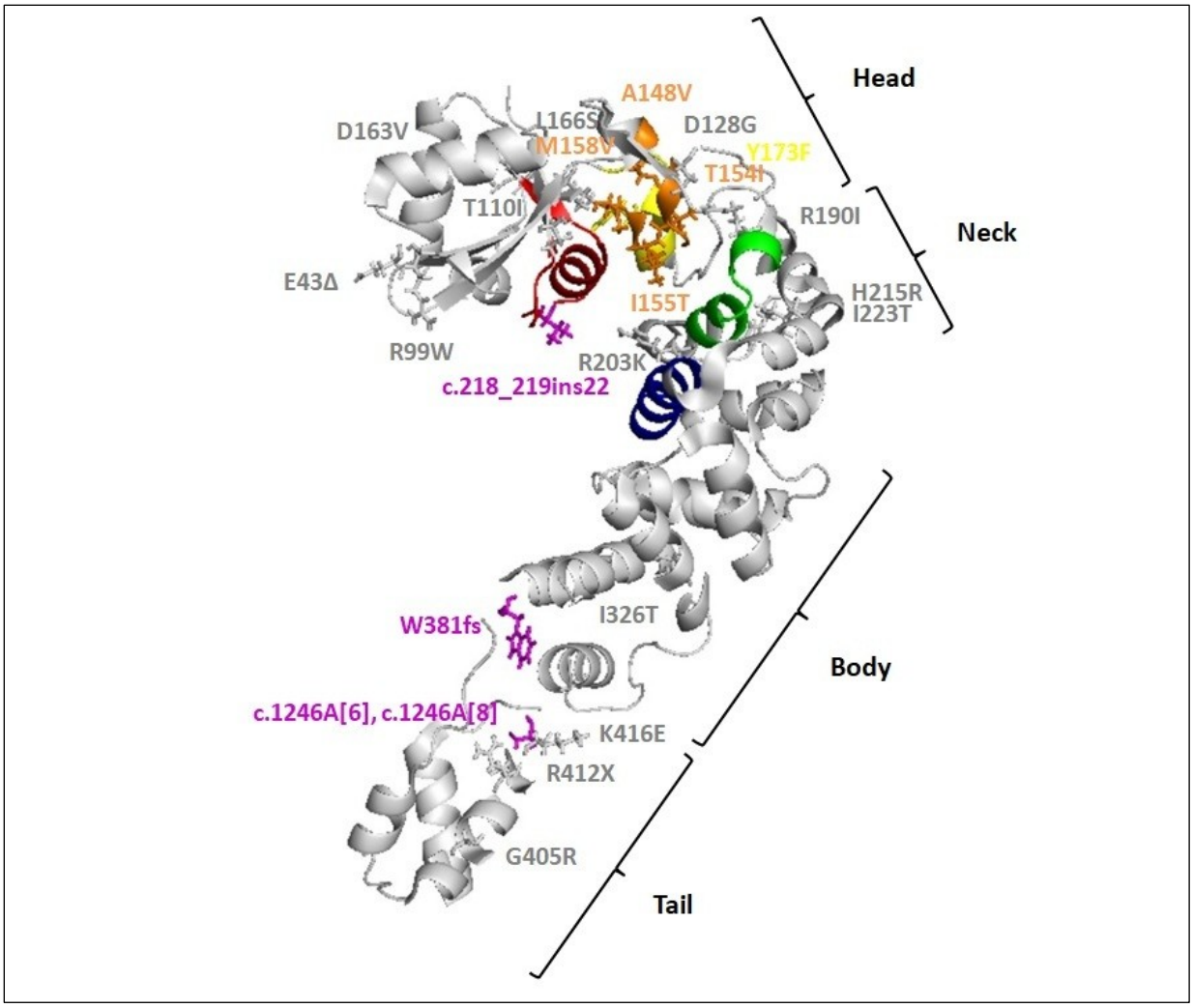

Figure 1-5: Locations in TRNT1 Corresponding to Known *TRNT1* Mutations. Amino acid changes and frame shifts are indicated. The naturally occurring amino acids are represented by stick models. Motifs A, B, C, D and E are represented by ribbons coloured red, orange, yellow, green and blue, respectively. Mutations in purple indicate frame shifts, and only the first altered N-terminal residue of each is displayed in stick model. This structure is visualized by PyMOL *(v1.7.4.5)* (Schrödinger 2018).

non-canonical mitochondrial $tRNA^{Ser(AGY)}$ (lacking a D arm) and a mini-tRNA derivative from *Bacillus subtilis* $tRNA^{Asp}$ (comprising only an acceptor stem and TΨC arm) as nucleic acid substrates (Leibovitch *et al.* 2018). In addition, the I326T variant has revealed an affinity for CTP four-fold lower than that of the native enzyme, and turnover numbers for nucleotide addition with a *B. subtilis* $tRNA^{Asp}$ substrate to be six- to nine-fold lower (Leibovitch *et al.* 2019).

1.4 This Work

Given the important roles of the conserved motifs in tRNA-NT function it is interesting that the amino acid changes in the head and neck region of the protein do not dramatically affect enzyme activity *in vitro*, but clearly do reduce the thermal stability of the protein (Leibovitch *et al.* 2018). Meanwhile, the amino acid change in the body region only mildly affects enzyme activity (Leibovitch *et al.* 2019). We were interested in seeing how additional amino acid alterations further from the active site would affect enzyme structure and function. We suspected that, as they are far from the active site, they are not residues specifically involved in catalysis, but more likely would alter the structure or stability of the enzyme.

1.4.1 Amino Acid Changes Investigated

We looked at three mutations that mapped to different regions of the resulting protein. The first mutation, a three-nucleotide deletion, resulted in the loss of a glutamate residue from the N-terminus of the protein (E43Δ). This amino acid is found at position 43 in the pre-mature form of the protein (containing its 29-residue mitochondrial targeting signal (MTS)) and is more N-terminal than any domains known to be required for enzyme activity (Figs. 1-3, 1-5). The second mutation is a missense mutation (cytosine being replaced by thymine) resulting in the change of the arginine residue at position 99 to tryptophan (R99W). The resulting amino acid substitution is between conserved motifs A and B and is adjacent to the single antiparallel β-sheet found in the enzyme (Figs. 1-3, 1-5). The final mutation is the addition of an adenosine residue in a string of seven adenosines beginning at nucleotide 1246 (c.1246A[8]) resulting in a frame shift such that the C-terminal 17 amino acids of the protein are replaced by eight different amino acids (Table 1-2, Fig. 1-5). All three of these mutations were identified in human disease phenotypes, principally associated with dysfunctions of the cardiovascular, immune, gastrointestinal, visual and nervous systems (Aksentijevich *et al.* 2014; Chakraborty *et al.* 2014; DeLuca *et al.* 2016; Hull *et al.* 2016; Frans *et al.* 2017; Giannelou *et al.* 2018; Kumaki *et al.* 2019) (Table 1-1).

Table 1-2: Carboxy-Terminal Sequences of Native and c.1246A[8] Frame Shift Variant

Variant	Amino acid sequence
Native	LREQWKKSGYQMEKDELLSYIKKT
c.1246A[8]	LREQWKKKWLPNGKR

Note: The first amino acid change resulting from the frame shift is highlighted in green, positively charged amino acids are shown in red and negatively charged amino acids are shown in blue.

In the case for the R99W variant, three young siblings (Hull *et al.* 2016) and one male patient (Frans *et al.* 2017) exhibit the homozygous recessive genotype, while two young unrelated girls exhibit a compound heterozygous R99W/D163V genotype (Aksentijevich *et al.* 2014) and one young boy exhibits a compound heterozygous R99W/R412X genotype (Kumaki *et al.* 2019). For the E43Δ variant, one male patient exhibits the compound heterozygous E43Δ/c.1246A[6] genotype (DeLuca *et al.* 2016). Finally, for the c.1246A[8] variant, two brothers exhibit a compound heterozygous c.1246A[8]/c.609-26T>C genotype (DeLuca *et al.* 2016), one young child exhibits a compound heterozygous c.1246A[8]/I223T genotype (Chakraborty *et al.* 2014; Giannelou *et al.* 2018) and one patient exhibits a compound heterozygous c.1246A[8]/K416E genotype (Giannelou *et al.* 2018). The young child with the c.1246A[8]/I223T genotype is confirmed to have SIFD (Chakraborty *et al.* 2014). Intriguingly, an atypical form of SIFD has been diagnosed in the case of the young boy exhibiting the R99W/R412X genotype, where sideroblastic anemia is conspicuously absent (Kumaki *et al.* 2019).

1.4.2 Thesis Objectives

The primary goal of this thesis is to perform a biophysical and biochemical analysis of the E43Δ, R99W, and c.1246A[8] (abbreviated as *A[8]*) variants of TRNT1 (Fig. 1-6) to determine if these properties are altered as compared to the native enzyme, and to see if these changes suggest how these mutations may contribute to human pathogenesis.

In addition, given how they are spread far across the sequence of TRNT1, including those in the N-terminus and C-terminus far from the active site, these amino acid alterations will be compared to the detailed characterization that already has been performed *in vitro* on the substitutions (T154I, M158V, L166S, R190I and I223T) mapping within or close to the active site and that mapping to the body domain (I326T), to see if new information on the structure or function of tRNA-NT can be determined. Moreover, an analysis of the R99W amino acid substitution may provide some insight into the role of this single antiparallel β-sheet in enzyme activity.

Ultimately, a more detailed understanding of the roles of these amino acids in tRNA-NT structure and function may provide insight into how this and other nucleotide-binding enzymes may function.

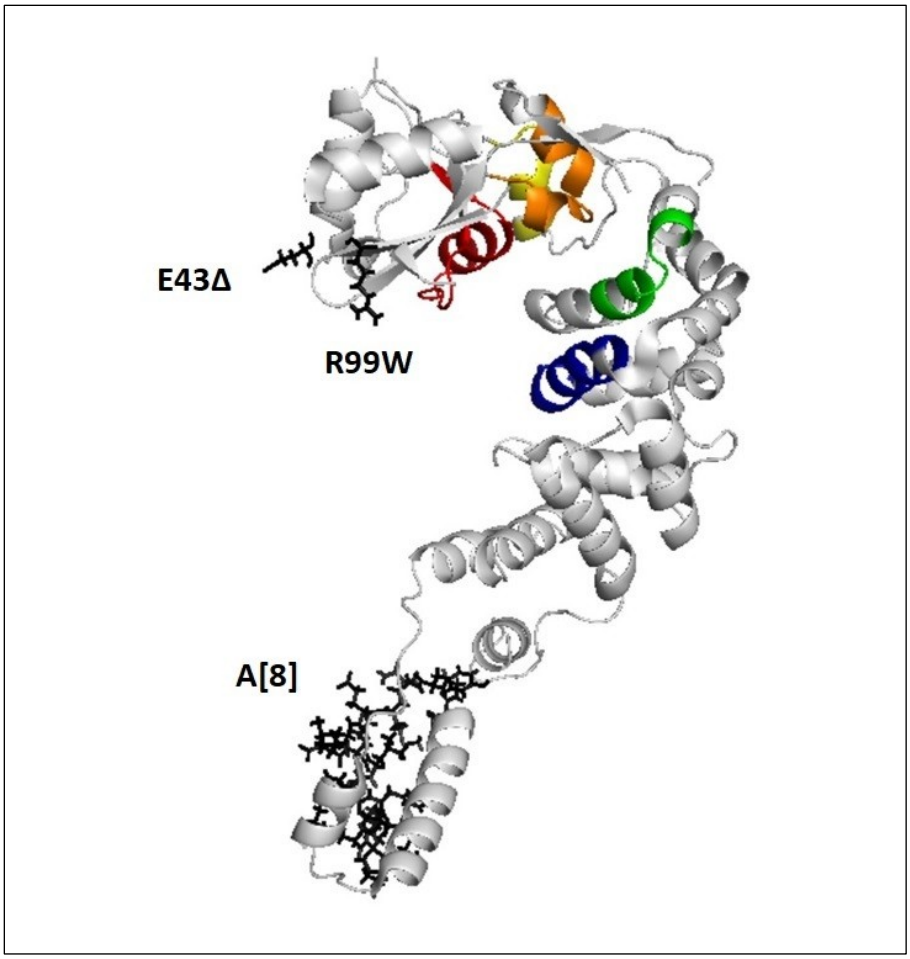

Figure 1-6: Locations in TRNT1 Corresponding to *TRNT1* Mutations in This Study. Amino acid changes resulting from mutations are shown as sticks. Motifs A, B, C, D and E are coloured red, orange, yellow, green and blue, respectively. This structure is visualized by PyMOL *(v1.7.4.5)* (Schrödinger 2018).

2.0 MATERIALS AND METHODS

2.1 Chemicals, Reagents, Enzymes, Solutions, Buffers and Growth Media

Table S0 in **Appendix (7.0)** lists all chemicals, reagents and enzymes used in this study (grades and suppliers indicated); Table 2-1 lists all solutions, buffers and growth media used (components indicated).

Table 2-1: Solutions, Buffers and Growth Media Used in This Study

Solution / Buffer / Growth Medium	Components
30% Acrylamide *(29:1)* Solution (Sambrook *et al.*, 1989)	232 g acrylamide, 8 g *bis* -acrylamide; filled to 800 mL with dH_2O
40% Acrylamide *(19:1)* Solution (Modified from Bio-Rad Laboratories, 1995)	304 g acrylamide, 16 g *bis* -acrylamide; filled to 800 mL with dH_2O
Agarose *(1%)* Gel (Modified from Meyers *et al.*, 1976)	0.5 g agarose; filled to 50 mL with TBE Buffer *(1X)* ; 2.5 µL Fluo-DNA/RNA Gel Staining Solution added
Native PAGE Loading Dye *(2X)* (Simpson *et al.*, 2009)	0.248 mL 0.5M-stock Tris-HCl *(pH 6.8)* , 0.02 mL 1% bromophenol blue, 0.2 mL glycerol, 0.532 mL dH_2O
Native PAGE Running Buffer *(pH 8.3) (5X)* (Simpson *et al.*, 2009)	15 g Tris, 72 g glycine; filled to 1 L with dH_2O; pH adjusted
Non-Reducing SDS-PAGE Loading Dye *(2X)* (Modified from Walker, 2002)	0.248 mL 0.5M-stock Tris-HCl *(pH 6.8)* , 0.02 mL 1% bromophenol blue, 0.2 mL glycerol, 0.4 mL 10% SDS, 0.132 mL dH_2O
PBS Solution *(pH 7.5)* (Sambrook *et al.*, 1989)	13.4 g sodium phosphate (dibasic) heptahydrate, 40 g NaCl, 1.25 g potassium phosphate (monobasic), 1 g KCl; filled to 5 L with dH_2O; pH adjusted with HCl
Peattie's Loading Dye *(2X)* (Peattie, 1979)	30.03 g urea, 0.030 g Tris, 0.015 g boric acid, 10 mL 0.5mM-stock EDTA, 0.025 g xylene cyanol, 0.025 g bromophenol blue; filled to 50 mL with dH_2O
Resuspension Buffer (Modified from Shan, 2005)	PBS Solution *(pH 7.5)* , EDTA *(1 mM final)*
SDS-PAGE Destaining Solution (Modified from Wong *et al.*, 2000)	10% isopropanol, 10% acetic acid, 80% dH_2O
SDS-PAGE Focusing Gel *(4%)* (Modified from Sambrook *et al.*, 1989)	1.4 mL 30% Acrylamide *(29:1)* Solution, 6 mL dH_2O, 2.5 mL 0.5M-stock Tris-HCl *(pH 6.8)* , 0.1 mL 10% SDS, 0.1 mL 10% APS, 0.01 mL TEMED
SDS-PAGE Loading Dye *(5X)* (Modified from Walker, 2002)	2.083 mL 1.5M-stock Tris-HCl *(pH 6.8)* , 5 mL glycerol, 0.025 g bromophenol blue, 1 g SDS, 2.5 mL β-mercaptoethanol; filled to 10 mL with dH_2O
SDS-PAGE Resolving Gel *(13%)* (Modified from Sambrook *et al.*, 1989)	4.3 mL 30% Acrylamide *(29:1)* Solution, 3 mL dH_2O, 2.5 mL 1.5M-stock Tris-HCl *(pH 8.8)* , 0.1 mL 10% SDS, 0.1 mL 10% APS, 0.01 mL TEMED
SDS-PAGE Running Buffer *(5X)* (Modified from Sambrook *et al.*, 1989)	72 g glycine, 15 g Tris, 5 g SDS; filled to 1 L with dH_2O

SDS-PAGE Staining Solution A (Wong *et al.*, 2000)	0.05% Coomassie Brilliant Blue R-250, 25% isopropanol, 10% acetic acid, 64.95% dH_2O
SDS-PAGE Staining Solution B (Wong *et al.*, 2000)	0.005% Coomassie Brilliant Blue R-250, 10% isopropanol, 10% acetic acid, 79.995% dH_2O
TBE Buffer *(5X)* (Modified from Sambrook *et al.*, 1989)	120 g Tris, 62 g boric acid, 40 mL 0.5M-stock EDTA *(pH 8)*; filled to 4 L with dH_2O
YT-Amp Agar Plate (Sambrook *et al.*, 1989)	0.8% bio-tryptone, 0.5% Yeast Extract, 0.5% NaCl, 1.5% agar, 0.1% 100 mg/mL-stock Amp solution, 96.6% dH_2O
YT Liquid Growth Medium (Sambrook *et al.*, 1989)	0.8% bio-tryptone, 0.5% Yeast Extract, 0.5% NaCl, 98.2 % dH_2O
7M Urea, 12% Polyacrylamide Gel (Modified from Bio-Rad Laboratories, 1995)	20 mL TBE Buffer *(5X)*, 20 mL dH_2O, 30 mL 40% Acrylamide *(19:1)* Solution, 42 g urea, 76.1 µL 25% APS,

2.2 Construction of Expression Systems

2.2.1 Generation, Propagation and Isolation of Plasmids Encoding *TRNT1* Variants

QuikChange™ site-directed mutagenesis (modified from Agilent Technologies 2015) was used to generate each *TRNT1* variant, using pET15b-*TRNT1* (provided by Dr. Matthew Leibovitch) encoding wild-type *TRNT1* as a template and forward and reverse primers (Table 2-2). The reaction conditions for each *TRNT1* variant are also listed (Table 2-3).

Table 2-2: Forward and Reverse Primers Used in Site-Directed Mutagenesis

***TRNT1* Variant**	**Oligonucleotides**
R99W [a]	*5′* - CAGTCGGCTGGGATCTGGATGATAAACAACAGAGG - *3′*
	5′ - CCTCTGTTGTTTATCATCCAGATCCCAGCCGACTG - *3′*
E43Δ	*5′* - GAATTCCAGTCACTTTTCACCGGTCTGAAGAGTCTGACAG - *3′*
	5′ - CTGTCAGACTCTTCAGACCGGTGAAAAGTGACTGGAATTC - *3′*
A[6]	*5′* - CAACAGTTGCGAGAACAGTGGAAAAAAGTGGTTACCAAATGGAAAAAGATG - *3′*
	5′ - CATCTTTTTCCATTTGGTAACCACTTTTTTCCACTGTTCTCGCAACTGTTG - *3′*
A[8]	*5′* - CAACAGTTGCGAGAACAGTGGAAAAAAAAGTGGTTACCAAATGGAAAAAGATG - *3′*
	5′ - CATCTTTTTCCATTTGGTAACCACTTTTTTTTCCACTGTTCTCGCAACTGTTG - *3′*

[a] *Designed by Dr. Matthew Leibovitch.*

Table 2-3: Reaction Conditions for Site-Directed Mutagenesis

		TRNT1 Variant			
		R99W [a]	E43Δ	A[6]	A[8]
Volume *(µL)*	pET15b-*TRNT1 (0.1X)*	1.7	5	5	5
	Phusion HF DNA Polymerase	0.2	0.3	0.3	0.3
	Phusion HF Buffer *(5X)*	9.9	10	10	10
	dNTPs *(2.5 mM)*	4	4	4	4
	dH_2O	33.7	28.7	28.7	28.7
	Forward Primer *(10 µM)*	0.25	1	1	1
	Reverse Primer *(10 µM)*	0.25	1	1	1
Temperature *(°C)*; time *(min)*	Denaturation *(initial)*	98; 3	98; 3	98; 3	98; 3
	19 X Denaturation	98; 0.25	98; 0.25	98; 0.25	98; 0.25
	19 X Annealing	45; 0.5	54; 0.5	65; 0.5	65; 0.5
	19 X Extension	72; 4	72; 4	72; 4	72; 4
	Extension *(final)*	72; 10	72; 10	72; 10	72; 10
		4; [hold]	4; [hold]	4; [hold]	4; [hold]

[a] *Performed by Dr. Matthew Leibovitch; total of 25 denaturation-annealing-extension cycles.*

After QuikChange™ site-directed mutagenesis, 5 µL of each reaction mixture was loaded onto a 1% agarose gel and electrophoresed at 110 V for 1 hour, in order to verify the presence of the amplicons. Restriction digestion of each reaction mixture at 37°C for 1 hour, with the enzyme *Dpn*I, was done to eliminate any parental methylated pET15b-*TRNT1*, and was followed by ethanol precipitation (Sambrook *et al.* 1989) and resuspension of the DNA in dH_2O. Plasmids of interest were transformed into *E. coli* XL2 competent cells (Ausubel *et al.* 1989), and single colonies were selected for growth in 10 mL volumes of YT liquid medium with Amp *(100 µg/mL)* for 16 hours with shaking at 225 rpm at 37°C. Plasmid purification from each culture was performed using the GeneJET Plasmid Miniprep Kit (Thermo Scientific), and ethanol precipitation was repeated to further concentrate plasmids. The sequence of each plasmid, encoding the desired *TRNT1* variant, was confirmed via Sanger sequencing and analysis (McGill University and Genome Quebec Innovation Centre).

2.2.2 Generation and Isolation of Run-Off Transcription Templates (Leibovitch *et al.* 2013)

Templates encoding target tRNA sequences for run-off transcription of tRNAs were generated as follows. Plasmids G73 and pmBsDCCA (each 35 µg) [both gifts from Dr. Alan Weiner, University of

Washington; originally constructed by Cho *et al.* (2003) and Oh and Pace (1994), respectively], encoding variants of the *B. subtilis* $tRNA^{Asp}$ gene, were digested by restriction enzymes at 37°C for 4 hours in order to produce linearized $tRNA^{Asp}$ templates, as described in Table 2-4.

Table 2-4: Components for Run-Off Transcription Template Generation

		Template		
		$tRNA^{Asp}$-N	$tRNA^{Asp}$-NC	$tRNA^{Asp}$-NCC
Volume *(µL)*	Plasmid G73	10	-	-
	Plasmid pmBsDCCA	-	10	10
	Fok I	5	5	-
	Bbs I	-	-	8
	NEBuffer 4 *(10X)*	10	10	-
	NEBuffer 2 *(10X)*	-	-	10
	dH_2O	75	75	72

Note: "N" denotes discriminator base.

After digestion, 5 µL of each reaction mixture was loaded onto a 1% agarose gel and electrophoresis was carried out, as described in Section 2.2.1, to verify the presence of the desired digestion products. Next, phenol/ether extraction (Sambrook *et al.* 1989) was performed to eliminate proteins and water-insoluble impurities, followed by ethanol precipitation, in order to isolate the desired $tRNA^{Asp}$ templates (Sambrook *et al.* 1989). The final concentration of each linearized template, to be used in a run-off reaction, was determined by UV-visible (UV-Vis) spectroscopy using an optical density of 260 nm (OD_{260}).

2.3 Production and Purification of TRNT1 Variant Proteins

2.3.1 Protein Production (modified from Leibovitch *et al.* 2018)

Plasmids encoding the *TRNT1* variants, from Section 2.2.1, or encoding the *TRNT1* native form were transformed into *E. coli* BL21(DE3) competent cells for heterologous protein production. *E. coli* cultures were subsequently transferred to Fernbach flasks containing 1.3 L of YT liquid growth medium with Amp *(100 µg/mL)*, and incubated for an average of 2 hours with shaking at 225 rpm and 37°C, in order to achieve a cell density measuring 0.4 to 0.5 at OD_{595}. This was followed by the addition of isopropyl-β-D-

thiogalactopyranoside (IPTG), at a final concentration of 0.25 or 0.5 mM, and further incubation for 16 to 24 hours with shaking at 16 or 19°C in order to induce cells.

2.3.2 Cell Lysis (modified from Leibovitch *et al.* 2018)

Following induction, each BL21(DE3) cell culture was transferred into two JA-10 centrifuge bottles and centrifuged for 10 minutes at 6 400 x *g* at 4°C in a Beckman J2-HS Centrifuge. After discarding the supernatant, 2 mL of cold Resuspension Buffer per gram of cell pellet was added, the cell mixtures were vortexed until homogeneous, and the cell suspensions were subsequently passed 3 to 4 times through a Thermo Spectronic French Pressure Cell Press at 1 000 psi. The resulting cell lysate was transferred to a JA-20 bottle and centrifuged twice for 25 minutes at 39 000 x *g* at 4°C, with the supernatant transferred to a new JA-20 bottle after the initial centrifugation.

2.3.3 Ni-NTA Resin Column (modified from Leibovitch *et al.* 2018)

All processes described here were conducted at 4°C. A Bio-Rad 10 cm x 1.5 cm column, packed with Ni-NTA agarose (QIAGEN) to a height of 1 cm, was equilibrated with two bed volumes of PBS Solution *(pH 7.5)* with 10% glycerol. The supernatant (8 to 16 mL) from Section 2.3.2 was cycled through this column for 30 minutes at a rate of one drop per 8 to 10 seconds. Non-specific binding to the resin was reduced via passage of two more bed volumes of PBS Solution *(pH 7.5)* with 10% glycerol, followed by two more bed volumes of the same containing 10 mM imidazole. Consecutive passages of 8, 6, 6 and 6 mL of PBS Solution *(pH 7.5)* containing 50, 100, 150 and 250 mM of imidazole, respectively, were performed in order to elute the His-tagged variant or native protein, at a rate of 1 drop per 3 to 5 seconds in 1.5 mL fractions. These fractions were kept on ice. The column was subsequently washed of residual protein with 2.5 mL of 6M Gdn-HCl and, as necessary, regenerated via passage of 5 mL of a solution of 100 mM nickel sulfate hexahydrate and 200 mM acetic acid.

2.3.4 SDS-PAGE, Non-Reducing SDS-PAGE and Native PAGE

Small aliquots (16 µL) from selected fractions were mixed with 1X SDS-PAGE Loading Dye (Table 2-1), heated for 2 minutes at 100°C, cooled to room temperature and centrifuged for 30 seconds before being loaded into the wells of a 4 cm x 10 cm x 0.075 cm SDS-PAGE gel (modified from Simpson *et al.* 2009). Electrophoresis was conducted at room temperature at 200 V, with a 4% stacking gel and 13% resolving gel, until the bromophenol blue dye front reached the bottom of the gel (typically 1.5 hours). For protein visualization, the gel was separated from its plates and stained with SDS-PAGE Staining Solution

A, SDS-PAGE Staining Solution B and SDS-PAGE Destaining Solution, with brief intervals of microwave heating (Wong *et al.* 2000). Densitometry analysis was subsequently performed, using ImageJ (Rasband 2018).

For non-reducing SDS-PAGE (modified from Simpson *et al.* 2009), the same procedure as that of SDS-PAGE was followed, however, 1X Non-Reducing SDS Loading Dye (Table 2-1) was used for sample mixing.

For native PAGE (Simpson *et al.* 2009), again the same procedure as that of SDS-PAGE was followed, however, 1X Native PAGE Loading Dye (Table 2-1) was used instead for sample mixing and 1X Native PAGE Running Buffer *(pH 8.3)* (Table 2-1) was used for electrophoresis. In addition, protein samples were not heated and all operations were performed in a 4°C environment.

2.3.5 Dialysis (modified from Leibovitch *et al.* 2018)

Appropriate fractions, as judged by SDS-PAGE from Section 2.3.4, were combined (totaling 7.5 mL) in a 50-kDa-MWCO Spectra/Por 7 Dialysis Membrane (Spectrum Labs) enclosure, and dialyzed against 1 L of PBS Solution *(pH 7.5)* with 10% glycerol for 1 hour at 4°C. This dialyzing solution was exchanged and dialysis was allowed to continue overnight. For biophysical analysis, dialysis was repeated an additional time, and dialysis buffer did not contain glycerol. Upon subsequent removal from the dialysis tubing, each variant or native protein solution was stored in 20 µL, 500 µL and 1 000 µL aliquots at -80°C, until further biophysical or biochemical analysis was performed.

2.3.6 Protein Concentration Determination

The concentration of each variant or native protein was determined by the Bradford assay (Bradford 1976; Bio-Rad Laboratories 2018). Briefly, 3 to 6 dilutions (ranging from 5-fold to 2 500-fold) of each variant or native protein were prepared in 800 µL volumes, to which 200 µL of Protein Assay Dye Reagent Concentrate was added. After mixing and 5 minute incubations, absorbance was measured at 595 nm (using a Shimadzu UV-260 UV-Visible Recording Spectrophotometer). As a standard, bovine serum albumen (BioShop) was prepared in 1.5, 4, 7 and 10 ng/µL 800 µL aliquots, and these were, similarly, combined with 200 µL of reagent and measured for absorbance. Upon establishment of a standard curve, concentrations of the diluted variant or native protein within the linear range of this

curve were determined, and the average value for the subsequent calculations of the initial concentration of the variant or native protein was computed.

2.4 Biophysical Characterization of TRNT1 Variant Proteins

2.4.1 UV-Visible Spectroscopy

To assess the amount of RNA that co-purified with the proteins, UV-visible (UV-Vis) spectroscopy was performed using a Varian Cary 100 Bio UV-Visible Spectrophotometer and the "Varian Cary WinUV Scan Application" *(v4.10(464))*. RNase-treated samples were prepared by incubation with RNase A (Pancreatic) (BioShop) at a final concentration of 20 ng/µL, at room temperature for one hour, prior to dialysis. After centrifugation for 3 minutes at 16 000 x *g* at 4°C to eliminate potential protein precipitate, 700 µL of native or variant protein was loaded into a 1.0 cm quartz cell and scanned at 20°C over a range of 200 to 400 nm.

2.4.2 Circular Dichroism Spectroscopy (Secondary Structure) (modified from Goring *et al.* 2013)

As in Section 2.4.1, aliquots of the native or variant TRNT1 protein were dialyzed against PBS Solution *(pH 7.5)*, either with or without prior RNase A treatment.

To determine the secondary structure, circular dichroism (CD) was performed using a Jasco J-815 Circular Dichroism Spectrometer. Nitrogen flow rate through the instrument was set to 3.8 L/minute and the "Spectrum Measurement" application was selected from the "Jasco Spectra Manager" software suite *(v1.54.03, Build 1)*. The scanning range was set between 200 and 260 nm; additional parameters were configured to standard sensitivity, a continuous scanning mode, a data pitch of 0.2 nm, a response of 1 second, a scan speed of 20 nm/min and a bandwidth of 1 nm. After centrifugation, as in Section 2.4.1, to eliminate potential protein precipitate, 300 µL of native or variant protein, at a concentration not exceeding 200 ng/µL, was loaded into a 0.2 cm cell cuvette, and the scan was conducted such that data were accumulated five times at 20°C. In the "Spectra Analysis" application *(v.1.53.04, Build 1)*, a Savitzky-Golay filter set to 25% was applied to smooth out the resulting data points.

2.4.3 Circular Dichroism Spectroscopy (Thermal Denaturation) (modified from Goring *et al.* 2013)

As in Section 2.4.1, aliquots of the native or variant TRNT1 protein were dialyzed against PBS Solution *(pH 7.5)*, either with or without prior RNase A treatment.

To profile thermal denaturation, a similar process as that of Section 2.4.2 was employed. However, the "Variable Temperature" application was selected instead. The scan was set to 222 nm and the temperature range as 20°C to 65°C; additional parameters were configured to a delay time of 30 seconds, a slope of 30°C/hour and a data pitch of 0.1°C. In the "Spectra Analysis" application, a Savitzky-Golay filter set to 25% was applied to smooth out the resulting data points, and a first-order derivative function was extracted to determine the protein's melting point (T_m).

2.4.4 Fluorescence Spectroscopy (modified from Leibovitch *et al.* 2013)

As in Section 2.4.1, aliquots of the native or variant TRNT1 protein were dialyzed against PBS Solution *(pH 7.5)*, either with or without prior RNase A treatment.

To determine the tertiary structure, fluorescence spectroscopy was performed using a Varian Cary Eclipse Fluorescence Spectrophotometer and the "Varian Cary Eclipse Scan Application" *(v1.1(132))*. An emission wavelength range of 310 to 400 nm was set, while an excitation wavelength of either 280 or 295 nm was selected. Additional parameters were configured to a scan speed of medium (600 nm/min), a data sampling interval of 1.0 nm, excitation and emission slit widths of 5 nm and a detector voltage of medium (600 V). After centrifugation, as above, to eliminate potential protein precipitate, 600 µL of native or variant protein, at a concentration not exceeding 200 ng/µL, was loaded into a 1.0 cm quartz cell, and the scan was conducted such that data were accumulated ten times (CAT scans) at 20°C. A "moving average" operation was subsequently applied to smooth out the resulting data points.

2.5 Biochemical Characterization of TRNT1 Variant Proteins

2.5.1 Run-Off Transcription and Purification of tRNA (modified from Leibovitch *et al.* 2013)

Run-off transcription from $tRNA^{Asp}$-N, $tRNA^{Asp}$-NC and $tRNA^{Asp}$-NCC templates was performed as follows. To initiate each reaction, appropriate amounts of linearized template, nucleoside triphosphates, buffer, T7 RNA polymerase and dH_2O were combined (Table 2-5), with incubation at 37°C for 3.5 to 8 hours.

Table 2-5: Components for Run-Off Transcription

Substrate / Buffer / Reagent / Catalyst	Volume *(µL)*
CTP *(10 mM)*	5
GTP *(10 mM)*	5
UTP *(10 mM)*	5
ATP *(1 mM)*	5
ATP, [α-^{32}P] *(10 µCi/µL, 3000 Ci/mmol)*	5
Transcription Buffer *(5X)*	20
RNAsecure Reagent *(25X)*	3.5
Linearized tRNA^{Asp} template [a]	4.5 - 12.5
T7 RNA Polymerase	4
dH_2O	44.5 - 36.5

[a] *5 µg tRNA^{Asp}-N, tRNA^{Asp}-NC or tRNA^{Asp}-NCC template required.*

Purification of tRNA^{Asp}-N, tRNA^{Asp}-NC and tRNA^{Asp}-NCC transcripts was achieved by a series of phenol extractions and ethanol precipitations, as in Section 2.2.2. After resuspending the RNA pellet in 10 µL dH_2O and 10 µL 2X Peattie's Loading Dye (Table 2-1), the sample was heated at 70°C for 10 minutes and subsequently loaded onto a 4 cm x 10 cm x 0.075 cm 7M urea, 20% polyacrylamide gel, where electrophoresis was performed at 230 to 260 V for 2 to 2.25 hours, until the bromophenol blue marker reached the bottom. Upon exposure to X-ray film (Super RX Fujifilm) for a period of time determined by the equation,

$$T = 30s \bullet 2^n$$

where *T* represents exposure time in seconds *(s)* and *n* represents the number of ^{32}P half-lives elapsed, the position of the relevant tRNA transcript was identified using a Kodak X-OMAT 1000A Processor, and the corresponding gel section excised. This excised gel fragment (typically ~100 µL as estimated based on gradation in an Eppendorf tube) was crushed using a spatula, and vortexed with 400 µL phenol, 360 µL dH_2O, 28 µL 7.5M ammonium acetate, 7.5 µL 0.5 mM EDTA and 4 µL 1M sodium acetate, and was left overnight at 4°C within a slowly rotating Eppendorf tube to allow for transcript to diffuse out of the gel (Rubin 1973). After centrifugation at 16 000 x *g* at 4°C for 10 min, the aqueous phase was collected and ethanol precipitation was performed, as described previously. The pellet containing the tRNA transcript was then resuspended in 110 µL dH_2O. The remaining organic phase, containing the original gel fragment, was subjected to additional vortexing with 360 µL dH_2O, 20 µL 7.5M ammonium acetate, 7 µL 0.5 mM EDTA and 4 µL 1M magnesium acetate, allowing for additional transcript to diffuse out

overnight at 4 °C. Isolation of the aqueous phase, ethanol precipitation and dH_2O resuspension were repeated with this solution, and the tRNA transcript was then combined with the initial sample. The concentration of total tRNA transcript was determined by ^{32}P scintillation counting using a LKB WALLAC-1217 RackBeta liquid scintillation counter, which was calibrated with unreacted [α-^{32}P]-labeled ATP.

2.5.2 Preparation of Baker's Yeast tRNA

For application in standard kinetic assays, in Section 2.5.4, bakers' yeast tRNA was prepared as follows. After resuspending 20 mg of crude baker's yeast tRNA (Roche) in 360 µL dH_2O and 40 µL 3M sodium acetate *(pH 5.2)*, four rounds of phenol extraction and two rounds of ether extraction were performed in sequence, followed by ethanol precipitation. To remove any amino acids attached to the 3'-ends of the tRNA, 2M Tris-HCl *(pH 8)* was added, vortexed and allowed to incubate for 2 hours at 37°C (modified from Sarin and Zamecnik 1964). Two more rounds each of phenol and ether extractions were then performed, and ethanol precipitation was repeated.

To remove any 3'-terminal CCA sequences, the tRNA was immediately resuspended in 280 µL dH_2O, 40 µL 100 mM $MgCl_2$, 40 µL 1M glycine buffer *(pH 9)* and 3 mg of snake venom phosphodiesterase I, type VI (from *Crotalus adamanteus*), and incubated for 1 hour at 37°C (modified from Yue *et al.* 1998). This was followed by three rounds of phenol extraction, two rounds of ether extraction and a final round of ethanol precipitation to eliminate the phosphodiesterase.

2.5.3 Standard Activity Assays (modified from Leibovitch *et al.* 2013)

A standard activity assay was set up as a series of mixtures consisting of 100 mM glycine buffer *(pH 9)*, 6 mM $MgCl_2$, 1 mM ATP and/or 0.1 mM CTP, 10 ng [α-^{32}P]-labeled $tRNA^{Asp}$-N, -NC or -NCC and dH_2O, in a total volume of 8 µL. After pre-heating the mixtures for 2 minutes at 37°C, nucleotide addition was initiated by the addition of 2 µL native or variant TRNT1 protein of varying concentrations at 37°C. Reactions were terminated after 2 minutes by the addition of 10 µL 2X Peattie's Loading Dye, and the resulting mixtures were heated for 10 minutes at 70°C in order to linearize the tRNA transcripts, followed by brief cooling on ice.

Samples were separated at 2 000 V for 7.5 to 8.5 hours on a 7M urea, 12% percent polyacrylamide gel (38 cm x 50 cm) in 1X TBE buffer, after the gel had been pre-run at 2 000 V for 1 hour. To locate products of interest, the gel was placed over a GE HealthCare Storage Phosphor Screen in an Amersham

Biosciences Exposure Cassette. Allowing for some error, the image on the Phosphor Screen developed according to the following equation,

$$T = \frac{d}{96} \bullet 2^{T+t/14}$$

where *T* represents exposure time in days *(d)* and *t* represents the time between synthesis of [α-^{32}P]-labeled ATP and the start of exposure in days *(d)*. The image was subsequently scanned using a GE Healthcare Typhoon Trio Variable Mode Imager and a Typhoon Scanner Control *(v5.0)* with a pixel size of 100 µm, and image analysis of the tRNA transcripts was conducted using the GE HealthCare ImageQuant TL 1D Gel Analysis program *(v7.0)*. This was accomplished by densitometry analysis, where bands corresponding to specific tRNA sizes before and after nucleotide incorporation were assessed for their relative intensities.

2.5.4 Standard Kinetics Assays (modified from Leibovitch *et al.* 2013)

A standard kinetic assay was set up as a series of mixtures containing the same components as in Section 2.5.3, however, all concentrations were fixed, including that of the added native or variant TRNT1 protein. For each reaction, the concentration of a single substrate (ATP, CTP, tRNA^{Asp}-NC or tRNA^{Asp}-NCC) was varied, in order to determine the specific kinetic parameters for that substrate. After each reaction was initiated by the addition of an appropriate amount of protein at 37°C, termination was achieved at each time point (10, 20 or 40 seconds) by withdrawing 10 µL of the reaction mixture and mixing it with 10 µL 2X Peattie's Loading Dye, followed by heating for 10 minutes at 70°C and brief cooling on ice. Each time point for each reaction was performed in duplicate or triplicate. For kinetic assays of varying tRNA^{Asp}-NC or tRNA^{Asp}-NCC concentrations, purified baker's yeast tRNA, as prepared in Section 2.5.2, was used to supplement for the higher tRNA concentrations demanded (typically above 1.2 ng/µL).

Electrophoresis of the mixtures, image exposure and analysis were conducted as described in Section 2.5.3.

Percent addition and initial velocity (v_o) of each reaction corresponding to each concentration of the varied substrate were determined, and nonlinear regression was performed using GraFit 7 (Leatherbarrow 2009), in order to model the resultant kinetics based on the Michaelis-Menten and Hill equations. For both models, the maximum reaction rate (V_{max}), apparent Michaelis constant ($K_{M,Apparent}$),

turnover number (k_{cat}) and specificity constant ($k_{cat}/K_{M,Apparent}$) were computed. For the Hill model, the Hill coefficient (*n*) was also determined.

2.6 Molecular Modeling and Visualization of TRNT1 Variant Proteins

The structure of the native TRNT1 protein was based on X-ray crystallographic data downloaded from the RCSB Protein Data Bank (PDB ID: 4X4W; Kuhn *et al.* 2015). To simulate the folded structure of each variant TRNT1 protein, a hybrid modeling approach called Robetta *(beta version)* was employed, combining both homology modeling and *ab initio* structure prediction (Kim *et al.* 2004), and upon output the top-ranking structure for each variant was selected.

To simulate the tertiary structure of the *B. subtilis* $tRNA^{Asp}$-NCCA, its sequence and corresponding secondary structure were downloaded from the Transfer RNA Database (Juhling *et al.* 2009) (tRNAdb ID: tdbD00000402; Yumada *et al.* 1983; Green *et al.* 1985), and the molecule was folded *in silico* without need for a structural template or sequence alignment, by RNAComposer (Popenda *et al.* 2012).

Finally, to simulate docking of the native or variant protein with the $tRNA^{Asp}$-NCCA, a hybrid algorithm of template-based modeling and *ab initio* free docking called HDOCK (Pearson and Lipman 1988; Remmert *et al.* 2012; Yan *et al.* 2017) was employed, and the complex with the lowest docking energy score was selected, given that the 3'-end of the $tRNA^{Asp}$-NCCA was within close proximity to the active site.

All models were visualized by the molecular visualization software, PyMOL *(v.1.7.4.5)* (Schrödinger 2018).

3.0 RESULTS

3.1 TRNT1 Variant Protein Amounts and Purities

Following production and purification of native, R99W, E43Δ and A[8] TRNT1 variant proteins, total protein amounts were determined by Bradford assay (Table S1); and SDS-PAGE (Fig. 3-1), non-reducing SDS-PAGE (Fig. 3-2) and native PAGE (Fig. 3-3) were carried out on aliquots of each. (In Figs. 3-1 to 3-3, the gap preceding the A[8] variant reflects the removal of lanes containing samples not pertinent to this discussion. For completeness, the original gel images are shown in Fig. S2.)

All recombinant proteins showed sizes in the ranges of those expected (Fig. 3-1) based on the predicted monomer sizes of 48.5, 48.6, 48.4 and 47.5 kDa for the native, R99W, E43Δ and A[8] variant proteins, respectively. For the sake of comparison, the mass of the A[8] variant was determined by mass spectrometry (MS) and this mass (47,360 Da) showed a good correlation with the mass determined by SDS-PAGE (~47.5 kDa) and the predicted mass based on the amino acid sequence (47,355 Da). Densitometry was performed on each SDS-PAGE sample to determine relative enzyme purity, defined as the relative ratio of protein of the expected molecular mass as compared to all proteins in the sample, and all samples showed >80% purity (Table S1, Fig. S1).

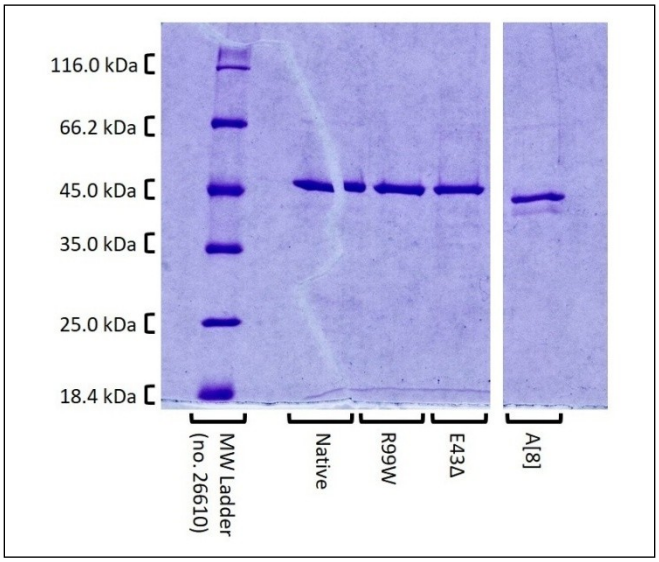

Figure 3-1: SDS-PAGE of Variant and Native TRNT1 Proteins. For each TRNT1 variant (and native) sample, 16 µL of a 100 ng/µL aliquot were loaded, followed by electrophoresis and gel staining. Unstained Protein Molecular Weight Marker (no. 26610) (Thermo Scientific) was used as a molecular weight ladder (6 µL) with the corresponding marker sizes shown. See **Figure S2A** for original gel image.

3.2 Quaternary Structures of TRNT1 Variants

In addition to SDS-PAGE, non-reducing SDS-PAGE and native PAGE of native and variant TRNT1 proteins were performed in order to gain insight into possible quaternary structures. Non-reducing SDS-PAGE with aliquots of each native and variant protein (Fig. 3-2) showed species at ~100 kDa, suggestive of dimerization products for the native, R99W, E43Δ and A[8] proteins. When native PAGE was performed (Fig. 3-3), all samples showed two major species, one of which migrated through the gel approximately half as far as the other, consistent with two forms of the native enzyme.

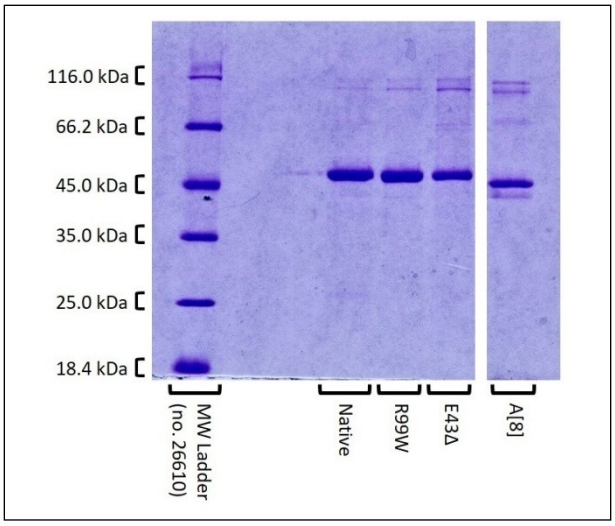

Figure 3-2: Non-Reducing SDS-PAGE of Variant and Native TRNT1 Proteins. For each TRNT1 variant (and native) sample, 8 µL of a 200 ng/µL aliquot were loaded (without β-mercaptoethanol), followed by electrophoresis and gel staining. (Molecular Weight Marker as in **Figure 3-1**). See **Figure S2B** for original gel image.

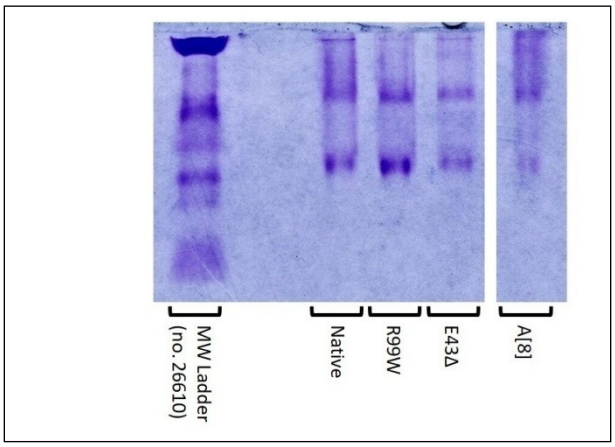

Figure 3-3: Native PAGE of Variant and Native TRNT1 Proteins. For each TRNT1 variant (and native) sample, 8 µL of a 200-ng/µL aliquot were loaded (without β-mercaptoethanol and SDS), followed by electrophoresis and gel staining. (Molecular Weight Marker as in **Figure 3-1**. No marker sizes could be confidently assigned.) See **Figure S2C** for original gel image.

3.3 Biophysical Characterization of TRNT1 Variants

3.3.1 Amount of Co-Purified RNA Bound

As this protein uses RNA as a substrate and nucleic acids have an absorption maximum at 260 nm, while aromatic amino acids show an absorption maximum at 280 nm, a ratio of absorbance at 280 nm to that at 260 nm (A_{280}:A_{260}) was calculated for each protein, either before or after RNase treatment, to assess the amount of *E. coli* nucleic acid that co-purified with the enzyme (Fig. 3-4). Before RNase treatment, the native, R99W and E43Δ proteins showed A_{280}:A_{260} ratios well below one resulting from a significant contribution from RNA, while the A[8] variant showed a ratio greater than one. After RNase treatment, all samples showed ratios between 1.34 and 1.59. The largest change in the A_{280}:A_{260} ratio upon RNase treatment was seen for the native enzyme (an increase of 0.94 ± 0.1), followed by the R99W variant (an increase of 0.71 ± 0.1) and the E43Δ variant (an increase of 0.69 ± 0.1). In contrast, the A[8] variant showed only a 0.17 ± 0.8 increase, primarily as a result of a limited reduction in $A_{260\ nm}$ as compared to the other samples.

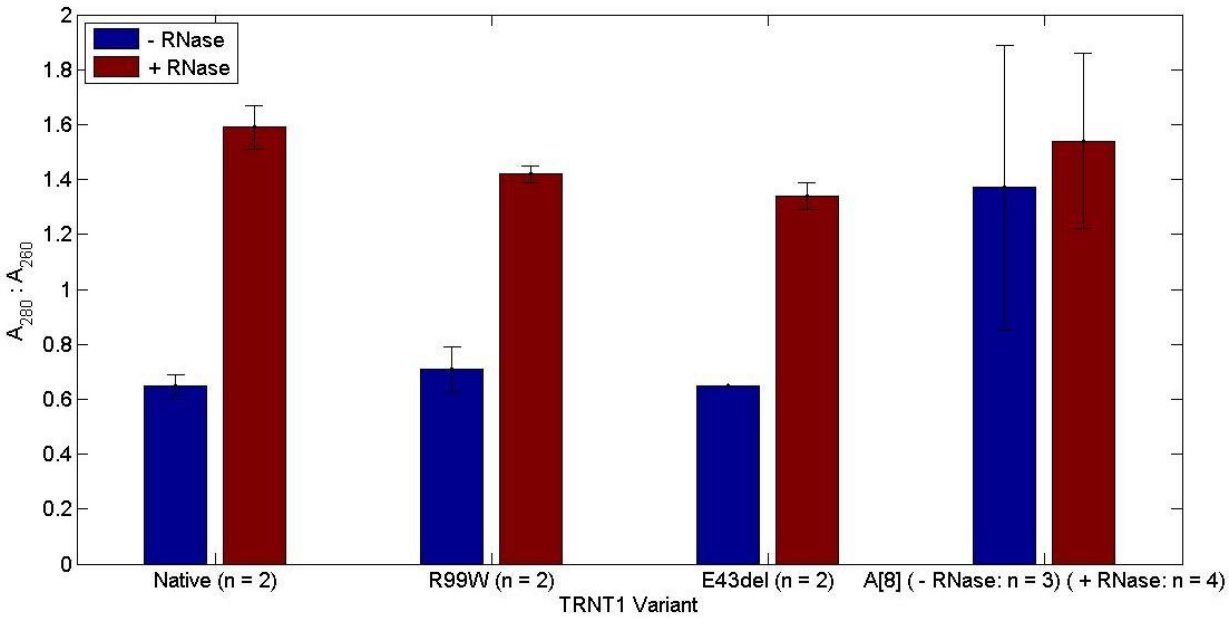

Figure 3-4: A_{280}:A_{260} Ratios of Native and Variant TRNT1 Proteins. The ratios of UV absorbance at 280 and 260 nm are displayed for native, R99W, E43Δ and A[8] TRNT1 proteins for samples treated (red) or untreated (blue) with RNAse A. The number of experimental replicates is denoted in parentheses, with error bars representing one SEM. Each replicate represents an individual experiment.

3.3.2 Secondary Structures

In order to assess any changes in the secondary structures of the TRNT1 variants, CD spectroscopy was performed on all samples before and after RNase treatment. In either condition, the CD spectra of all proteins were characteristic of a mixed α-helix/β-strand structure indicative of minimal or no change in secondary structure from that of native TRNT1. CD signal traces of the raw data are shown in Fig. S3A and Fig. S3B, while traces normalized to those of the native enzyme are shown in Fig. S3C.

3.3.3 Thermal Stabilities

In order to assess any changes in the thermal stabilities of the TRNT1 variants, thermal denaturation was performed by following the ellipticity of each protein at 222 nm as the temperature was raised from 20 to 65°C in order to follow total remaining α-helical content (Fig. S4A). Using these data, a T_m, defined as the temperature at which 50% of the α-helical content is unfolded (20°C is assigned 100% α-helical content), was calculated for each sample. There was a difference of only 3°C or less in T_m (thermal stability) between all samples upon comparison either before or after RNase treatment (Fig. 3-5). A decrease of ~2.5°C in T_m was observed for the native enzyme upon RNase treatment, while smaller decreases upon RNase treatment were seen in the other samples. The T_m for the native enzyme was in excellent agreement with that determined previously (Leibovitch *et al.* 2018) for the native enzyme (42.4°C). Thermal denaturation curves normalized to those of the native enzyme are shown in Fig. S4B, while fractions unfolded are shown in Fig. S4C.

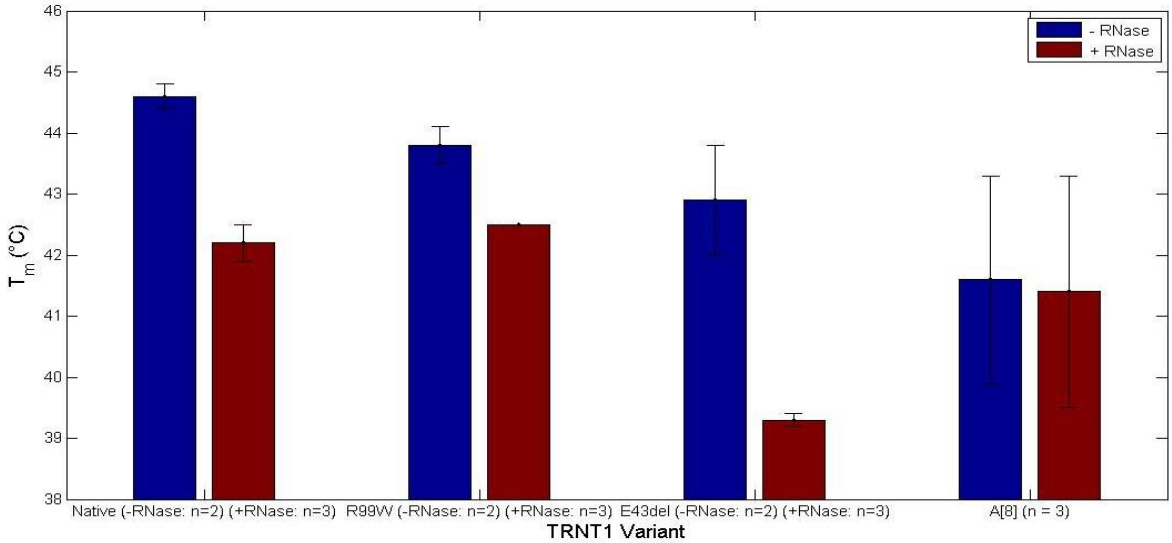

Figure 3-5: Melting temperatures (T_m's) of Native and Variant TRNT1 Proteins. T_m's are displayed for native, R99W, E43Δ and A[8] TRNT1 proteins before (red) and after (blue) treatment with RNAse A. The number of experimental replicates is denoted in parentheses, with error bars representing one SEM.

3.3.4 Tertiary Structures

In order to assess any changes in the tertiary structures of the TRNT1 variants, fluorescence spectroscopy was performed. Whether assayed for fluorescence after excitation at 280 nm or 295 nm, or before or after RNase treatment, emission spectrum peaks were red-shifted by only up to a maximum of ~4 nm for excitation at 280 nm and ~2.7 nm for excitation at 295 nm, as compared to the native enzyme (Fig. 3-6). Fluorescence emission traces of the raw data are shown in Fig. S5A (without RNase) and Fig. S6A (with RNase), while traces normalized to those of the native enzyme are shown in Fig. S5B (without RNase) and Fig. S6B (with RNase).

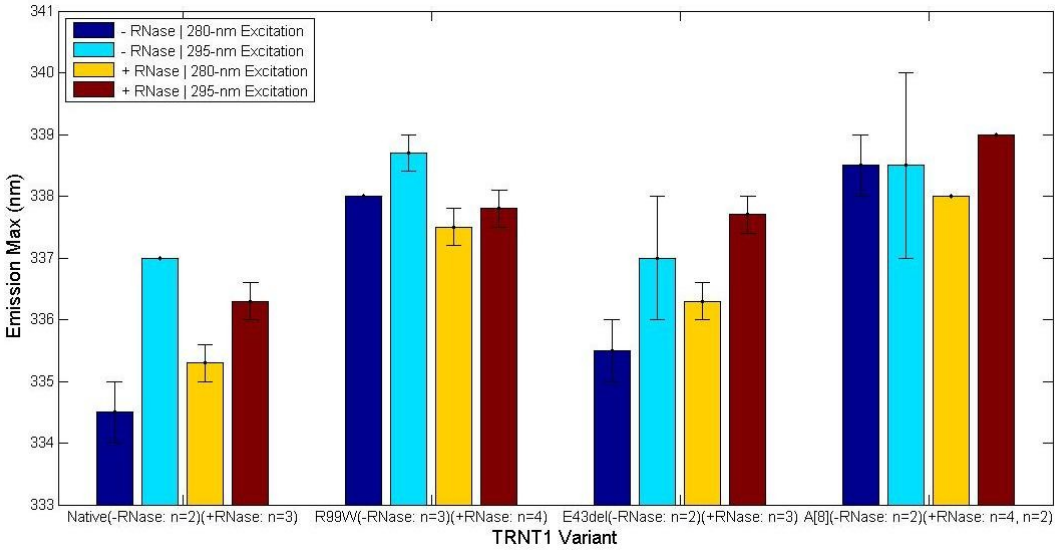

Figure 3-6: Fluorescence Emission Maxima of Native and Variant TRNT1 Proteins. Fluorescence emission maxima are displayed for native, R99W, E43Δ and A[8] TRNT1 proteins. Maxima for non-RNase-treated aliquots after excitation at 280 and 295 nm are represented by dark and light blue bars, respectively, and maxima for RNase-treated aliquots after excitation at 280 and 295 nm are represented by yellow and red bars, respectively. The number of experimental replicates for each maximum is denoted in parentheses, with error bars representing one SEM.

3.4 Biochemical Characterization of TRNT1 Variants

3.4.1 Activities

To address any changes in enzyme activities of the TRNT1 variants, standard end point assays (Leibovitch *et al.* 2013) were set up in order to gauge the amount of enzyme required for AMP and/or CMP incorporation (A- and/or C-addition, respectively) on different tRNA transcripts. Four separate experimental conditions were used – $tRNA^{Asp}$-NCC and ATP (Fig. 3-7), $tRNA^{Asp}$-NC and CTP (Fig. 3-8), $tRNA^{Asp}$-N and CTP (Fig. 3-9), and $tRNA^{Asp}$-N and CTP and ATP (Fig. 3-10).

3.4.1.1 AMP Addition to the tRNA^{Asp}-NCC Transcript

In the assay measuring AMP addition to the tRNA^{Asp}-NCC transcript (Fig. 3-7), at the highest protein amount tested (9.2 ng), the native enzyme showed 74% final product formation. All variant enzymes tested showed considerably less AMP incorporation, with 26%, 18% and 11% by the R99W, E43Δ and A[8] variants, respectively, at similar protein amounts. Furthermore, a similar level of product formation to that of the native enzyme was observed for the A[8] variant only when its amount was increased by approximately 10-fold to 83.9 ng (63% product formed).

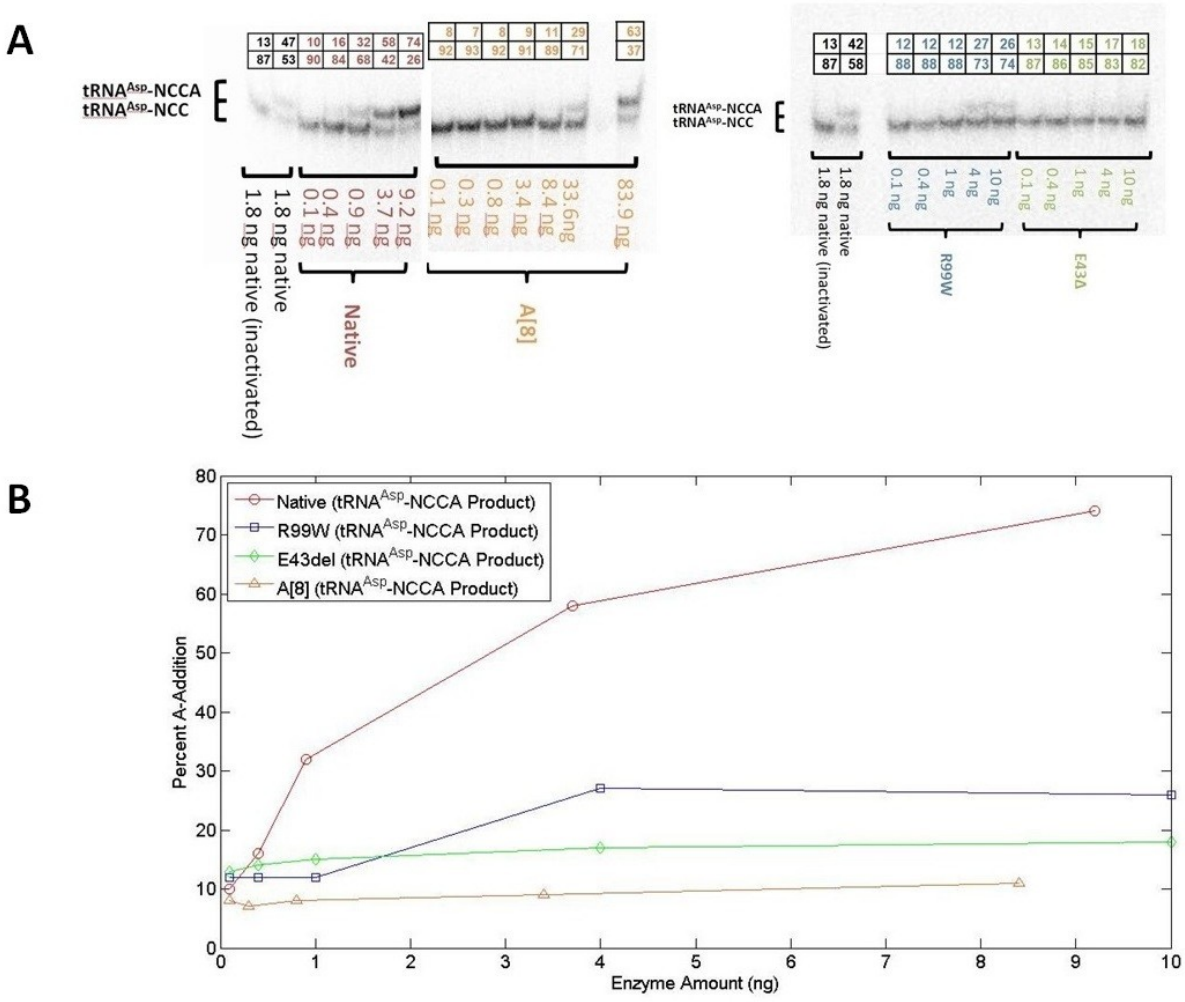

Figure 3-7: Activity Assay of Native and Variant TRNT1 Enzymes (AMP Incorporation onto tRNA^{Asp}-NCC). (A) Enzyme and amount used are indicated beneath each lane, while numbers above each lane indicate relative amounts of tRNA^{Asp}-NCCA and tRNA^{Asp}-NCC at the completion of each two-minute reaction. **(B)** Graphical representation of data from **(A)**.

3.4.1.2 CMP Addition to the tRNA^{Asp}-NC Transcript

In the assay measuring CMP addition to the tRNA^{Asp}-NC transcript (Fig. 3-8), at 3.7 ng, the native enzyme showed 48% final product formation, while at similar levels, 26% and 13% were seen for the E43Δ and A[8] variants. A comparable level of product formation to that of the native enzyme was only attainable by the A[8] variant when its amount was increased by approximately 25-fold to 83.9 ng (76% product formed). Surprisingly, for the R99W variant, 74% final product formation was observed at only 5 ng, suggesting an increased ability of this variant, as compared to the native enzyme, to incorporate CMP onto the tRNA^{Asp}-NC transcript.

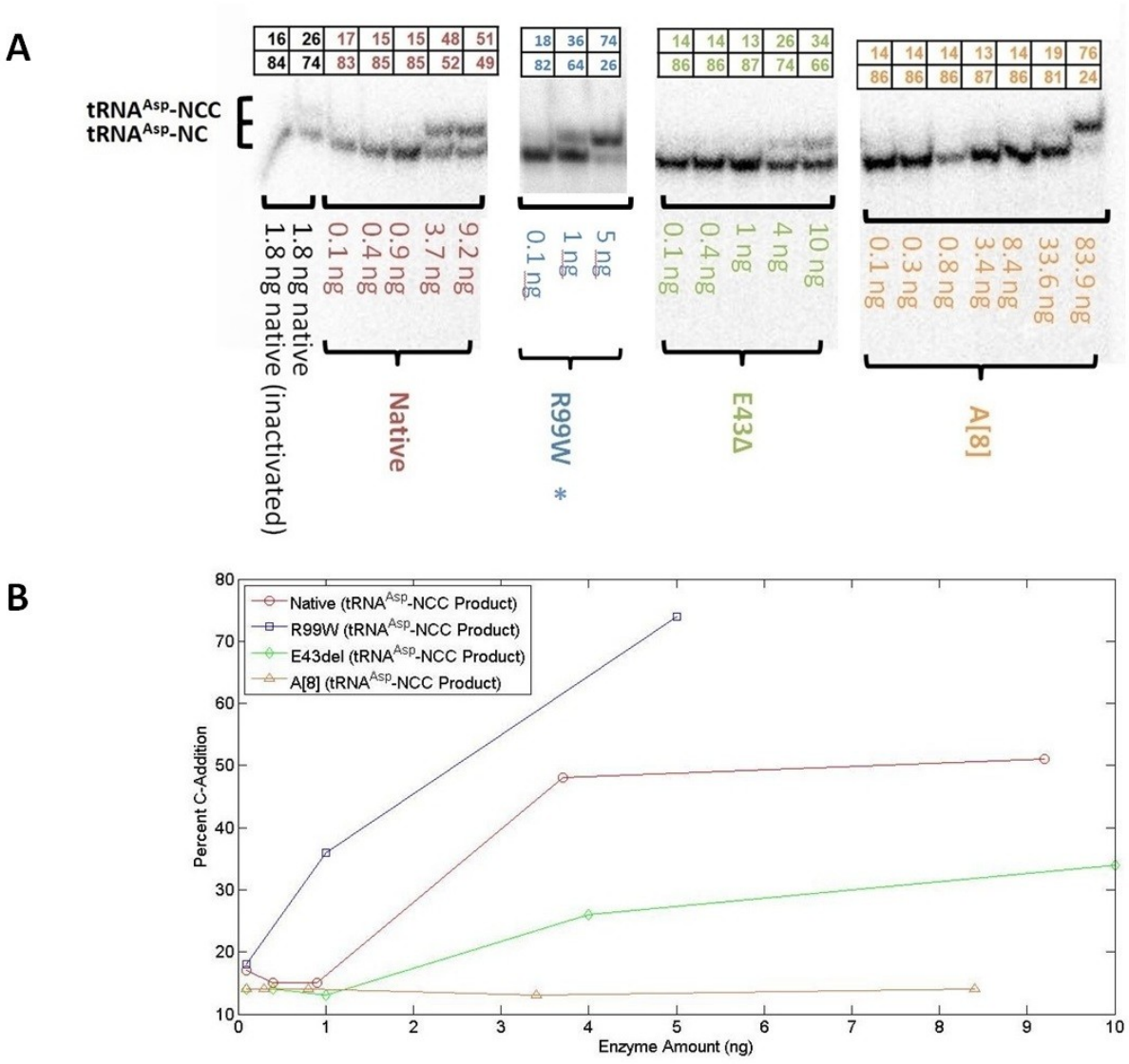

Figure 3-8: Activity Assay of Native and Variant TRNT1 Enzymes (CMP Incorporation onto tRNA^{Asp}-NC). **(A)** Enzyme and amount used are indicated beneath each lane, while numbers above each lane indicate relative amounts of tRNA^{Asp}-NCC and tRNA^{Asp}-NC at the completion of each two-minute reaction. **(B)** Graphical representation of data from **(A)**. ***: Performed by Nathalie Reid.***

3.4.1.3 CMP Addition to the tRNA^{Asp}-N Transcript

In the assay measuring CMP addition to the tRNA^{Asp}-N transcript (Fig. 3-9), all enzymes showed much reduced activity with tRNA^{Asp}-NCC product formation at roughly 5% at approximately 10 ng of protein in nearly all cases. The exception is the E43Δ variant, which showed 23% tRNA^{Asp}-NCC product formation at this amount, suggesting an increased ability, as compared to the native enzyme, of the E43Δ variant to incorporate CMP onto the tRNA^{Asp}-N transcript.

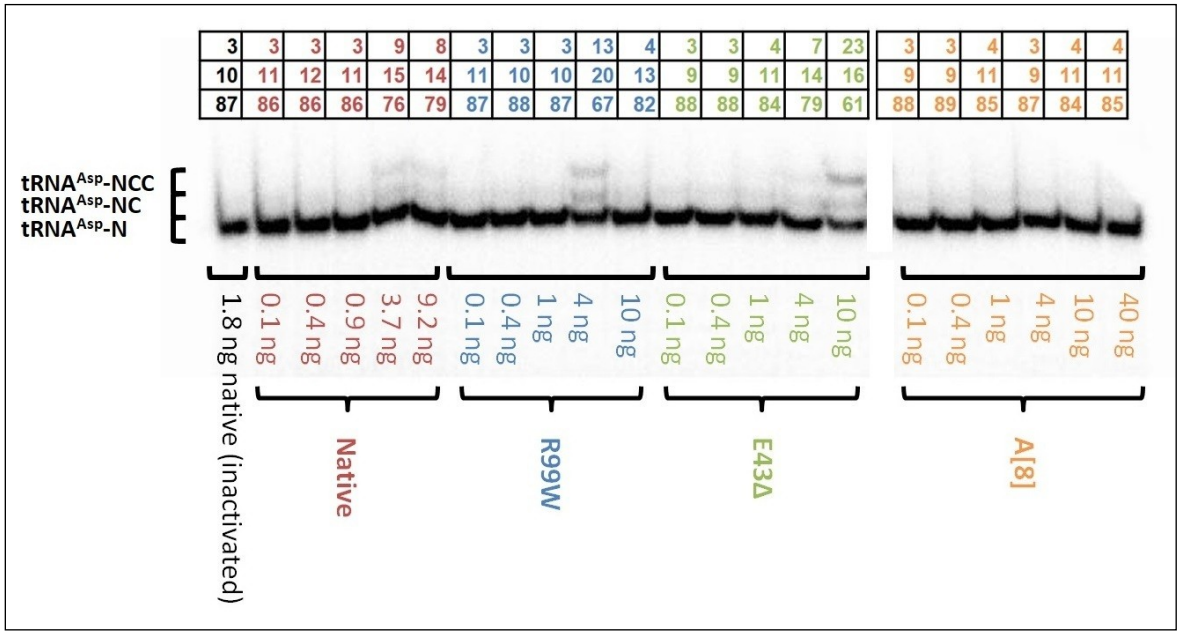

Figure 3-9: Activity Assay of Native and Variant TRNT1 Enzymes (CMP Incorporation onto tRNA^{Asp}-N). Enzyme and amount used are indicated beneath each lane, while numbers above each lane indicate relative amounts of tRNA^{Asp}-NCC, tRNA^{Asp}-NC and tRNA^{Asp}-N at the completion of each two-minute reaction.

3.4.1.4 CMP and/or AMP Addition to the tRNA^{Asp}-N Transcript

In the assay with tRNA^{Asp}-N, CTP and ATP as substrates (Fig. 3-10), a similar pattern to that of the assay using tRNA^{Asp}-N and CTP (Fig. 3-9) was observed. This experiment differs from those described above, in that in this case both ATP and CTP can be incorporated. Given the results shown in Fig. 3-9 for CMP incorporation alone, it is reasonable to assume that the addition of the first two nucleotides represents CMP incorporation and that of the final nucleotide represents AMP incorporation. Here, at 9.2 ng, the native enzyme showed 37% tRNA^{Asp}-NCCA product formation, while the R99W, E43Δ and A[8] variants showed considerably less (≤11%) at similar protein amounts (Fig. 3-10). Again, a comparable level of final product formation to that of the native was observed for the A[8] variant only when its amount was increased by approximately 10-fold to 83.9 ng (54% tRNA^{Asp}-NCCA product formed).

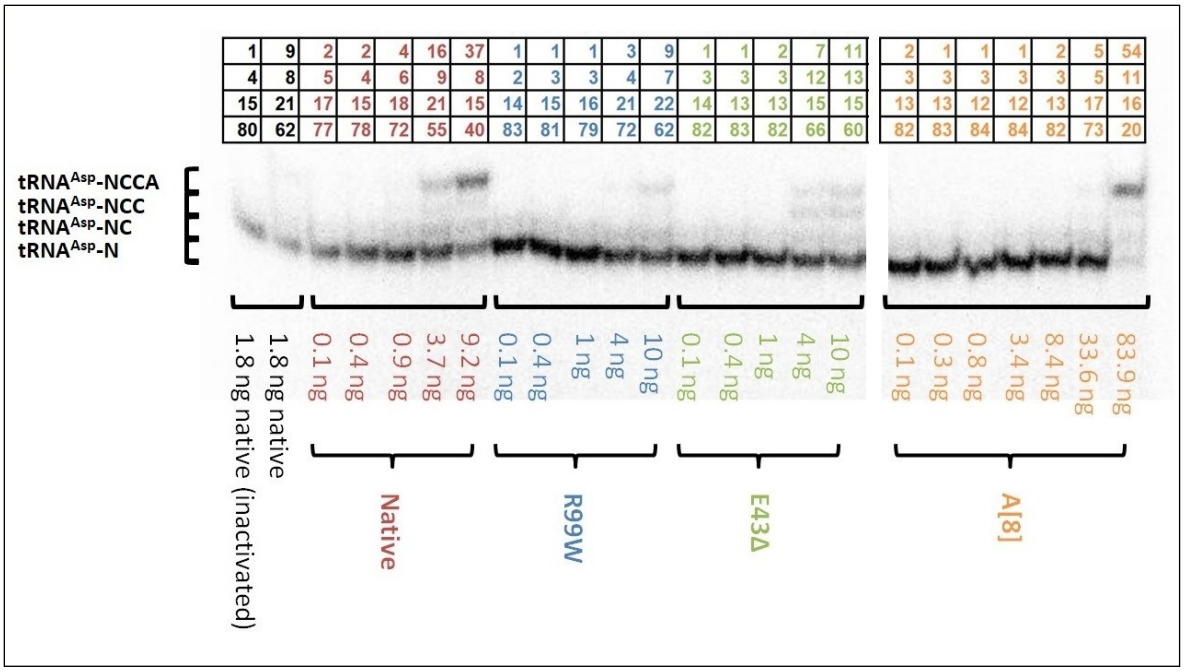

Figure 3-10: Activity Assay of Native and Variant TRNT1 Enzymes (CMP and AMP Addition to tRNA^{Asp}-N). Enzyme and amount used are indicated beneath each lane, while numbers above each lane indicate relative amounts of tRNA^{Asp}-NCCA, tRNA^{Asp}-NCC, tRNA^{Asp}-NC and tRNA^{Asp}-N at the completion of each two-minute reaction.

3.4.1.5 Misincorporation of CMP and/or AMP onto tRNA^{Asp} Transcripts By the E43Δ Variant

Given that the E43Δ variant showed better final product formation when CMP was incorporated onto tRNA^{Asp}-N than did the native enzyme (23% versus 8%, respectively, at approximately 10 ng in Fig. 3-9), but less final product formation when ATP was also present in the reaction (11% versus 37%, respectively in Fig. 3-10) or when AMP was incorporated onto tRNA^{Asp}-NCC (18% versus 74%, respectively, in Fig. 3-7), a difference in the ability to incorporate CMP or AMP by the E43Δ variant was suggested.

Therefore, the ability of the E43Δ variant to incorporate CMP onto tRNA^{Asp}-N or tRNA^{Asp}-NC was tested at higher enzyme amounts. CMP incorporation onto the tRNA^{Asp}-NC transcript showed run-on transcription with tRNA^{Asp}-NCCC and -NC$_{(4)}$ products forming at 11.5 and 46.2 ng of E43Δ protein, respectively (Fig. 3-11A). In comparison, the native enzyme showed a tRNA^{Asp}-NCCC product only starting to form at 24.1 ng (Fig. 3-11A). Similarly, CMP incorporation onto the tRNA^{Asp}-N transcript showed tRNA^{Asp}-NCCC, -NC$_{(4)}$ and -NC$_{(5)}$ products forming at 11.5, 46.2 and 115.4 ng of E43Δ protein, respectively (Fig. 3-11B). Here, run-on C-adding activity with the E43Δ protein was seen as early as 4.6

ng, where a tRNA^{Asp}-NCCC product was first evident (Fig. 3-11B), in contrast to that of the native enzyme, which only showed this run-on product at 96.5 ng of protein.

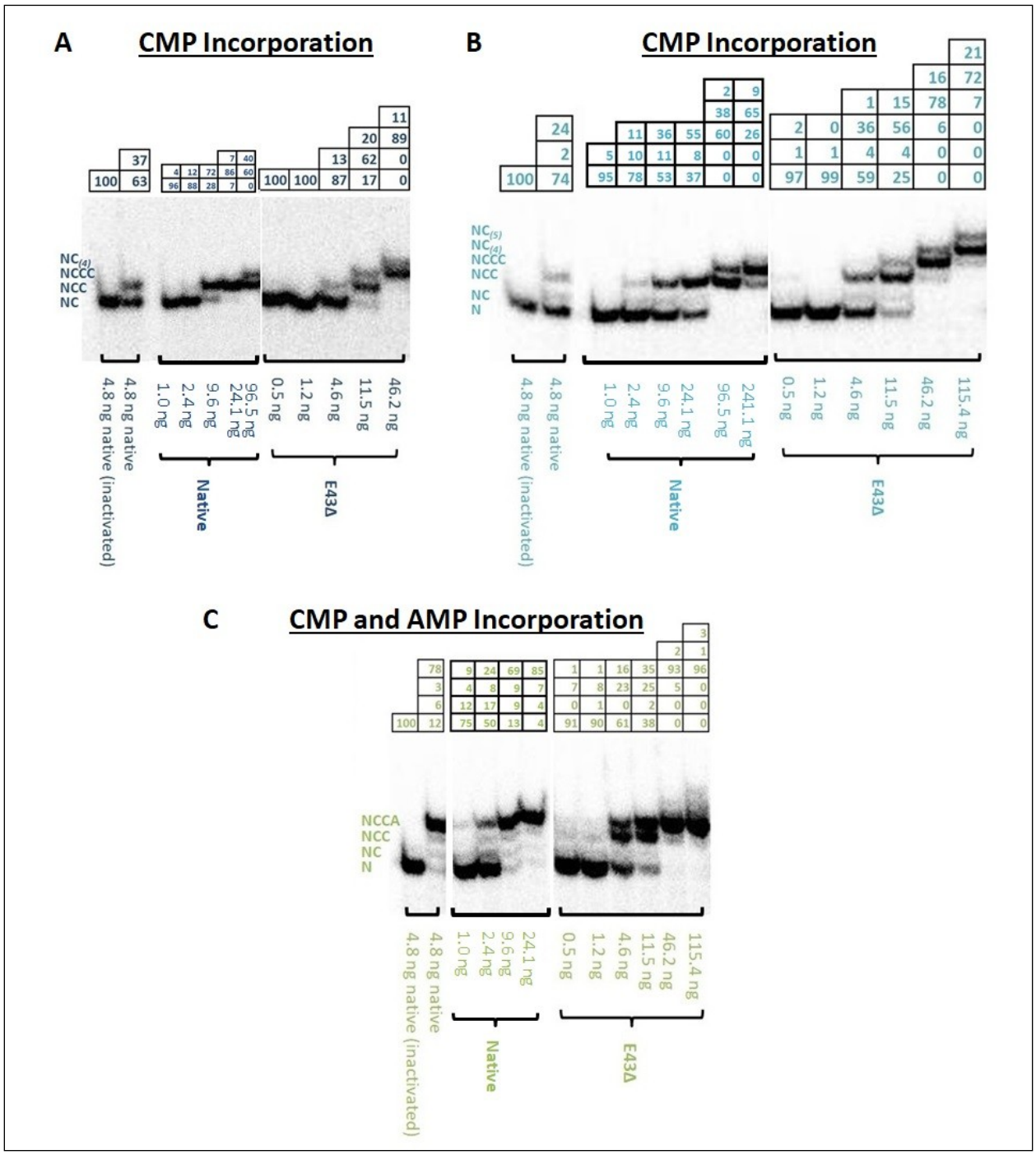

Figure 3-11: Activity Assays of E43Δ Variant. (A) CMP incorporation onto tRNA^{Asp}-NC. **(B)** CMP incorporation onto tRNA^{Asp}-N. **(C)** CMP and AMP incorporation onto tRNA^{Asp}-N. Enzyme and amount used are indicated beneath each lane, while numbers above each lane indicate relative amounts of transcript products and reactants at the completion of each two-minute reaction.

When both ATP and CTP were provided to the $tRNA^{Asp}$-N transcript, interestingly, there was limited extension beyond the third (typically -NCCA) position (Fig. 3-11C), observable with E43Δ protein amounts of 46.2 and 115.4 ng.

3.4.2 Kinetics

Based on the data generated from the end point assays, it seemed worthwhile to define more specific kinetic parameters for these TRNT1 variants. Specifically, kinetic analyses were performed to determine any changes in apparent Michaelis constants ($K_{M,Apparent}$'s) for nucleoside triphosphates (NTPs) or nucleic acids, or for turnover numbers (k_{cat}'s), as compared to the native enzyme. Four different experimental conditions were employed by altering ATP, CTP, $tRNA^{Asp}$-NCC or $tRNA^{Asp}$-NC concentrations (Tables 3-1, 3-2, 3-3 and 3-4, respectively). A subset of representative kinetic assay plots for the native enzyme is shown in Fig. S7.

3.4.2.1 Varying ATP Concentration

When the ATP concentration was varied and the amount of $tRNA^{Asp}$-NCC transcript was fixed (Table 3-1), in terms of $K_{M,Apparent}$ for ATP binding, the E43Δ and A[8] variants showed less than a three-fold increase compared to that of the native enzyme, while the R99W variant showed an approximately 100-fold decrease compared to that of the native enzyme (1.14 ± 0.6 μM versus 124.31 ± 39.3 μM). In terms of k_{cat}, the E43Δ variant showed no real change, although it showed less product formation in the end point assay (Fig. 3-7). In contrast, the R99W and A[8] variants showed a 5-fold (0.04 ± 0.0 s^{-1}) and 10-fold (0.02 ± 0.0 s^{-1}) decrease in k_{cat}, respectively, compared to that of the native enzyme (0.17 ± 0.0 s^{-1}), which agrees well with the reduced activity seen previously in the end point assays (Fig. 3-7).

3.4.2.2 Varying CTP Concentration

When the CTP concentration was varied and the amount of $tRNA^{Asp}$-NC transcript was fixed (Table 3-2), the R99W and E43Δ variants showed a 20-fold (0.22 ± 0.4 μM) and 3-fold (1.61 ± 0.2 μM) decrease in $K_{M,Apparent}$, respectively, compared to that of the native enzyme (4.60 ± 0.6 μM), while the A[8] variant showed a 7-fold increase (32.03 ± 38.5 μM). In comparing all variants and the native enzyme to each other, there was on the order of a greater than 100-fold difference in $K_{M,Apparent}$ values. In contrast, differences in k_{cat} values among all enzymes were three-fold or less (ranging from 0.07 ± 0.0 s^{-1} for the R99W variant to 0.21 ± 0.1 s^{-1} for the A[8] variant).

Table 3-1: Kinetic Assay of Native and Variant TRNT1 Enzymes (Varying ATP and Fixed $tRNA^{Asp}$-NCC)

A

TRNT1 Variant	$K_{M,Apparent}$ (μM)	k_{cat} (s^{-1})	$k_{cat}/K_{M,Apparent}$ ($\mu M^{-1} s^{-1}$)
Native	124.31 ± 39.3	0.17 ± 0.0	0.001 ± 0.001
R99W	1.14 ± 0.6	0.04 ± 0.0	0.03 ± 0.04
E43Δ	373.02 ± 127.3	0.22 ± 0.0	0.0006 ± 0.0005
A[8]	182.90 ± 17.7	0.02 ± 0.0	0.0001 ± 0.0000

B

TRNT1 Variant	$K_{M,Apparent} : K_{M,Apparent,0}$	$k_{cat} : k_{cat,0}$	$k_{cat}/K_{M,Apparent} : k_{cat,0}/K_{M,Apparent,0}$
Native	1.00 ± 0.9	1.0 ± 0.3	*n / a*
R99W	0.01 ± 0.01	0.2 ± 0.1	*n / a*
E43Δ	3.00 ± 2.9	1.3 ± 0.4	*n / a*
A[8]	1.47 ± 0.9	0.1 ± 0.0	*n / a*

(A) *Calculated values.*
(B) *Calculated values from* ***(A)*** *normalized to those of native TRNT1.*
Note: Green, native values; red, "weaker" than native values; blue, "stronger" than native values.
Note: The SEM is included where applicable.

Table 3-2: Kinetic Assay of Native and Variant TRNT1 Enzymes (Varying CTP and Fixed $tRNA^{Asp}$-NC)

A

TRNT1 Variant	$K_{M,Apparent}$ (μM)	k_{cat} (s^{-1})	$k_{cat}/K_{M,Apparent}$ ($\mu M^{-1} s^{-1}$)
Native	4.60 ± 0.6	0.17 ± 0.0	0.04 ± 0.01
R99W	0.22 ± 0.4	0.07 ± 0.0	0.34 ± 1.0
E43Δ	1.61 ± 0.2	0.21 ± 0.0	0.13 ± 0.0
A[8]	32.03 ± 38.5	0.21 ± 0.1	0.01 ± 0.06

B

TRNT1 Variant	$K_{M,Apparent} : K_{M,Apparent,0}$	$k_{cat} : k_{cat,0}$	$k_{cat}/K_{M,Apparent} : k_{cat,0}/K_{M,Apparent,0}$
Native	1.00 ± 0.3	1.0 ± 0.1	1 ± 1
R99W	0.05 ± 0.1	0.4 ± 0.1	9 ± 36
E43Δ	0.35 ± 0.1	1.2 ± 0.1	3 ± 2
A[8]	6.96 ± 10.9	1.2 ± 1.0	0.3 ± 2.0

(A) *Calculated values.*
(B) *Calculated values from* ***(A)*** *normalized to those of native TRNT1.*
Note: Green, native values; red, "weaker" than native values; blue, "stronger" than native values.
Note: The SEM is included where applicable.

3.4.2.3 Varying $tRNA^{Asp}$-NCC Concentration

When assayed using the Michaelis-Menten model of enzyme kinetics and varying the amount of $tRNA^{Asp}$-NCC transcript (Table 3-3), the R99W variant showed an 11-fold increase in $K_{M,Apparent}$ as compared to the $K_{M,Apparent}$ of the native enzyme (0.14 ± 0.0 μM), while the E43Δ and A[8] variants showed only a two-fold decrease or increase, respectively. In terms of $k_{cat,}$ the R99W, E43Δ and A[8] variants showed a 2-fold (2.06 ± 0.2 s^{-1}), 6-fold (0.61 ± 0.1 s^{-1}) and 33-fold (0.10 ± 0.0 s^{-1}) decrease, respectively, as compared to that of the native enzyme (3.86 ± 0.2 s^{-1}), again agreeing well with the reduced activity seen previously in the end point assays (Fig. 3-7). Not surprisingly, $k_{cat}/K_{M,Apparent}$'s for $tRNA^{Asp}$-NCC were lower than those of the native enzyme (20-fold, 3-fold and 100-fold lower for the R99W, E43Δ and A[8] variants, respectively). Similar trends were seen when these data were fitted to the Hill model. Only the R99W variant showed a Hill coefficient greater than one (n = 1.11 ± 0.0), with apparent 2-fold (0.31 ± 0.0 μM), 7-fold (0.59 ± 0.0 s^{-1}) and 14-fold (1.86 ± 0.3 μM^{-1} s^{-1}) differences in $K_{M,Apparent}$, k_{cat} or $k_{cat}/K_{M,Apparent}$, respectively. This suggests that under these conditions, cooperativity is not an issue.

Table 3-3: Kinetic Assay of Native and Variant TRNT1 Enzymes (Varying $tRNA^{Asp}$-NCC and Fixed ATP)

A

TRNT1 Variant	$K_{M,Apparent}$ (μM)	k_{cat} (s^{-1})	$k_{cat}/K_{M,Apparent}$ (μM^{-1} s^{-1})
Native	0.14 ± 0.0	3.86 ± 0.2	26.64 ± 4.2
R99W	1.56 ± 0.2	2.06 ± 0.2	1.32 ± 0.3
	0.31 ± 0.0 [a]	0.59 ± 0.0 [a]	1.86 ± 0.3 [a]
E43Δ	0.07 ± 0.01	0.61 ± 0.1	9.06 ± 3.6
A[8]	0.27 ± 0.0	0.10 ± 0.0	0.38 ± 0.1

B

TRNT1 Variant	$K_{M,Apparent} : K_{M,Apparent,0}$	$k_{cat} : k_{cat,0}$	$k_{cat}/K_{M,Apparent} : k_{cat,0}/K_{M,Apparent,0}$
Native	1.0 ± 0.2	1.00 ± 0.1	1.00 ± 0.4
R99W	11 ± 2	0.53 ± 0.1	0.05 ± 0.02
	2.2 ± 0.4 [a]	0.15 ± 0.0 [a]	0.07 ± 0.03 [a]
E43Δ	0.5 ± 0.1	0.16 ± 0.0	0.34 ± 0.2
A[8]	1.9 ± 0.3	0.03 ± 0.0	0.01 ± 0.01

(A) *Calculated values.*
(B) *Calculated values from* ***(A)*** *normalized to those of native TRNT1.*
All data fitted to Michaelis-Menten model except for [a] *which is fitted to Hill model.*
Note: Green, native values; red, "weaker" than native values; blue, "stronger" than native values.
Note: The SEM is included where applicable.

3.4.2.4 Varying $tRNA^{Asp}$-NC Concentration

Given that the A[8] variant showed the greatest increase in K_M for CTP binding when the amount of $tRNA^{Asp}$-NC transcript was held constant, we tried the reverse experiment by holding the CTP amount constant and altering the $tRNA^{Asp}$-NC concentration (Table 3-4). As a result, the A[8] variant showed an 80-fold increase in $K_{M,Apparent}$ for $tRNA^{Asp}$-NC upon fitting to the Michaelis-Menten model when compared to the native enzyme (3.01 ± 0.6 *μM* versus 0.04 ± 0.0 *μM*). Interestingly, when the data were analyzed based on the Hill model, this difference in $K_{M,Apparent}$ was much less (at approximately 10-fold at 0.47 ± 0.1 *μM*), suggesting there may be some cooperativity (Hill coefficient, n = 1.42 ± 0.1) involved in $tRNA^{Asp}$-NC binding. In either case, no major change in k_{cat} was observed (less than three-fold), although less product formation was seen in the end point assay (Fig. 3-8). Based on these data, the specificity constants ($k_{cat}/K_{M,Apparent}$'s) for $tRNA^{Asp}$-NC were more than 10-fold lower than that of the native enzyme and almost identical within experimental error. Again, this suggests that overall cooperativity is not an issue.

Table 3-4: Kinetic Assay of Native and Variant TRNT1 Enzymes (Varying $tRNA^{Asp}$-NC and Fixed CTP)

A

TRNT1 Variant	$K_{M,Apparent}$ *(μM)*	k_{cat} *(s^{-1})*	$k_{cat}/K_{M,Apparent}$ *($\mu M^{-1}\ s^{-1}$)*
Native	0.04 ± 0.0	1.34 ± 0.1	30.40 ± 3.4
A[8]	3.01 ± 0.6	3.78 ± 0.5	1.25 ± 0.5
	0.47 ± 0.1 [a]	1.11 ± 0.1 [a]	2.34 ± 0.4 [a]

B

TRNT1 Variant	$K_{M,Apparent} : K_{M,Apparent,0}$	$k_{cat} : k_{cat,0}$	$k_{cat}/K_{M,Apparent} : k_{cat,0}/K_{M,Apparent,0}$
Native	1 ± 0	1.00 ± 0.1	1.00 ± 0.3
A[8]	80 ± 19	2.82 ± 0.5	0.04 ± 0.02
	10 ± 3 [a]	0.83 ± 0.1 [a]	0.08 ± 0.03 [a]

(A) *Calculated values.*
(B) *Calculated values from* ***(A)*** *normalized to those of native TRNT1.*
All data fitted to Michaelis-Menten model except for [a] which is fitted to Hill model.
Note: Green, native values; red, "weaker" than native values.
Note: The SEM is included where applicable.

3.5 *In Silico* Folding and Docking of TRNT1 Variants to *Bacillus subtilis* $tRNA^{Asp}$-NCCA

In order to place into context the biophysical and/or biochemical alterations of the TRNT1 enzyme variants relative to the native enzyme, *in silico* folding of these variants was performed using Robetta (Kim *et al.* 2004). The tertiary structure of the *B. subtilis* $tRNA^{Asp}$-NCCA transcript was determined via *in silico* folding of the secondary structure of the transcript by RNAComposer (Popenda *et al.* 2012), and this was followed by *in silico* docking to the crystal structure of the native enzyme or to the folded structure of each variant enzyme using HDOCK (Pearson and Lipman 1988; Remmert *et al.* 2012; Yan *et al.* 2017).

The models for the R99W variant (discussed further in Section 4.1) suggest a local change in the tertiary structure of the protein (Fig. 3-12), display the location of the residue corresponding to R99 relative to nearby regions of the native protein (Fig. 3-13), and suggest displacement of one or more disordered loop and/or flexible loop residues in the variant protein (Fig. 3-14).

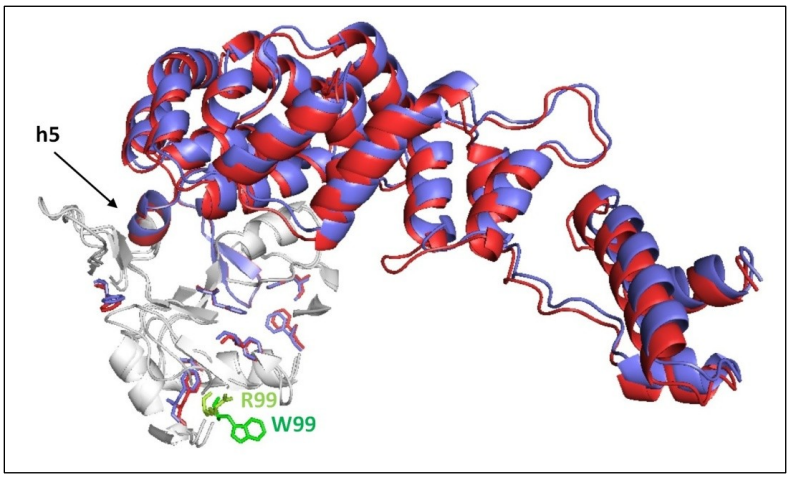

Figure 3-12: Local Change in Tertiary Structure of the R99W Variant. The native TRNT1 enzyme (blue ribbon) and R99W variant (red ribbon) are shown superimposed. The region N-terminal to α-helix 5 (h5) for both enzymes is coloured white. Phenylalanine residues in this region of the proteins (blue and red sticks) and the arginine or tryptophan residue at position 99 (light and dark green sticks, respectively) in an unstructured region of the enzyme are shown. These structures are visualized by PyMOL *(v1.7.4.5)* (Schrödinger 2018).

Figure 3-13: Location of the Residue Corresponding to R99, Motifs A and B, the Disordered Loop and the Flexible Loop in the Native TRNT1 Enzyme. (A) The regions to be discussed are shown on the primary sequence of TRNT1. Residue R99 is shown in large font. The first "DF" residues (red) represent the last two amino acids of motif A and the last "DA" residues (orange) represent the first two amino acids of motif B. Based on the crystal structure of Augustin *et al.* (2003), α-helix 4 (h4) is shown in bold, β-strands 2, 3 and 4 (s2, s3 and s4, respectively) are shown in italics and a turn is underlined. The disordered loop (Toh *et al.* 2009) is displayed in light gray and the flexible loop (Neuenfeldt *et al.* 2008; Hoffmeier *et al.* 2010) in black. **(B)** The native TRNT1 enzyme (blue ribbon) is shown with motif A (red), motif B (orange), the disordered loop (light gray) and the flexible loop (black) displayed. Unresolved regions of the crystal structure are indicated as dashed blue lines. Residue R99 (blue stick) is flanked by β-strand 2 (s2) or α-helix 4 (h4) and β-strand 3 (s3). This structure is visualized by PyMOL *(v1.7.4.5)* (Schrödinger 2018) and is a composite of two structures (PDB ID: 4X4W, 1OU5).

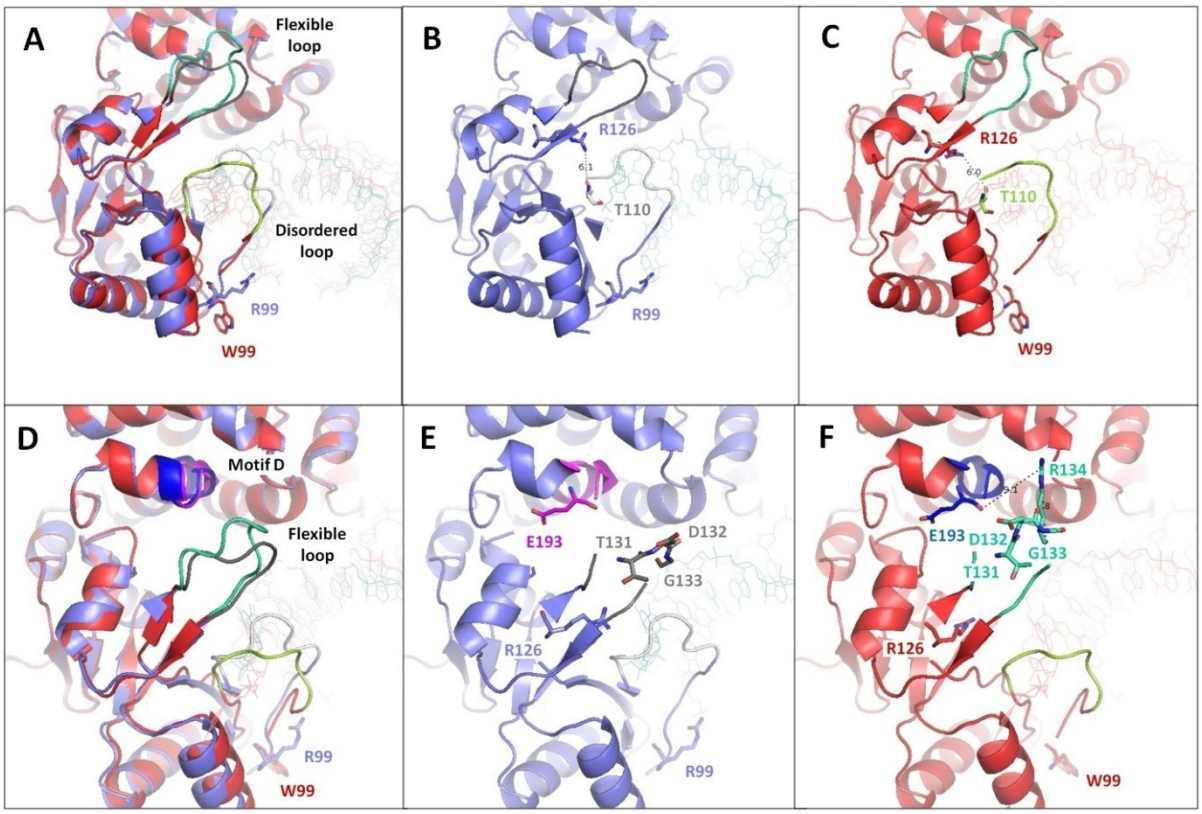

Figure 3-14: Displacement of One or More Disordered Loop and/or Flexible Loop Residues by the R99W Substitution. The native TRNT1 enzyme (blue ribbon) and R99W variant (red ribbon) are superimposed and their bound tRNAs (light blue and light red lines, respectively) are shown. Residues R99 and W99 are represented by blue and red sticks, respectively. Oxygen and nitrogen atoms are coloured dark red and dark blue, respectively. **(A)** In the native enzyme and the R99W variant, the disordered loop (white and green, respectively) and the flexible loop (gray and teal, respectively) are displayed. **(B, C)** In each of these, key residues in the disordered loop and flexible loop are indicated and hydrogen bond interactions are represented by dotted lines (displayed lengths in Ångströms). **(D)** In the native enzyme and the R99W variant, the flexible loop (gray and teal, respectively) and motif D (purple and dark blue, respectively) are displayed. **(E, F)** In each of these, key residues in the flexible loop and motif D are indicated and hydrogen bond interactions are represented by dotted lines (displayed lengths in Ångströms). (In the native enzyme, the lack of a hydrogen bond between R134 and E193 results from the absence of R134 in the crystal structure.) These structures are visualized by PyMOL *(v1.7.4.5)* (Schrödinger 2018) and the native enzyme is a composite of two structures (PDB ID: 4X4W, 1OU5).

The models for the E43Δ variant (discussed further in Section 4.2) suggest an alteration in structure of the protein promoted by a loss of a defined α-helix and displacement of an adjacent loop (Fig. 3-15), display the location of the residue corresponding to E43 relative to nearby regions of the native protein (Fig. 3-16), suggest a shift of the nucleotide binding pocket in the variant protein (Fig. 3-17), displacement of one or more disordered loop and/or flexible loop residues (Fig. 3-18), retention of

hydrogen bonds between residues R60 and A81 (Fig. 3-19) and displacement of one or more motif C residues (Fig. 3-20).

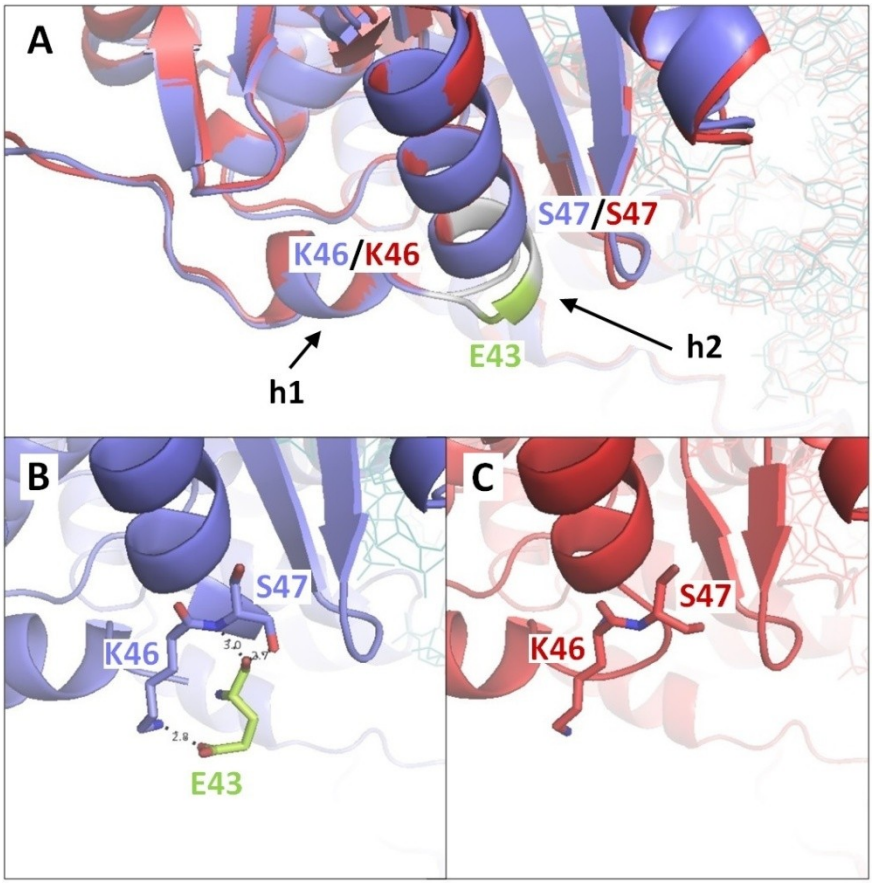

Figure 3-15: Loss of Defined Structural Elements of the E43Δ Variant. (A) The native TRNT1 enzyme (blue ribbon) and E43Δ variant (red ribbon) are shown superimposed. The region between α-helix 1 (h1) and α-helix 2 (h2) deviating in space between the structures is coloured white, and residue E43 of the native TRNT1 enzyme is coloured green. **(B)** In the native TRNT1 enzyme, residue E43 (green stick) at the N-terminus of α-helix 2 hydrogen bonds to K46 and S47 (blue sticks) within the helix, where hydrogen bonds are represented by dotted lines (displayed lengths in Ångströms). **(C)** In the E43Δ variant, a lack of stabilizing hydrogen bonds to K46 and S47 might lead to destabilization of α-helix 2 and a slight structural change in the loop connecting α-helix 1 to α-helix 2. In **(B)** and **(C)**, oxygen and nitrogen atoms are coloured dark red and dark blue, respectively. These structures are visualized by PyMOL *(v1.7.4.5)* (Schrödinger 2018).

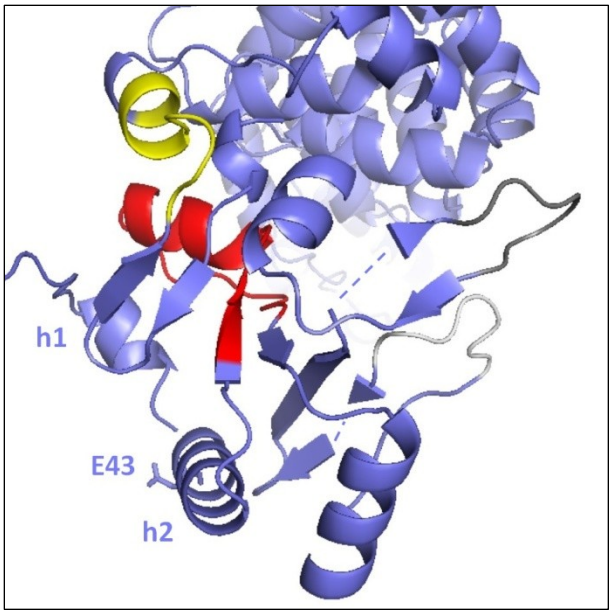

Figure 3-16: Location of the Residue Corresponding to E43, Motifs A and C, the Disordered Loop and the Flexible Loop in the Native TRNT1 Enzyme. The native TRNT1 enzyme (blue ribbon) is shown with motif A (red), motif C (yellow), the disordered loop (white) and the flexible loop (gray) displayed. Unresolved regions of the crystal structure are indicated as dashed blue lines. Residue E43 (blue stick) is situated at the N-terminus of α-helix 2 (h2) and is located C-terminal to α-helix 1 (h1). This structure is visualized by PyMOL *(v1.7.4.5)* (Schrödinger 2018) and is a composite of two structures (PDB ID: 4X4W, 1OU5).

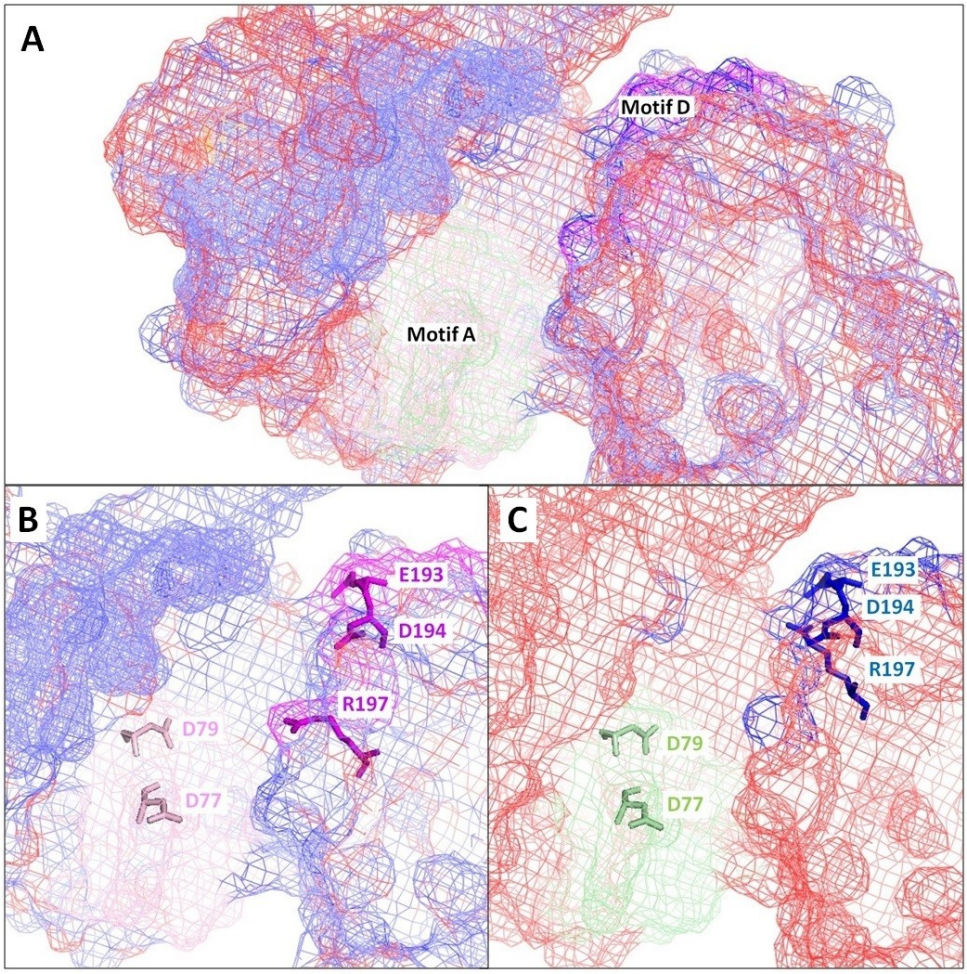

Figure 3-17: Shift of the Nucleotide Binding Pocket Relative to the Two-Metal Binding Carboxylates by the E43 Deletion. The native TRNT1 enzyme (blue surface mesh) and E43Δ variant (red surface mesh) are superimposed. **(A)** In the native enzyme and the E43Δ variant, motif A (pink and light green surface mesh, respectively) and motif D (purple and dark blue surface mesh, respectively) are displayed. **(B, C)** In each of these, the conserved residues in motif A and motif D are indicated. In the E43Δ variant, the nucleotide binding pocket defined by residues E193, D194 and R197 of motif D has an alternative structural organization and may pull the bound ATP away from the two-metal binding catalytic carboxylates D77 and D79 of motif A. These structures are visualized by PyMOL *(v1.7.4.5)* (Schrödinger 2018) and the native enzyme is a composite of two structures (PDB ID: 4X4W, 1OU5).

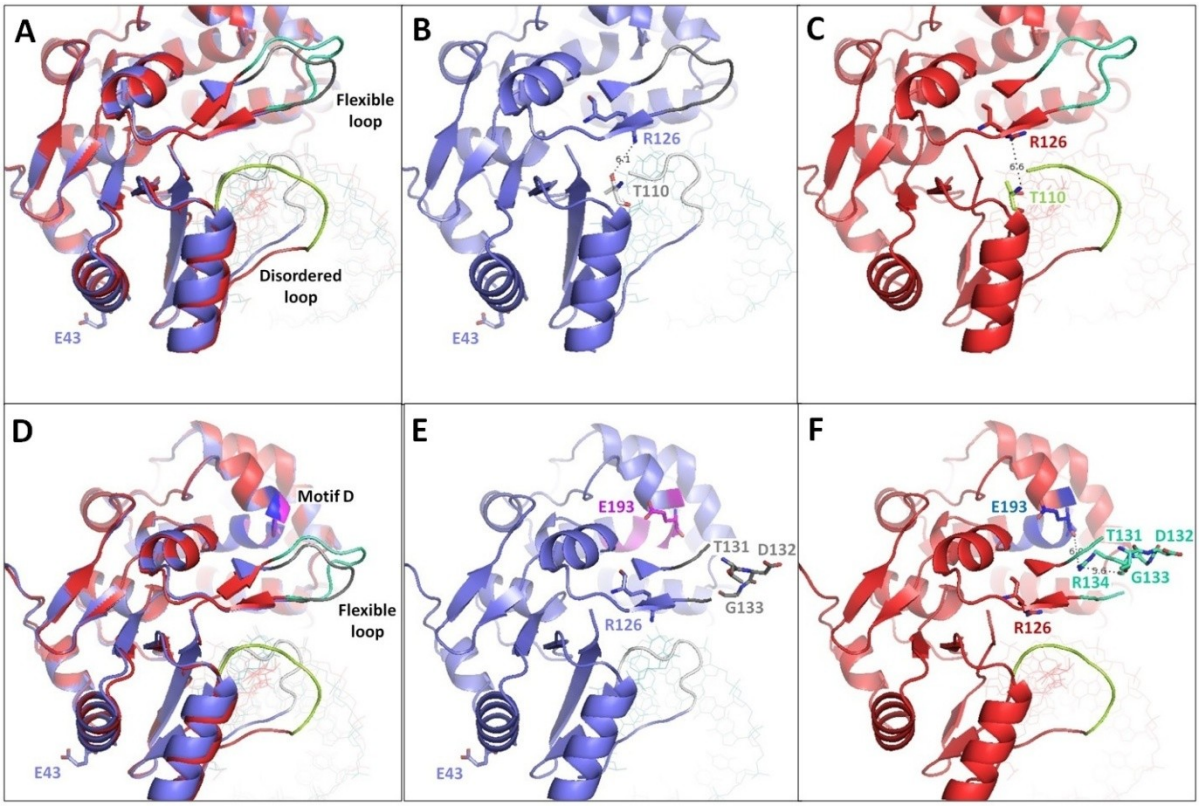

Figure 3-18: Displacement of One or More Disordered Loop and/or Flexible Loop Residues by the E43 Deletion. The native TRNT1 enzyme (blue ribbon) and E43Δ variant (red ribbon) are superimposed and their bound tRNAs (light blue and light red lines, respectively) are shown. Residue E43 is represented by a blue stick. Oxygen and nitrogen atoms are coloured dark red and dark blue, respectively. **(A)** In the native enzyme and the E43Δ variant, the disordered loop (white and green, respectively) and the flexible loop (gray and teal, respectively) are displayed. **(B, C)** In each of these, key residues in the disordered loop and flexible loop are indicated and hydrogen bond interactions are represented by dotted lines (displayed lengths in Ångströms). **(D)** In the native enzyme and the E43Δ variant, the flexible loop (gray and teal, respectively) and motif D (purple and dark blue, respectively) are displayed. **(E, F)** In each of these, key residues in the flexible loop and motif D are indicated and hydrogen bond interactions are represented by dotted lines (displayed lengths in Ångströms). (In the native enzyme, the lack of a hydrogen bond between R134 and E193 results from the absence of R134 in the crystal structure.) These structures are visualized by PyMOL *(v1.7.4.5)* (Schrödinger 2018) and the native enzyme is a composite of two structures (PDB ID: 4X4W, 1OU5).

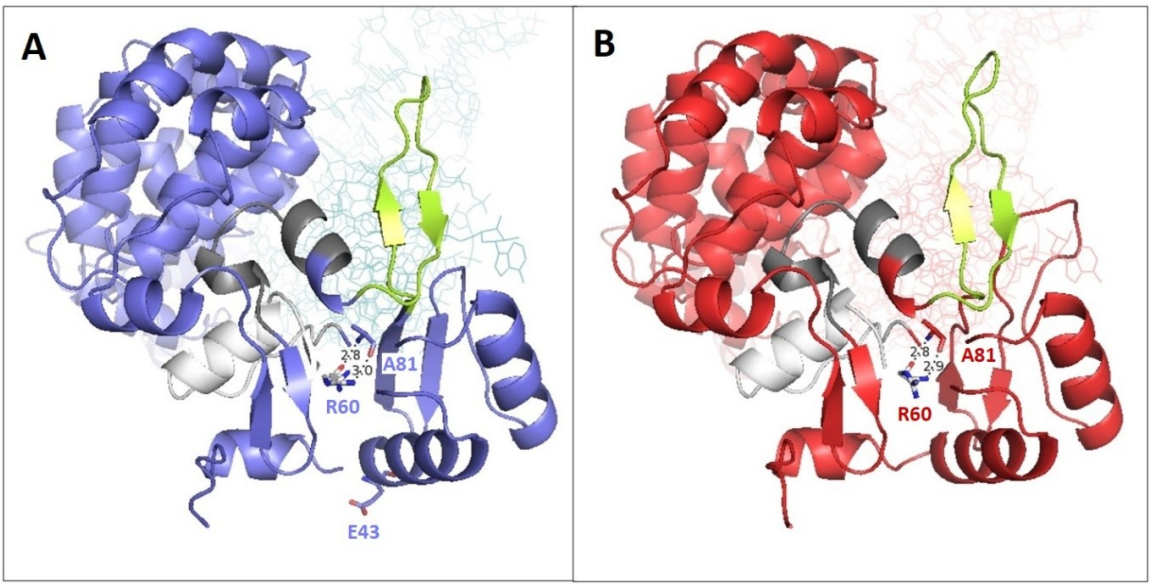

Figure 3-19: Retention of Hydrogen Bonds between Residues R60 and A81 of the E43Δ Variant. (A) The native TRNT1 enzyme (blue ribbon) and **(B)** E43Δ variant (red ribbon) are shown. Motif A (white), the flexible loop (green) and motif B (gray) are displayed with residues E43, R60 and A81 represented by sticks, where A81 normally makes direct contact with the flexible loop. The hydrogen bonds between the amide and carbonyl groups of the main chains of R60 and A81, which are located on adjacent β-strands, are retained upon the deletion of E43 and no alteration in the position of the flexible loop is apparent. Hydrogen bonds are represented by dotted lines (displayed lengths in Ångströms), and oxygen and nitrogen atoms are coloured dark red and dark blue, respectively. These structures are visualized by PyMOL *(v1.7.4.5)* (Schrödinger 2018).

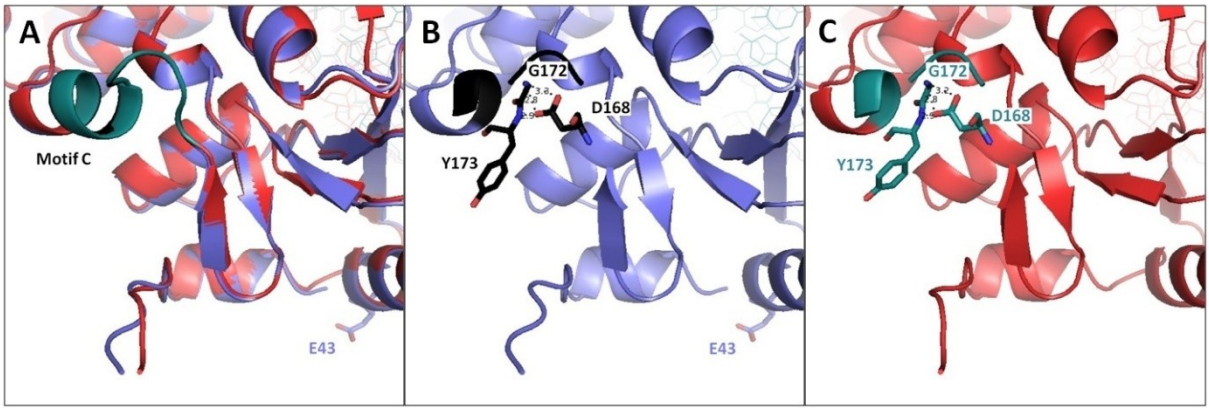

Figure 3-20: Displacement of One or More Motif C Residues by the E43 Deletion. The native TRNT1 enzyme (blue ribbon) and E43Δ variant (red ribbon) are superimposed and their bound tRNAs (light blue and light red lines, respectively) are shown. Residue E43 is represented by a blue stick. Oxygen and nitrogen atoms are coloured dark red and dark blue, respectively. **(A)** In the native enzyme and the E43Δ variant, motif C (black and deep teal, respectively) is displayed. **(B, C)** In each of these, key residues in motif C are indicated and hydrogen bond interactions are represented by dotted lines (displayed lengths in Ångströms). These structures are visualized by PyMOL *(v1.7.4.5)* (Schrödinger 2018) and the native enzyme is a composite of two structures (PDB ID: 4X4W, 1OU5).

The models for the A[8] variant (discussed further in Section 4.3) display the location of altered residues of the protein from the A[8] frame shift (Fig. 3-21) and reveal newly exposed surfaces of the two C-terminal α-helices (Fig. 3-22).

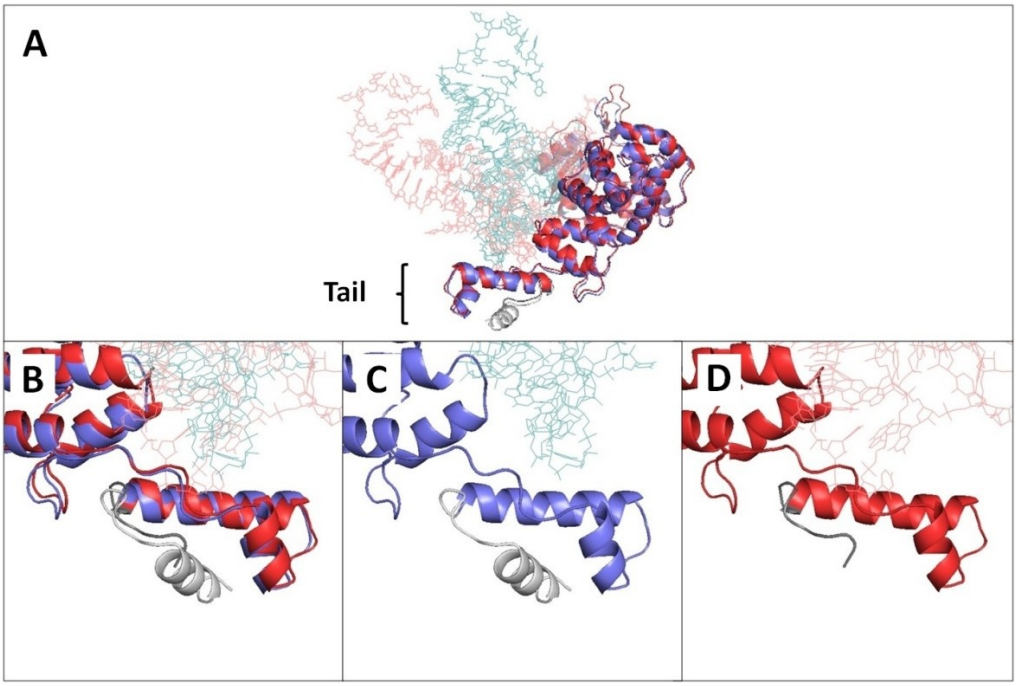

Figure 3-21: Location of Altered Residues from the A[8] Frame Shift in the TRNT1 Enzyme. The native TRNT1 enzyme (blue ribbon) and A[8] variant (red ribbon) are superimposed and their bound tRNAs (light blue and light red lines, respectively) are shown. In the tail domain, the 17 C-terminal residues (white) of the native enzyme and the eight C-terminal residues (gray) of the A[8] variant are displayed. **(A)** The bound tRNAs of the native enzyme and the A[8] variant reveal a large difference in rotational position. **(B)** In the A[8] variant, the C-terminal α-helix is replaced by a small disordered region. These views of the native enzyme and the A[8] variant are shown separately in **(C)** and **(D)**, respectively. In **(B-D)**, the molecular complex is rotated 180° relative to **(A)** with respect to the vertical. These structures are visualized by PyMOL *(v1.7.4.5)* (Schrödinger 2018).

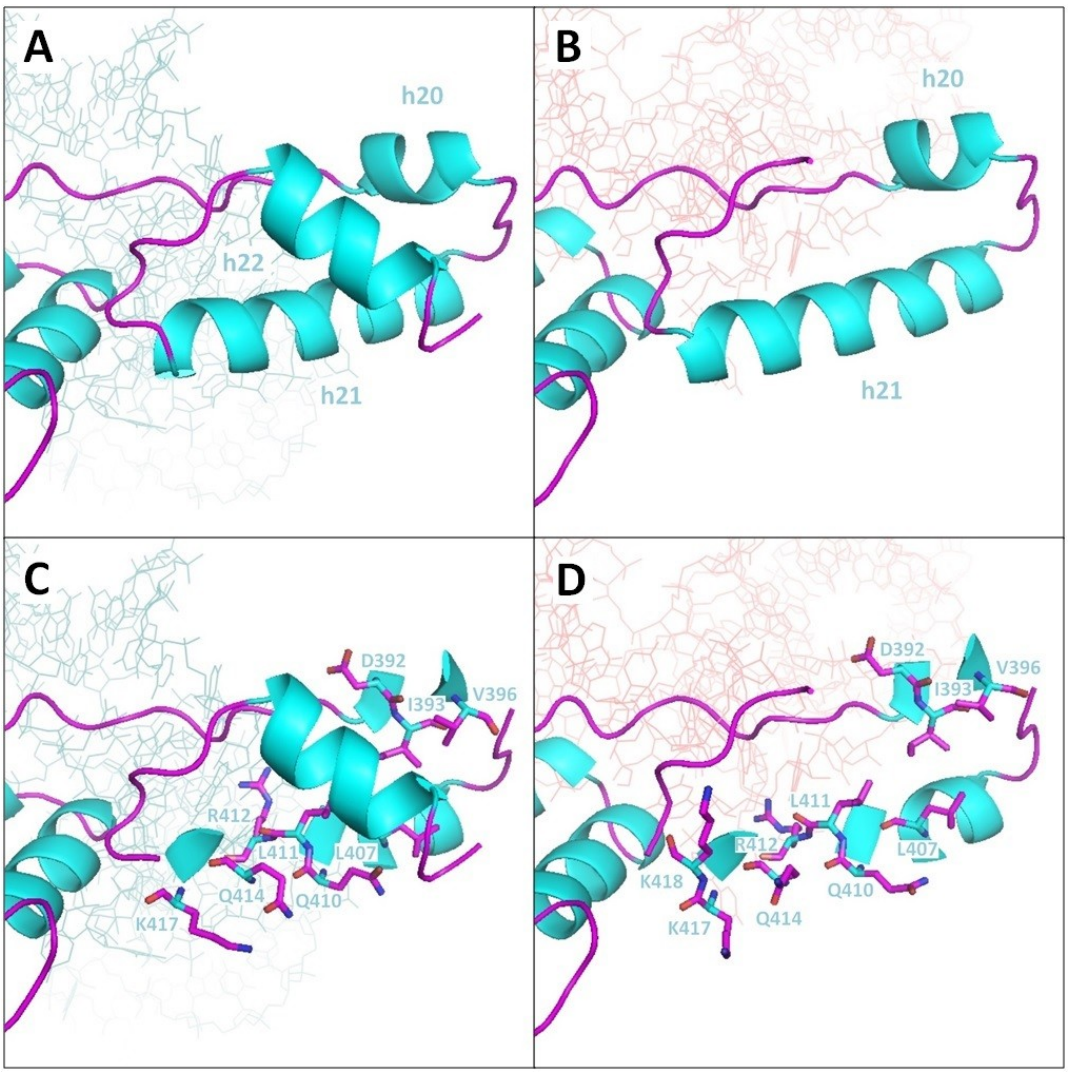

Figure 3-22: Newly Exposed Surfaces of the Two C-Terminal α-Helices of the A[8] Variant. (A, C) In **(A)**, the three C-terminal α-helices (h20, h21 and h22 as cyan ribbons) of the tail domain in the native TRNT1 enzyme and bound tRNA (light blue lines) are shown. In **(C)**, residues of h20 and h21 which interact with h22 are represented by sticks. **(B, D)** In **(B)**, the two C-terminal α-helices (h20 and h21 as cyan ribbons) of the tail domain in the A[8] variant and bound tRNA (light red lines) are shown. In **(D)**, the same residues of the α-helices from **(C)**, with the exception of residue K418 resulting from the A[8] frame shift, are surface-exposed and are represented by sticks. Carbon, α-carbon, oxygen and nitrogen atoms are coloured purple, cyan, dark red and dark blue, respectively. These structures are visualized by PyMOL *(v1.7.4.5)* (Schrödinger 2018).

4.0 DISCUSSION

In eukaryotes, the role of tRNA nucleotidyltransferase (tRNA-NT) is paramount in the fundamental functioning of the cell as tRNAs must undergo an essential maturation step in which a cytidine-cytidine-adenosine (CCA) trinucleotide sequence is attached to the 3'-end of each tRNA. This specific series of nucleotide additions is accomplished by tRNA-NT without the need for a nucleic-acid template (Deutscher 1983). Partial loss-of-function (LOF) mutations in *TRNT1*, encoding human tRNA-NT, have been demonstrated to cause a wide spectrum of human diseases, as evidenced by the rapidly growing body of medical literature in the past five years (Aksentijevich *et al.* 2014; Chakraborty *et al.* 2014; Sasarman *et al.* 2015; DeLuca *et al.* 2016; Hull *et al.* 2016; Wedatilake *et al.* 2016; Frans *et al.* 2017; Lougaris *et al.* 2018; Giannelou *et al.* 2018; Bader-Meunier *et al.* 2018; Gorodetsky *et al.* 2018; Kumaki *et al.* 2019; Abdulhadi *et al.* 2019).

SIFD, the most severe of these disease phenotypes, has been recently linked to reduced thermal stabilities and catalytic activities of TRNT1 enzyme variants (Leibovitch *et al.* 2018, 2019) that arise from six single amino acid substitutions (T154I, M158V, L166S, R190I, I223T and I326T) first identified by Chakraborty *et al.* (2014). Of these substitutions, the first five map within or close to the active site in the head and neck domains of the protein, while the last (I326T) maps further from the active site in the body domain. Despite their different locations in the protein, all of these substitutions lead to decreases in thermal stability and/or catalytic activity.

In light of these observations, this work explores three additional *TRNT1* mutations yielding the E43Δ (DeLuca *et al.* 2016), R99W (Aksentijevich *et al.* 2014; Hull *et al.* 2016; Frans *et al.* 2017; Kumaki *et al.* 2019) and A[8] (Chakraborty *et al.* 2014; DeLuca *et al.* 2016; Giannelou *et al.* 2018) variants. These amino acid changes map near the amino-terminus (E43Δ), between conserved motifs A and B in the head domain but far from the previously characterized mutations (R99W), and to the tail domain far from the active site of the protein (A[8]). Moreover, these changes result from a three-nucleotide deletion (E43Δ), a missense mutation (a single cytosine-to-thymine transition generating R99W) and a frame shift resulting from a single nucleotide insertion (A[8], eight adenosines instead of seven). By exploring these three variants resulting from different types of mutations found near the amino-terminus (N-terminus), the active site or the carboxy-terminus (C-terminus) of the resulting protein, we hoped to see effects on enzyme structure and/or function to determine potential contributions to

TRNT1-linked pathogenesis and to see if there are unifying features linked to pathogenesis, regardless of the type or location of mutation introduced.

4.1 R99W Variant

The R99W variant will be discussed first as it is found near the active site as are the T154I, M158V, L166S, R190I and I223T variants which have been characterized previously (Leibovitch *et al.* 2018). The R99W variant results from a transition at nucleotide position 295 in the *TRNT1* open reading frame where a cytosine is converted to a thymine changing a CGG codon to UGG (Aksentijevich *et al.* 2014; Hull *et al.* 2016; Frans *et al.* 2017; Kumaki *et al.* 2019). Located between conserved motifs A and B (Figs. 1-3, 3-13A), R99 is situated in an unstructured region between strands 2 and 3 of the single antiparallel β-sheet of the enzyme and based on the available crystal structures of TRNT1 (Augustin *et al.* 2003; Kuhn *et al.* 2015) is found on the surface of the protein (Fig. 3-13B). Substitution of this hydrophilic amino acid in the primary-sequence context of alanine-glycine-isoleucine-arginine-methionine-isoleucine (Figs. 1-3, 3-13A) with the more hydrophobic tryptophan residue (Engelman *et al.* 1986) may be expected to lead to a reorganization of this region of the protein and the movement of these amino acids into a more hydrophobic environment. This reorganization may be expected to alter nucleoside triphosphate (NTP) binding or discrimination as motif A contains the two-metal binding catalytic carboxylates (D*x*D) that interact with the triphosphate moiety of CTP or ATP (Steitz *et al.* 1994; Yue *et al.* 1996; Steitz 1998), while motif B contains the residues required to ensure that deoxyribonucleoside triphosphates (dNTPs) do not bind (Li *et al.* 2002; Cho *et al.* 2007). Moreover, it has been proposed that this region of the protein contains a flexible loop that acts to ensure complete CCA addition by changing conformation during CMP and AMP incorporation (McGann and Deutscher 1980; Zhu *et al.* 1986; Li *et al.* 2002; Augustin *et al.* 2003; Tomita *et al.* 2004; Neuenfeldt *et al.* 2008; Just *et al.* 2008; Toh *et al.* 2009; Hoffmeier *et al.* 2010).

4.1.1 Local Change in Tertiary Structure

Rearrangement of this region of the protein may have changed the environments of other aromatic amino acids in the vicinity of position 99 (*e.g.*, F93, or F80 and F120 in the single β-sheet) such that their fluorescence spectra were altered, changing the fluorescence intensity or the wavelength of the maximum fluorescence signal. Also, given that in this study we used the mature TRNT1 enzyme (lacking its mitochondrial targeting signal (MTS)) such that it contains only four tryptophan residues (W144 in motif B, W239 in motif E, and W381 and W415 in the C-terminal tail domain), the addition of a fifth

tryptophan may have been expected to change the fluorescence signal more dramatically after excitation at 295 nm, since at this wavelength tryptophan fluorescence dominates over that of phenylalanine or tyrosine. Surprisingly, when assayed for excitation at 295 nm, the fluorescence maximum for tryptophan, there was no real red-shift of the fluorescence signal (~1.5 nm), suggesting no major change in overall higher order structure and surprisingly no effect of adding an additional tryptophan residue to the protein. More interestingly, a larger change in wavelength of fluorescence maximum of approximately 3 nm (Fig. 3-6, with or without RNase) was seen after excitation at 280 nm (which should excite phenylalanine, tryptophan and tyrosine). Given that there was no major change in fluorescence seen with the excitation at 295 nm which suggested no dramatic alteration of the overall structure of the protein, the change in fluorescence maximum after excitation at 280 nm may be linked to a more localized rearrangement of tyrosine and phenylalanine residues. If one concentrates on the region near R99 and N-terminal to α-helix 5 (helix numbering according to Augustin *et al.* (2003)), one notes that this region contains seven phenylalanine residues (accounting for one third of all phenylalanines in TRNT1), one tryptophan and no tyrosines. Importantly, this region of the protein includes the disordered region containing R99 and most of the single β-sheet found in TRNT1 (Fig. 3-12). The red-shift in wavelength of the emission maximum indicates that some aromatic residues have been moved into a more hydrophilic environment perhaps resulting in a reorganization of this important region.

4.1.2 Dimerization as a Probe for Determining Biophysical Properties

Recently, Leibovitch *et al.* (2019) showed that even a small change in tertiary structure could manifest itself in the inability of TRNT1 to form a covalent dimer *in vitro*, so we checked for dimerization of the R99W variant. Similar to the native protein, the R99W variant was capable of forming a covalent dimer under non-reducing conditions (Fig. 3-2), and native PAGE suggests no apparent change in size or conformation of the R99W monomer or dimer as compared to those of the native enzyme (Fig. 3-3). This is not surprising as substitutions of other amino acids (T154I, M158V, L166S, R190I and I223T) clustering near the active site also did not inhibit covalent dimer formation (Leibovitch *et al.* 2019). Given that dimerization requires the presence of residue C373 found at the C-terminal end of the body domain far from R99, this again supports the idea that the change of R99 to tryptophan does not result in major structural changes in the protein, again suggesting that a local change in structure (Fig. 3-12) is responsible for the phenotype observed *in vivo*.

The loss of covalent dimerization *in vitro* was also linked to a decrease in tRNA binding in the I326T variant (Leibovitch *et al.* 2019), however, as the R99W variant and the native enzyme show similar A_{280}:A_{260} ratios before or after RNase treatment (Fig. 3-4), this suggests a similar level of binding of the tRNA substrate to the enzyme during purification and supports the hypothesis that the change in the enzyme is confined to the N-terminal region of the head domain far from where tRNA binds.

4.1.3 No Change in Secondary Structure but Minor Decrease in Stability

The data to this point support a change in higher order structure confined to a small region of the protein rather than reflecting a major change in higher order structure. To see if this change is revealed in a loss or gain of specific secondary structures, we used circular dichroism (CD) spectroscopy. Based on a comparison of the CD spectra of the native and variant enzyme, no change in the secondary structure of the R99W variant was detected (Fig. S3 A-C). In addition, we used CD spectra to determine the thermal stability of the native and variant enzymes. We noted that there was a greater difference in melting temperature within the native enzyme with or without RNA (~2.5°C) than there was between the R99W variant and the native enzyme (<1°C) under either of these conditions (Fig. 3-5). This is a novel observation with respect to amino acid substitutions near the active site, as the other characterized variants all showed a drop of 5-7°C in melting temperature as compared to the native enzyme (Leibovitch *et al.* 2018). However, this observation fits well with the finding that production of the R99W variant protein is normal in skin-derived fibroblasts in one male patient with progressive B-cell immunodeficiency, who is homozygous for R99W (Table 1-1), suggesting that thermal instability does not lead to pathogenesis in this case (Frans *et al.* 2017). The increase in T_m seen when either sample was compared to its non-RNase treated counterpart (Fig. 3-5) likely reflects a contribution from bound tRNA in thermal denaturation as more energy is needed in the presence of tRNA to denature both the tRNA and the protein.

As no dramatic alteration was observed in any of the biophysical parameters we tested (secondary, tertiary or quaternary structure, thermal stability, or the amount of tRNA associated with the R99W variant as compared to the native TRNT1 enzyme), this suggested that neither a major loss of structure nor stability was responsible for the phenotype observed. Therefore, we proceeded to gauge the level of catalytic activity exhibited by the R99W variant.

4.1.4 Altered CMP and AMP Incorporation

Previous *in vitro* characterizations of the T154I, M158V, L166S, R190I, I223T and I326T variants have all revealed, to various degrees, decreased AMP incorporation onto the *B. subtilis* $tRNA^{Asp}$-NCC and -NC transcripts (Leibovitch *et al.* 2018, 2019). Based on the location of the R99 residue between conserved motifs A and B in the catalytic core of the enzyme (Fig. 3-13), the R99W substitution may also affect enzyme activity.

Indeed, reduced A-addition onto the $tRNA^{Asp}$-NCC was seen with the R99W variant as compared to the native enzyme in end point assays (Fig. 3-7). At the highest enzyme amount tested (~10 ng), the R99 variant showed three-fold less product formation as compared to the native enzyme. This suggests that the ability to either bind or incorporate AMP is affected. Given the role of motif A in binding the triphosphate portion of NTPs, and the role of the region between motifs A and B in allowing the switch from C-addition to A-addition (Toh *et al.* 2009; Hoffmeier *et al.* 2010), these observations were not surprising. We wished to know if the reduced ability to incorporate AMP also was seen with CMP incorporation and so assayed for C-addition to the $tRNA^{Asp}$-NC (Fig. 3-8) and $tRNA^{Asp}$-N transcripts (Fig. 3-9). When looking at the addition of two C residues, at any enzyme amount tested, CMP incorporation was comparable between the native enzyme and the R99W variant (Fig. 3-9). Moreover, when we used the $tRNA^{Asp}$-NC transcript and added a single C residue, we saw perhaps even more efficient incorporation of the second C by the R99W variant than by the native enzyme (Fig. 3-8). This suggests that the defect in this enzyme is reflected in AMP incorporation and not in CMP incorporation. This is supported when both ATP and CTP are incubated with the $tRNA^{Asp}$-N transcript, as similar levels of CMP seem to be incorporated while almost no AMP is incorporated by the R99W variant (Fig. 3-10). In order to characterize this decrease in A-adding activity, kinetic assays were performed.

4.1.5 Kinetic Analysis and Possible Mechanisms of TRNT1 Alteration

As the end point assays suggested that A-addition was the limiting factor, we first characterized AMP incorporation onto the $tRNA^{Asp}$-NCC transcript. The k_{cat} that we calculated for AMP incorporation by the R99W variant suggested that less efficient chemistry of the reaction may play some role in generating the phenotype observed, as the R99W variant showed a turnover number (k_{cat}) that was approximately 20% that of the native enzyme (Table 3-1). A five-fold reduction in turnover number correlates well with the reduced AMP incorporation that we saw in the end point assays (Fig. 3-7). Previously, an *E. coli* tRNA-NT variant has been identified which showed an approximately five-fold decrease in the ability to

incorporate AMP but not CMP (McGann and Deutscher 1980), and the amino acid alteration was determined to be a glycine-to-aspartic acid substitution in the G*x*G*xx*G nucleotide-binding domain of the *E. coli* tRNA-NT which also is in the region between motifs A and B (Zhu *et al.* 1986). Also, with the *E. coli* enzyme, Kim *et al.* (2009) have carried out single turnover kinetics and have shown that the kinetics of AMP incorporation depends on pre-chemistry conformational changes of the active site. By carrying out the experiment in increasing glycerol concentrations, they showed that they could decrease the incorporation of AMP by approximately five-fold, similar to what we saw here with the R99W variant. Moreover, under the same experimental conditions they have seen no effect on CMP incorporation. When this same region of the *E. coli* tRNA-NT was replaced with the corresponding region of the *E. coli* poly(A) polymerase, AMP incorporation but not CMP incorporation was lost (Just *et al.* 2008). Neuenfeldt *et al.* (2008) further have shown that a small deletion in this region of the *E. coli* enzyme near what would be R99 in the human enzyme between motifs A and B resulted in the loss of the ability to incorporate AMP but not CMP, again suggesting the loss of an ability to alter the conformation of this region of the protein to switch from CMP to AMP incorporation during the course of the reaction. Furthermore, they also have indicated (data not shown, Neuenfeldt *et al.* (2008)) that additional mutations in the corresponding region of the human enzyme also interfere dramatically with A-addition. Taken together, all of these observations suggest that the ability to alter the conformation of the enzyme to incorporate AMP but not CMP is impaired in the R99W variant.

Interestingly, while the turnover number for AMP incorporation was reduced approximately five-fold in the R99W variant as compared to the native enzyme, an even more dramatic change (approximately 100-fold smaller) in the apparent Michaelis constant ($K_{M,Apparent}$) for ATP binding was observed in the R99W variant as compared to the native enzyme (Table 3-1). This much smaller $K_{M,Apparent}$ for the variant as compared to the native enzyme suggests that ATP binds more tightly to the R99W variant than it does to the native enzyme. It is difficult to reconcile this increase in ATP binding with the decrease in specific activity that we observed, but it may reflect the decreased ability of the variant enzyme to perform the conformational changes required during the course of the reaction. If we consider that under the conditions for this reaction (*Eq. 1*), k_2 is not rate-limiting, then $K_{M,Apparent}$ is defined by *Eq. 2*,

$$E + S \underset{}{\overset{k_1}{\rightleftharpoons}} ES \xrightarrow{k_2} E + P \qquad \textit{Eq. 1}$$

$$E + S \underset{k_{-1}}{\overset{k_1}{\rightleftharpoons}} ES \qquad \textit{Eq. 2}$$

where *E*, *S*, *ES* and *P* represent enzyme, substrate, enzyme-substrate complex and product, respectively. Thus, $K_{M,Apparent} \approx k_{-1}/k_1$ and the ~100-fold decrease in $K_{M,Apparent}$ for the variant as compared to the native enzyme may reflect either a much smaller rate of substrate release or a much greater rate of substrate binding. The significance of this decrease in $K_{M,Apparent}$ and how the R99W substitution leads to it remains unclear, but perhaps the conformational change that reduces the turnover number does so by more tightly binding the ATP substrate.

As the experiments described above all suggest that amino acid substitutions in this region of the protein reduce activity with respect to AMP incorporation but not CMP incorporation, we also wanted to test for changes in any kinetic parameters associated with CMP incorporation. As we previously saw an apparent increase in catalytic activity for CMP incorporation in our end point assay (Fig. 3-8), we were not surprised to see a nine-fold increase in the specificity constant ($k_{cat}/K_{M,Apparent}$) for CMP incorporation onto the $tRNA^{Asp}$-NC transcript owing largely to a 20-fold increase in affinity (*e.g.*, 20-fold decrease in $K_{M,Apparent}$) for CTP (Table 3-2). These parameters for CMP incorporation, when taken with those for AMP incorporation (Table 3-1), suggest that while there is a small decrease in k_{cat} in either case, there is a much more important change in $K_{M,Apparent}$ especially for AMP incorporation. As discussed, this change in $K_{M,Apparent}$ reflects either a much greater recognition and binding of substrate or a much reduced rate of substrate release. The fact that both ATP and CTP binding seem to be increased in the R99W variant suggests that this amino acid substitution in part alters the organization around the NTP-binding D*x*D sequence in motif A (Li *et al.* 2002). In fact, our data suggest that these decreases in $K_{M,Apparent}$ (*e.g.*, increases in affinity) are limited to NTPs, as when $K_{M,Apparent}$ was calculated for $tRNA^{Asp}$-NCC binding, an 11- or 2-fold increase in $K_{M,Apparent}$ (*e.g.*, decrease in affinity) was instead observed in comparison to the native enzyme (Table 3-3). The differences in the binding of ATP and CTP may reflect changes in motif D which is responsible for distinguishing between these two bases (Li *et al.* 2002), but as described above, changes in conformation during the course of the reaction also may be involved.

An intriguing possibility may involve the role of a disordered region in the structure between motifs A and B (Fig. 3-13) in contributing to the bias toward CMP incorporation. In the *T. maritima* tRNA-NT, a β-turn links strands 4 and 5 in the single β-sheet in this protein, and residues within this β-turn have been proposed to play a role in the recognition of the phosphate backbone of the 3'-end of the bound tRNA during CMP incorporation and the subsequent positioning of the tRNA 3'-end for AMP incorporation

(Toh *et al.* 2009). When this region of the *T. maritima* protein is compared to that of the human enzyme (Fig. 4-1), we see that this β-turn aligns well with the disordered region in the human enzyme.

```
TRNT1           NHELRIAGGAVRDLLNGVKPQDIDFATTATPTQMKEMFQSAGIRMINNRGEKHGT-ITAR
                N  + + GG VRDLL G+K  DID        +    F     R +  +  KH   +TA
T. maritima     NMPVYVVGGFVRDLLLGIKNLDIDIVVEGNALE----FAEYAKRFLPGKLVKHDKFMTAS
```

Figure 4-1: Sequence Alignment of a Region of the Human and *Thermotoga maritima* tRNA-NTs. Residue R99 in the human enzyme is shown in bold. The disordered region in the human enzyme is underlined once and the β-turn in the *T. maritima* enzyme is underlined twice. Residue T87 in the β-turn is displayed in bold and green.

Upon substitution of a threonine residue at position 87 within this β-turn (Fig. 4-1) by alanine, Toh *et al.* (2009) demonstrated slightly augmented C-addition and reduced A-addition into *T. maritima* $tRNA^{Phe}$-derived mini-helices initially ending with -N or -NC and -NCC, respectively. As this threonine residue has been shown to form a hydrogen bond with R104 of the flexible loop, which in turn rearranges the nucleotide binding pocket formed by motif D to facilitate ATP binding and fixes the tRNA 3'-end during AMP incorporation, the replacement of the threonine in this loop might have abolished this hydrogen bond and weakened incorporation of AMP in the *T. maritima* tRNA-NT (Toh *et al.* 2009). Given the alignment of this β-turn with the disordered region of TRNT1 (Fig. 4-1), a similar scenario may occur with TRNT1. The R99W substitution in TRNT1 might lead to a rearrangement of the disordered loop that leads to displacement of one or more functionally critical residues (Fig. 3-14 A-C) such that the disordered loop can no longer reposition the 3'-end of the tRNA for AMP incorporation, resulting in augmented CMP incorporation and reduced AMP incorporation. This suggests that the important change seen in the R99W variant is in the arrangement of the amino acids required to align the substrates appropriately for catalysis rather than simply in the binding of the substrates.

The altered incorporation of CMP and AMP, respectively, may also reflect changes in the flexible loop of TRNT1 that result when R99 is changed to tryptophan. Given the position of the R99 residue and the flexible loop between motifs A and B (Fig. 3-13), it is conceivable that the R99W substitution might also disrupt the function of the flexible loop. The flexible loop, located near the β-sheet, is highly disordered and non-resolved in most crystal structures of Class II tRNA-NTs (Fig. 3-13). It consists of 10 to 20 amino acids and lacks sequence conservation (Li *et al.* 2002; Augustin *et al.* 2003; Tomita *et al.* 2004; Neuenfeldt *et al.* 2008; Toh *et al.* 2009), but is demonstrated to directly interact with conserved residues

of motif D. It is known to effectuate a lever-like motion that triggers movement of these conserved residues, thus rearranging the nucleotide binding pocket of motif D for a CTP-to-ATP specificity switch. The flexible loop initially detects and fixes the tRNA 3'-end after two rounds of C-addition, and subsequently promotes terminal A-addition by mediating the movement of adjacent domains of the enzyme (Neuenfeldt *et al.* 2008; Toh *et al.* 2009; Hoffmeier *et al.* 2010) (Fig. 1-4). Supporting what has been described above for the importance of hydrogen bonding between T87 and R104 in the *T. maritima* tRNA-NT, conversion of R104 of the flexible loop to alanine also showed reduced AMP incorporation at the 3' terminal position of a *T. maritima* $tRNA^{Phe}$-derived mini-helix although the rate of CMP incorporation was unchanged at the penultimate position (Toh *et al.* 2009). In addition, these authors have shown that upon replacing Y108 of the flexible loop with alanine, AMP incorporation was reduced to below 30% of that of the native *T. maritima* tRNA-NT. Both of these scenarios demonstrate that single amino acid substitution can lead to the loss of the ability of the flexible loop to direct the nucleotide binding pocket of motif D to switch from CTP to ATP specificity. Since R104 of the *T. maritima* tRNA-NT is also part of the highly conserved B/A motif of CCA-adding enzymes (Neuenfeldt *et al.* 2008) and Y108 is mildly conserved among these (Hoffmeier *et al.* 2010), a similar scenario might occur with TRNT1. With respect to the flexible loop in the human enzyme, Hoffmeier *et al.* (2010) have shown that alanine substitutions at D132, G133 or R134 (numbering as in Augustin *et al.* (2003)) in this region of the human enzyme almost completely abolish AMP incorporation at the 3' terminal position, while CMP incorporation at the two preceding positions remains intact. All of these results agree well with what we observed for the R99W variant in end point assays where AMP incorporation was reduced while CMP incorporation was not (Figs. 3-7 to 3-9). Taken together, these data suggest that the R99W substitution in TRNT1 might propagate a conformational change via tertiary structural alterations that displaces residues R126 and/or T131 (homologues of R104 and Y108 in the *T. maritima* tRNA-NT, respectively) in the flexible loop (Fig. 3-14 D-F), such that the flexible loop becomes unable to induce the switch of the nucleotide binding pocket to ATP specificity. Mechanistically, R134 in the human enzyme is responsible for inducing the nucleotide specificity switch of motif D by forming a salt bridge to the conserved E193 residue in the nucleotide binding pocket to bring the head and neck domains together (Hoffmeier *et al.* 2010). Considering what we have seen for C- and A-addition by the R99W variant in our end point assays, it is plausible that the R99W substitution might effect a conformation change that displaces D132, G133 and/or R134 (Fig. 3-14 D-F) with the end result being the inability of the flexible loop to induce toggling of the nucleotide binding pocket toward ATP specificity.

However, the problem with this interpretation is that we see an approximately 100-fold decrease in $K_{M,Apparent}$ for ATP in the R99W variant as compared to the native enzyme. This suggests that reduced ATP binding is not the issue, but rather catalysis (an approximately five-fold decrease in k_{cat} for AMP incorporation was observed in the R99W variant). In the experiments of Hoffmeier *et al.* (2010) with the human enzyme, they also showed a decrease in K_M for ATP binding (albeit much smaller at 30-60% for the T130A and R134A variants, respectively) with a much more dramatic decrease in k_{cat} (by 77-fold) for the R134A variant. Based on their observations, Hoffmeier *et al.* (2010) proposed that in addition to being involved in the switch from CTP binding to ATP binding, the loop element also contributed to the catalysis of A-addition. This is supported by our observation of an approximately five-fold reduction in k_{cat} and crystallographic studies with bound substrates (Toh *et al.* 2009) indicating that in the *T. maritima* enzyme the loop was involved in positioning the 3'-OH group of the final cytidine residue (C75) of the tRNA for nucleophilic attack on the triphosphate moiety of the ATP that also is bound to the enzyme.

In summary, it appears that the R99W variant can still bind ATP and CTP efficiently, however, the mechanism that prevents efficient incorporation of AMP likely involves the lack of correct local conformational changes allowing the nucleotide specificity switch from CTP to ATP, as well as a lack of correct local structural changes that direct its catalysis. Both of these instances suggest that multiple structural elements or motifs, in the N-terminal region of TRNT1, are implicated in the impairment of AMP incorporation.

4.1.6 The R99W Variant Is Associated With Mild Phenotypes

Taking into account the small biophysical and biochemical changes in the R99W variant that we report here, it is not surprising that the resultant phenotypes linked to this substitution are mild compared to those linked to other reported mutations (Table 1-1) (Chakraborty *et al.* 2014). Indeed, Leibovitch *et al.* (2018) have shown reduced thermal stability for the T154I variant which is likely to account for its significantly reduced level in cultured patient fibroblasts as reported by Chakraborty *et al.* (2014). Meanwhile, the more severe I223T variant exhibited a 20-fold decrease in affinity for CTP binding and has been suggested to be detrimental in blood cells where CTP concentrations are relatively low (Leibovitch *et al.* 2018). That no aberration in thermal stability or dramatic decrease in affinity for CTP or ATP was observed for the R99W variant is likely indicative of the mild clinical manifestations (and lack of fatalities) associated with this variant. Upon identifying a male patient homozygous for R99W who

was diagnosed at 23 years of age, Frans *et al.* (2017) suggested that the mild phenotype was linked to a lack of conservation of this residue and its surrounding primary sequence (Fig. 1-3). Three young siblings homozygous for R99W also show a mild systemic phenotype (Table 1-1) (Hull *et al.* 2016). The remaining patients, though, display a different set of symptoms including more systemic pathologies such as anemia (Aksentijevich *et al.* 2014) and autoinflammation (Kumaki *et al.* 2019) (Table 1-1). In the latter cases, however, R99W is compound heterozygous with another allele and so it is likely that the partial LOF of the other mutation also contributes to these phenotypes. Nonetheless, all patients exhibit a form of immunodeficiency (Table 1-1) and thus it is conceivable that, although not lethal, phenotypes arising from an R99W substitution may appear in B- and/or T-cells in which high levels of protein synthesis continually occur (Kumaki *et al.* 2019) and therefore are particularly sensitive to perturbations in the amount of functional enzyme.

Hence, it is likely that the patients harboring the allele for the R99W substitution are sick due to inefficient AMP incorporation by the variant enzyme, as demonstrated by the five-fold decrease in turnover number with ATP as a substrate relative to that of the native enzyme (Table 3-1). That this particular facet of the enzyme is only mildly compromised may therefore explain why disease manifestations are non-life threatening in patients and are limited in scope and severity.

4.2 E43Δ Variant

The E43Δ variant results from the deletion of nucleotides 126 to 128 (AGA) in the *TRNT1* open reading frame such that a single glutamate residue is lost (DeLuca *et al.* 2016). This is the most N-terminal mutation discovered to date as the original glutamate represents the 14th residue of the probable cytosolic form of the protein synthesized from its second N-terminal in-frame start codon. (The variant proteins used in these experiments also are synthesized from this start codon). *In vivo*, it is possible that the glutamate is even more N-terminal, depending on how many amino acids are removed by the mitochondrial processing protease upon import of this protein into mitochondria. E43 is situated at the N-terminus of α-helix 2 of the enzyme and is located N-terminal to conserved motif A (Fig. 1-3). Based on the crystal structures of TRNT1 (Augustin *et al.* 2003; Kuhn *et al.* 2015), E43 is surface-exposed (Fig. 1-6). Deletion of this negatively charged amino acid from the vicinity of the N-terminus of α-helix 2 may lead to destabilization of this helix or may alter the organization of α-helices 1 and 2 with respect to one another. In either event, this change may alter some of the conformational character of this region of the protein. Given that the C-terminus of α-helix 2 is separated by only three amino acids from the N-

terminus of β-strand 1 that begins at motif A, perhaps changes in the stability or arrangement in space of α-helix 2 are propagated through the protein to alter this β-sheet or more specifically motif A.

We previously have shown that in yeast tRNA-NT, an arginine-to-tryptophan substitution at the beginning of motif A and in the first β-strand (corresponding to a substitution only 17 amino acids from E43 in TRNT1) can suppress a temperature-sensitive (*ts*) mutation in motif C (Goring *et al.* 2013). This suppression is linked to an increase in enzyme activity and not to an increase in the thermal stability of yeast tRNA-NT. More precisely, this yeast R64WE189F double variant showed on the order of a 6- to 10-fold increase in the turnover number (depending on the substrate tested) as compared to the E189F *ts* variant (Rahman 2017). Furthermore, we have shown that the R64W variant increased misincorporation of AMP onto a growing 3' CCA-end (Rahman 2017). We wondered if the removal of the glutamate from a similar position in TRNT1 (close to the β-sheet and motif A) would show a similar effect.

Given the importance of the two-metal binding catalytic carboxylates (D*x*D) in motif A (Steitz *et al.* 1994; Yue *et al.* 1996; Steitz 1998), altering the structure of this region of the protein may result in altered NTP binding or discrimination. If this change in structure is not confined to this region of the protein, we may also see effects on tRNA binding and catalysis as other important motifs are reoriented in space. To address these possibilities, we first looked at the stability and higher order structure of the E43Δ variant as compared to the native enzyme.

4.2.1 Minor Decrease in Structural Stability

Although we previously have shown that converting R64 to W64 in the yeast enzyme did not alter the protein structure or stability (Goring *et al.* 2013), we wished to confirm that this also was the case in the human E43Δ variant and so we proceeded to assess these characteristics using CD spectroscopy and thermal denaturation, respectively. No change in secondary structure of the E43Δ variant was seen (Fig. S3 A-C) though a minor drop in melting temperature (~2°C) from that of the native enzyme was observed (Fig. 3-5). Although this change in T_m is considerably less than the 5-7°C drop seen in other characterized human variants (Leibovitch *et al*. 2018, 2019), it is more pronounced than that of the R99W variant described above (Fig. 3-5). If the reduced negative charge resulting from the removal of E43 at the N-terminus of α-helix 2 (Fig. 3-15A) destabilizes this helix, it also may eliminate the potential for hydrogen bonding between E43 and K46 (via the side chains) and S47 (via the main chain of E43) in

α-helix 2 (Fig. 3-15B) to further destabilize the structure of α-helix 2, and also alter the arrangement of the connecting turn between α-helices 1 and 2 (Fig. 3-15 A, C). This modeling agrees well with the structural model generated by DeLuca *et al.* (2016) (who have used an alternative modeling software).

A subsequent propagation of these conformational changes within the protein might thus account for the minor decrease in stability, though it remains unclear whether this effect could be global or simply confined to one or more regions, as thermal stability was determined based on the change in signal intensity at 222 nm reflecting the loss of α-helical character. This minor decrease in thermal stability is consistent with the finding that E43Δ variant protein levels were reduced by over two-fold, as compared to native protein levels in fibroblasts in a healthy control, in dermal fibroblasts in one male patient with retinitis pigmentosa who exhibited a compound heterozygous E43Δ/c.1246A[6] genotype (Table 1-1) (DeLuca *et al.* 2016). However, E43Δ variant protein levels are significantly reduced in induced pluripotent stem cell (iPSC)-derived retinal organoids specific for this patient, as compared to native protein levels in control retinal organoids from an age-matched individual (Sharma *et al.* 2017), suggesting that the stability of the protein in general may be reduced. These reports suggest that the overall reduced stability of the E43Δ variant contributes to pathogenesis involving retinitis pigmentosa. In fact, DeLuca *et al.* (2016) have shown that knockdown of the tRNA-NT gene in zebrafish leads to more pronounced defects in the visual response than in other affected cells or tissues, similar to the effect of reduced E43Δ variant protein levels in the human patient. Moreover, DeLuca *et al.* (2016) have demonstrated that while a relatively mild knockdown of the tRNA-NT gene restricts phenotypes to the visual system in zebrafish, a more complete knockdown encompasses multiple systems and processes including eye development, heart development and red blood cell maturation suggesting therefore a dependence of phenotypes on TRNT1 protein levels in humans, or in this specific case, stability of the E43Δ variant.

4.2.2 No Change in Tertiary Structure

To see if the reduced stability of the protein resulted from altered tertiary structure, fluorescence spectroscopy was used. As E43 is found near the N-terminus of the protein, it seemed unlikely that the loss of this amino acid would have an effect on the overall tertiary structure of the protein, but a rearrangement of this region may have affected the environments of nearby aromatic amino acids (*e.g.*, F37, F41, F52 and F93, or F80 in the single β-sheet) such that their fluorescence spectra at 295 nm were shifted. The wavelength of maximum fluorescence of the E43Δ variant upon excitation at either 280 or

295 nm revealed no substantial change (~1 nm or less) compared to that of the native enzyme (Fig. 3-6), suggesting no major change in overall higher order structure. These findings suggest limited effects on the tertiary structure of the protein either resulting from any destabilization of α-helix 2 or rearrangement of the region connecting α-helices 1 and 2 due to the deletion of E43.

4.2.3 No Change in Dimerization or tRNA Binding

Given that there were no apparent changes in secondary or tertiary structure and that the ability to form a covalent dimer *in vitro* depends on interactions in the C-terminal portion of the enzyme far from E43, we did not expect to see any effect on dimerization in the E43Δ variant and this was the case (Fig. 3-2). In addition, no apparent change in the size or conformation of the E43Δ monomer or dimer was seen as compared to those of the native enzyme (Fig. 3-3). Based on these data it appears that, as with the R99W variant, the E43Δ variant shows no major structural changes.

Similarly, as the loss of *in vitro* dimerization for the I326T variant reflected a decrease in tRNA binding (Leibovitch *et al.* 2019), like the R99W variant, the E43Δ variant instead shows A_{280}:A_{260} ratios similar to those of the native enzyme before or after RNase treatment (Fig. 3-4). This suggests a similar level of binding of the tRNA substrate to the E43Δ variant during purification and also supports the notion that overall structural changes in the protein are minimal.

4.2.4 Altered CMP and AMP Incorporation

As described previously, we have already characterized the differences in enzyme activity in a yeast enzyme with amino acid substitutions in this region of the protein. More specifically, in the yeast R64W variant we have seen no change in turnover number, tRNA or ATP binding, but an approximately three-fold increase in $K_{M,Apparent}$ for CTP binding (Rahman 2017). While R64 is predicted to lie within motif A and the first β-strand of the β-sheet, E43 in the human enzyme is N-terminal to and separated from motif A by α-helix 2 and a short connecting segment (Fig. 3-16). Hence, it is possible that the deletion of E43 in TRNT1 may affect enzyme activity via a structural perturbation of motif A by weakening the normal functions of motif A in NTP binding and/or polymerization. In addition, since in the higher order structure of the protein, E43 is not far from the region connecting motifs A and B, or motif C (Fig. 3-16), it is possible that these structures may be functionally affected as well. As described in Section 4.1, the region between motifs A and B may be involved in the recognition of the tRNA 3'-end for AMP

incorporation at its terminal position. In addition, motif C is known to mediate this process by bringing the head and neck domains of the enzyme together (Ernst *et al.* 2015).

A reduction in AMP incorporation onto the $tRNA^{Asp}$-NCC transcript was seen with the E43Δ variant as compared to the native enzyme in end point assays (Fig. 3-7). At the highest enzyme amount tested (~10 ng), the E43Δ variant showed four-fold less product formation as compared to the native enzyme. Much like the R99W variant, this suggests that the ability to bind or incorporate AMP was affected. To determine if the reduced ability to incorporate AMP was also seen for CMP incorporation, C-addition to the $tRNA^{Asp}$-NC (Fig. 3-8) and $tRNA^{Asp}$-N transcripts (Fig. 3-9) was assayed. Using the $tRNA^{Asp}$-NC transcript at ~10 ng of enzyme, the E43Δ variant showed 1.5-fold less incorporation of the second C as compared to the native enzyme (Fig. 3-8), however, with the $tRNA^{Asp}$-N transcript at the same enzyme amount, higher incorporation of the first and second C's by this variant was observed especially with respect to incorporation of the second C (which showed product formation three-fold higher with the variant than the native enzyme) (Fig. 3-9). When both ATP and CTP were incubated with the $tRNA^{Asp}$-N transcript, no substantial changes were seen for CMP incorporation at either of the expected positions on the transcript, however, a decrease in AMP incorporation was evident at the terminal position (Fig. 3-10). Therefore, like the R99W variant, these results suggest that the E43Δ variant may be defective in AMP but not CMP incorporation and so kinetic assays were performed in order to gauge the extent of impairment.

4.2.5 No Change in $K_{M,Apparent}$ for Substrate Binding

Regarding substrate affinities, the $K_{M,Apparent}$ values for ATP, CTP and $tRNA^{Asp}$-NCC binding to the E43Δ variant were all within three-fold of those of the native enzyme (Tables 3-1 to 3-3), suggesting that substrate binding is not affected by the loss of E43. These data are consistent with the yeast R64W variant which also showed only small changes in these values (Rahman 2017). Likewise, in most cases the previously characterized human variants showed $K_{M,Apparent}$ values that differed by at most two-fold as compared to the native human enzyme (Leibovitch *et al.* 2018, 2019). So the data presented here agree well with what had been seen previously and suggest that there are no changes in substrate binding in the E43Δ variant that are linked to the disease phenotype. We therefore looked at catalytic activity as the factor that may be involved.

4.2.6 Different ATP and CTP Catalysis

With respect to AMP incorporation into the $tRNA^{Asp}$-NCC transcript, the calculated k_{cat} of the E43Δ variant was between 16% and 30% of that of the native enzyme depending on which substrate was varied (Tables 3-1, 3-3). When incorporating CMP into the $tRNA^{Asp}$-NC transcript, the calculated k_{cat} of the E43Δ variant actually was 120% that of the native enzyme (Table 3-2). These values are in good agreement with what we have seen previously for the yeast R64W variant where the turnover number with varying CTP concentration decreased by a small amount (~25%) (Rahman 2017), and for the previously characterized human variants (Leibovitch *et al.* 2018) which showed values within 30% above or below that of the native enzyme, with the exception of the more C-terminal I326T variant for which the k_{cat} dropped approximately six-fold (Leibovitch *et al*. 2019). This suggests that, in terms of nucleotide incorporation kinetics, what is happening in the E43Δ variant is more similar to what is happening in the other N-terminal variants than in the C-terminal variant. This again seems reasonable, given the biophysical data, suggesting that there are no major changes in the structure of the protein (Sections 4.2.1 to 4.2.3).

4.2.7 Potential Contributions of Motif A, the Disordered and Flexible Loops, and Motif C

As the C-terminus of α-helix 2 is separated by only three amino acids from the N-terminus of β-strand 1, which in turn constitutes the beginning of motif A (Fig. 3-16), the deletion of E43 may lead to the destabilization of α-helix 2 and the propagation of this destabilization that primarily affects motif A. Motif A, the most N-terminal element of the Class II tRNA-NT, is located in the head domain (Figs. 1-5, 3-16) and contains two highly conserved catalytic carboxylates (D*x*D) (Yue *et al*. 1996). Polymerization via AMP or CMP incorporation onto the 3'-end of the tRNA normally occurs by a two-metal ion binding mechanism which was first described for DNA polymerases (Steitz *et al.* 1994; Steitz 1998). The two carboxylates bind and coordinate two Mg^{2+} ions at the catalytic core such that the first Mg^{2+} ion deprotonates the 3'-OH of the ribose of the terminal nucleotide of the tRNA. This initiates a nucleophilic attack by the 3'-O^- at the α-phosphate of the incoming ATP or CTP. The second Mg^{2+} ion stabilizes the triphosphate moiety of ATP or CTP and promotes the release of the pyrophosphate group following the attack. Both metal ions also stabilize the transition state intermediate. Given the roles of these residues in the chemistry of the reaction, one would expect changes in their organization to alter k_{cat} and not $K_{M,Apparent}$. However, here we see only small changes in either of these parameters, suggesting that the E43Δ variant does not alter the structure of motif A to affect the role of ATP or CTP in the reaction. Interestingly, the greatest drop in k_{cat} (to approximately 16% of native) was seen when the ATP

concentration was held constant and the $tRNA^{Asp}$-NCC concentration was varied. This may suggest that alterations in structure at motif A are not manifested with respect to ATP or CTP, but with respect to the tRNA transcript. Nonetheless, *in silico* protein-folding and subsequent *in silico* docking to $tRNA^{Asp}$-NCCA revealed an increased distance between the two aspartates of motif A and the conserved R197 residue of motif D in the E43Δ variant as compared to that of the native enzyme (Fig. 3-17). Assuming that the snapshot of the structures represents the A-adding reaction, this change may reflect an alteration of conformation of the nucleotide binding pocket due to the displacement of the R197 contact point for ATP away from the two carboxylates, such that the bound ATP is pulled away from motif A resulting in a decrease in turnover.

In the structure of TRNT1, E43 is located in the head domain of TRNT1 which contains not only motif A, but also the disordered loop and the flexible loop (Fig. 3-16) described previously in Section 4.1.5 for the R99W variant. It is possible that the deletion of E43 does not alter motif A, but may disrupt the function of the disordered loop or the flexible loop. Similar to what we have proposed for the R99W variant, the deletion of E43 may disrupt the function of the flexible loop near E43 (Fig. 3-16) such that residues R126 and/or T131 in the flexible loop (Fig. 3-18 D-F) are unable to induce the transition of the nucleotide binding pocket toward an ATP specificity. It is equally likely that the E43 deletion initiates conformation changes (perhaps through disruption of a hydrogen bonding network) that displace residues D132, G133 and/or R134 in the flexible loop (Fig. 3-18 D-F) resulting in the inability of the flexible loop to induce toggling of the nucleotide binding pocket toward an ATP specificity. In contrast to the R99W variant, the latter effect in the E43Δ variant involving displacement of R134 is conceivable, since the k_{cat} with varying $tRNA^{Asp}$-NCC concentration showed a six-fold reduction (Table 3-3) and the k_{cat} with varying ATP concentration of the R134A variant showed a 77-fold reduction (Hoffmeier *et al.* 2010), while the change in $K_{M,Apparent}$ for ATP binding for either variant was minimal to none (Table 3-1) (Hoffmeier *et al.* 2010).

In addition, in the yeast R64W variant, functional alteration of the flexible loop has been suggested by Rahman (2017) to occur if the hydrogen bonding network between residues R64 and A85, on adjacent β-strands in the β-sheet of yeast tRNA-NT, is disrupted. Residue A85 has been proposed to be normally in direct contact with the flexible loop, and so Rahman (2017) has predicted that disruption of this bonding network to residue A85 would subsequently affect the flexible loop and alter its function. As the R64W substitution showed only a slight increase in CTP affinity, Rahman (2017) has suggested that as a

hydrogen bonding network is maintained with A85 regardless of the residue involved, the flexible loop would retain its normal function of mediating the CTP-to-ATP specificity switch. As residues R64 and A85 in the yeast enzyme are conserved in the human enzyme (homologous to residues R60 and A81, respectively), and assuming that the secondary and tertiary structures of the two β-strands of the yeast enzyme are similar enough to those of the human enzyme (the crystal structure of yeast tRNA-NT has not yet been solved), the involvement of this hydrogen bonding network may also apply in the case of the deletion of E43. Upon closer inspection, the two hydrogen bonds formed between R60 and A81 in the human enzyme (Fig. 3-19A) appear to be preserved when E43 is deleted (Fig. 3-19B), and since there are no changes to the secondary (Fig. S3C) or tertiary structure (Fig. 3-6) of the E43Δ variant as compared to that of the native human enzyme, this is not surprising. These observations support our model that much smaller structural perturbations, as determined by thermal denaturation (Fig. 3-5), are involved in altering different regions of the human enzyme upon deletion of E43 such that AMP incorporation is reduced and CMP incorporation is increased, and argue against a major structural change in the single β-sheet in the enzyme.

The results we obtained with the E43Δ variant may reflect changes in motif C of TRNT1. Due to the proximity of residue E43 to motif C (Fig. 3-16), one can imagine how deletion of E43 might disrupt its function. Motif C, located between the head and neck domains, contains a sequence which is sparsely conserved in Class II tRNA-NTs (D$x_{(3,4)}$G$x_{(9)}$R, where $x_{(n)}$ represents any *n* number of consecutive amino acids; the sequence of TRNT1 is D*YFN*G*YEDLKNKKV*R), and acts as a spring element between the head and neck domains (Ernst *et al*. 2015) (Figs. 1-5, 3-16). Although it makes no contact with tRNA or nucleotides, motif C has been demonstrated to modulate the overall flexibility of the enzyme by properly orienting the tRNA and nucleotides in the catalytic core. This is accomplished by the stretching of motif C upon binding of tRNA to the body domain so that the catalytic core is adjusted through precise stages in order to accommodate the growing tRNA. In the human enzyme, Ernst *et al.* (2015) have shown that replacement of residue D168, in the sequence context of DYFNG above, with an alanine in the sparsely conserved sequence compromised this stretching such that the resulting enzyme variant was unable to incorporate AMP efficiently. This being the case, the K_M values for ATP and tRNA remained unchanged, demonstrating a general independence of motif C from the binding of these two substrates; however k_{cat} for this variant was reduced 15-fold relative to the native enzyme (Ernst *et al.* 2015). Moreover, D168 has an equally vital function as it promotes a helix-capping interaction (Aurora and Rose 1998; Makhatadze 2005) with an α-helix. Located between β-strand 6 and α-helix 6 (H6), D168

hydrogen bonds with G172 and Y173 in order to stabilize the α-helical conformation of helix 6 and subsequently influence the spring function of motif C (Ernst *et al.* 2015). Naturally, the replacement of this aspartate with alanine has been envisaged to disrupt this helix-capping interaction and displace this α-helix (Ernst *et al*. 2015). Thus, given our kinetics data for the E43Δ variant, which showed a six-fold decrease in k_{cat} in AMP incorporation with varying $tRNA^{Asp}$-NCC (Table 3-3) but little change in $K_{M,Apparent}$ for ATP or $tRNA^{Asp}$-NCC binding (Tables 3-1 and 3-3, respectively), it is plausible that the deletion of E43 may also effect a conformation change that displaces D168 in motif C (Fig. 3-20 A-C) with similar outcomes as that of the D168A substitution. This also would demonstrate the independence of the deletion of E43 from ATP or $tRNA^{Asp}$-NCC binding, but nevertheless would lead to reduced AMP incorporation. Furthermore, as the spring function of motif C would be altered, multiple rounds of C-addition may also result yielding the run-on transcription products ($tRNA^{Asp}$-$NC_{(4)}$ and $tRNA^{Asp}$-$NC_{(5)}$) observed (Fig. 3-11 A, B).

4.2.8 Augmented CMP Incorporation and Run-On Transcription

As described above, if the ability of motif C to function as a spring is compromised, we may see multiple rounds of CMP incorporation. To further explore the phenomenon of run-on transcription, additional activity assays were performed using the $tRNA^{Asp}$-N and $tRNA^{Asp}$-NC transcripts with higher enzyme amounts. Under these conditions, we discovered that in addition to being more efficient at incorporating CMP into the penultimate and antepenultimate positions of the tRNA transcripts than was the native enzyme, the E43Δ variant also generated run-on transcription products of both the $tRNA^{Asp}$-NC (Fig. 3-11A) and $tRNA^{Asp}$-N (Fig. 3-11B) transcripts more efficiently than did the native enzyme. In fact, while the native enzyme seemed able to generate some $tRNA^{Asp}$-NCCC run-on products under these conditions, the variant enzyme efficiently generated $tRNA^{Asp}$-$NC_{(4)}$ (Fig. 3-11A) and $tRNA^{Asp}$-$NC_{(5)}$ (Fig. 3-11B) run-on products.

When the $tRNA^{Asp}$-N transcript was used in the presence of both CTP and ATP (Fig. 3-11C), extension was limited to three nucleotides suggesting that competition between ATP and CTP occurs at the third position 3' to the discriminator base, and that if AMP is incorporated ($tRNA^{Asp}$-NCCA) extension is terminated and the final transcript product is released, but if CMP is incorporated ($tRNA^{Asp}$-NCCC) C-addition can continue. Nevertheless, the ability of the E43Δ variant to incorporate CMP still far exceeds that of the native enzyme at enzyme amounts of at least 10 ng (Fig. 3-11C).

Perhaps in the E43Δ variant, the nucleotide binding pocket as defined by motif D or the flexible loop that plays a role in the conversion from CTP binding to ATP binding is rearranged in such a way that incoming CTP is much more readily accommodated by the E43Δ variant than it is by the native enzyme, due to the increase in affinity (Table 3-2). This seems unlikely, given that the difference in the $K_{M,Apparent}$ values for CTP in the native and variant proteins differs by only about three-fold. However, if we consider $K_{M,Apparent}$ values for both ATP and CTP, there is an almost 10-fold difference between them as the $K_{M,Apparent}$ value for ATP increases by three-fold as compared to the native enzyme. However, when ATP is added to the reaction, run-on transcription is dramatically reduced (Fig. 3-11), suggesting that ATP can bind efficiently and once incorporated into tRNA terminates transcription.

4.2.9 The E43Δ Variant Is Associated With Retinitis Pigmentosa and Erythrocyte-Linked Phenotypes

Much like the R99W variant, the phenotypes associated with the E43 deletion are mild compared to those associated with other reported mutations (Table 1-1). In fact, the only symptoms manifested in the one male patient reported to date are retinitis pigmentosa with erythrocytic microcytosis and anisocytosis with mild anemia (DeLuca *et al.* 2016) – a far cry from much more severe manifestations such as SIFD or B-cell immunodeficiency. As described in Section 4.2.1, a minor decrease in thermal stability of this variant (Fig. 3-5) is likely to account for its decrease in abundance in dermal fibroblasts and iPSC-derived retinal organoids particular to this patient, relative to native protein levels in healthy control patients, and to contribute to the retinitis pigmentosa phenotype (DeLuca *et al.* 2016; Sharma *et al.* 2017). Another aspect of the E43Δ variant is the three-fold decrease in the affinity for ATP (373.02 ± 127.3 µM) that it shows relative to the native enzyme (124.31 ± 39.3 µM) (Table 3-1) – though the intracellular ATP concentrations of most cells in the human body are at least 1 mM, those of human lymphocytes have been reported to be as low as 390 or 463 µM (de Korte *et al.* 1985; Pagani *et al.* 1991). This suggests that the reduced affinity for ATP exhibited by this variant may be relevant in human lymphocytes. This is interesting as there is no clinical evidence of any aberration in this cell type in the patient, yet red blood cells are more affected by this variant (*e.g.*, microcytosis, anisocytosis and anemia) (DeLuca *et al.* 2016). The intracellular ATP concentration in human red blood cells is known to be at least 1.5 mM (Torrance and Whittaker 1979; de Korte *et al.* 1985; Werner *et al.* 1987), and so the altered ATP affinity cannot be the cause of these reported red blood cell-linked pathologies.

Considering all our data, we surmise that patients harboring the E43Δ variant are most likely sick due to the combination of a minor decrease in structural stability which may account for the red blood cell-

linked pathologies, inefficient AMP incorporation arising from decreased affinity for ATP and a reduction in turnover number with respect to varying $tRNA^{Asp}$-NCC concentrations, relative to the parameters of the native enzyme. Regarding the red blood cell abnormalities, it has been proposed that this mutation might trigger an imbalanced synthesis of alpha or beta globin chains in hematopoietic cells (DeLuca *et al.* 2016) and also adversely affect iron utilization (Taher *et al.* 2013).

Because retinitis pigmentosa is characterized by the gradual degeneration of photoreceptor cells of the outer neural retina (DeLuca *et al.* 2016) and photoreceptor cells typically regenerate ~10% of their outer segments daily (Wangsa-Wirawan 2003), the function of which is photon detection, it is not surprising that one or more of these aberrations in TRNT1 structure or function could selectively and adversely affect the function of this cell type. Indeed, as photoreceptor cells are highly metabolically active, a very high demand for protein synthesis is continually required and so any perturbation in this process would likely result in a dramatic change in phenotype. Furthermore, Sharma *et al.* (2017) have demonstrated that the iPSC-derived retinal organoids harboring the E43Δ variant were deficient in autophagy and possessed high levels of oxidative stress, thought to be a major cause of photoreceptor cell injury and death. Ultimately, as the E43 deletion only mildly compromises TRNT1, it stands to reason that these disease manifestations are non-life threatening and are also limited in scope and severity. One caveat however is the recognition that the other allele of the patient, c.1246A[6] (DeLuca *et al.* 2016), may very well play an equally important role, if not a stronger one, in the development of these phenotypes, and so this work represents at best a partial study of the link between TRNT1 variant characteristics and disease manifestation. To this end, work to define the biophysical and biochemical features of the A[6] variant is ongoing.

4.3 A[8] Variant

Although we were unable to characterize the A[6] variant, we did characterize the A[8] variant which like the A[6] variant results from a frame shift in the *TRNT1* open reading frame, whereby an adenosine is deleted (A[6]) or inserted (A[8]) into a stretch of seven adenosine residues beginning at nucleotide 1246 of the open reading frame. These two variants yield proteins with their C-terminal amino acids replaced by others (DeLuca *et al.* 2016) (Table 4-1), which correspond to the most C-terminal mutations discovered to date as they occur near the end of the tail domain of TRNT1.

Table 4-1: Carboxy-Terminal Sequences of Native and c.1246A Frame Shift Variants

Variant	Amino acid sequence
Native	LREQWKKSGYQMEKDELLSYIKKT
c.1246A[6]	LREQWKKVVTKWKKMNF
c.1246A[8]	LREQWKKKWLPNGKR

Note: The first amino acid change resulting from the frame shift is highlighted in green, positively charged amino acids are shown in red and negatively charged amino acids are shown in blue.

The extra nucleotide in the A[8] variant results in a change in the primary sequence of the protein such that the most C-terminal α-helix of the protein (Fig. 1-6) is replaced by a short disordered region (Fig. 3-21) such that the overall charge on this region of the protein changes from zero to +3 (Table 4-1) and the overall molecular mass of the protein is reduced by approximately 1 kDa.

4.3.1 Increased Dimerization and Amount of Higher Molecular Weight Species

As expected, SDS-PAGE denaturing gel electrophoresis showed no real difference in apparent mass between the native and A[8] monomers (Fig. 3-1). Since the ability of TRNT1 to dimerize reflects the organization of the C-terminal body and tail domains of TRNT1 (Leibovitch *et al.* 2019), we tested for *in vitro* dimerization of the A[8] variant. Like the native enzyme and most of the other variant proteins, but not the I326T variant (Leibovitch *et al.* 2019), the A[8] variant showed a covalent dimerization product on electrophoresis in the absence of reducing agent (Fig. 3-2). In fact, under these conditions the A[8] variant actually showed a greater amount of dimer than did any of the other proteins tested (Fig. 3-2). We previously have argued that the loss of covalent dimer in the I326T variant is linked to a change in the higher order structure of the monomer (Leibovitch *et al.* 2019), so perhaps an increase in the amount of covalent dimer also reflects a change in the structure of the protein. That something has changed in the structure of the A[8] variant also may be reflected in non-denaturing gel electrophoresis, where a relative increase in the amount of high molecular weight species as compared to the native enzyme and the E43Δ and R99W variants is seen (Fig. 3-3). To address the possibility that the higher order structure of the protein has changed, we used fluorescence and CD spectroscopies to look for changes in tertiary and secondary structure, respectively.

4.3.2 No Change in Tertiary or Secondary Structure

The mature native TRNT1 contains four tryptophan residues: W144, W239, W381 and W415; one in the region between conserved motifs A and B in the head domain of the protein (discussed previously in the

context of R99), one in the highly conserved motif E in the neck domain, and one each in the less well conserved body and tail domains of the protein, respectively. In contrast, the A[8] variant contains five tryptophan residues with translation of the frame shift mutation resulting in an altered protein sequence and the introduction of the fifth tryptophan (W419) near W415 (Table 4-1). Given this, fluorescence spectroscopy (upon excitation of tryptophan residues at 295 nm) was used to determine if any changes in the tertiary structure of A[8] as compared to the native enzyme could be detected. Surprisingly, no change (within error) was observed in the wavelength of maximum fluorescence for the A[8] variant as compared to the native enzyme (Fig. 3-6). This suggests not only that there is no major change in tertiary structure but also that the addition of a tryptophan residue in the variant shows no effect on fluorescence. The small red-shift (<3 nm) for the A[8] variant may reflect that either the new W419 or the existing W415 is more solvent-exposed as nine amino acids have been removed from the C-terminus of the protein and the terminal α-helix has been lost. The same approximately 3 nm red-shift in the wavelength of maximum fluorescence emission was also seen when all aromatic amino acids were excited at 280 nm (Fig. 3-6). As excitation at this wavelength will account for all aromatic amino acids in the protein, this supports the idea that there is not a major change in tertiary structure in the A[8] variant as compared to the native enzyme.

Similarly, no change in secondary structure of the A[8] variant was seen using CD spectroscopy (Fig. S3 A-C). This is not surprising given the overall primarily α-helical character of the protein (~60% α-helix) such that the loss of a single C-terminal α-helix resulted only in a small change in overall CD spectrum.

So perhaps the increase in the amount of higher molecular weight species under non-denaturing conditions and the increase in the amount of covalent dimer seen do not reflect changes in the tertiary or secondary structure of the protein, but simply result from the loss of the C-terminal α-helix. If one compares the predicted structure of the C-terminus of the A[8] variant (Fig. 3-21C) with the C-terminus of the native enzyme (Fig. 3-21D), one can see that with the loss of the C-terminal α-helix in the A[8] variant the antepenultimate and penultimate α-helices of the protein each has an additional surface exposed. Perhaps exposing these surfaces allows monomers to associate in a different way such that the disulfide bond required for covalent dimerization can form more easily (Fig. 3-2) or that monomers may associate more easily under non-denaturing conditions (Fig. 3-3). It is interesting that with the loss of the C-terminal helix (h22) some amino acids that would have been involved in interactions with this helix are now surface-exposed (Fig. 3-22). In the A[8] variant, the new C-terminal helix (h21) now has

surface-exposed arginine and lysine residues in addition to a number of surface-exposed polar and hydrophobic residues (Fig. 3-22 B, D). Also, the smaller helix (h20) N-terminal to this helix has a surface-exposed aspartate along with two surface-exposed hydrophobic residues (Fig. 3-22 B, D). It is possible that the newly exposed hydrophobic residues (L407 and L411 in the new C-terminal helix (h21) and I393 and V396 in the smaller helix (h20)) (Fig. 3-22 B, D) may create part of a binding surface that facilitates association with another A[8] monomer and/or more easily promote disulfide bond formation at residue C373. Moreover, the binding orientation of the tRNA to the A[8] variant also may be altered as the contact sites with helix h22 are removed and the newly exposed surfaces of helices h20 and h21 may interact with the tRNA (Figs. 3-21D, 3-22B, 3-22D).

4.3.3 Minor Decrease in Structural Stability

In terms of melting temperature, the change in T_m of this variant as compared to the native enzyme is much less than that seen with most of the other characterized human variants (5-7°C) (Leibovitch *et al.* 2018, 2019), however, it is on par with that of the E43Δ variant, described above, as the latter variant also showed a decrease of T_m of ~2°C (Fig. 3-5). Given that the E43Δ and A[8] changes are near the N- and C-terminus of the protein, respectively, perhaps it is not surprising that they have less of an effect on protein stability than do amino acid substitutions within the protein. There is no difference in thermal stability whether the A[8] protein is pretreated with RNase or not, while for the native enzyme there is a ~2°C reduction in melting temperature after RNase treatment. We previously attributed the increase in T_m in the presence of RNA to a contribution from bound tRNA as more energy is needed in the presence of the tRNA to denature both the tRNA and the protein. This may suggest that in contrast to the native, R99W and E43Δ proteins, the A[8] variant binds tRNA less efficiently. As with the E43Δ variant, the decrease in thermal stability associated with the A[8] variant is consistent with the reduced variant protein levels seen in dermal fibroblasts of two patients with retinitis pigmentosa showing the compound heterozygous A[8]/c.609-26T>C genotype (Table 1-1) (DeLuca *et al.* 2016). Moreover, A[8] variant protein levels were significantly reduced in iPSC-derived retinal organoids specific for these two patients (Sharma *et al*. 2017), suggesting that the stability of the protein in general may be reduced. Like the E43Δ variant, these reports suggest that the overall reduced stability of the A[8] variant contributes to pathogenesis involving retinitis pigmentosa.

4.3.4 Major Decrease in tRNA Binding and Role of the Tail Domain

If we use the A_{280}:A_{260} ratio as an indicator of tRNA association with the variant during purification, we see that there is essentially no change in the A_{280}:A_{260} ratio for the variant before or after RNase treatment (Fig. 3-4), while the native, R99W and E43Δ variants show at least a two-fold difference before and after RNAse treatment. This supports the hypothesis that tRNA binds less efficiently to the A[8] variant, which has a C-terminal change in the protein's primary structure, as compared to the native enzyme and the other variants with amino acid substitutions that are more N-terminal. That a C-terminal alteration in the protein's primary structure should affect tRNA binding is not surprising.

Available crystal structures and co-crystal structures of tRNA-NT enzymes with bound tRNA revealed that the body and tail domains of the protein are important for tRNA binding (Li *et al.* 2002; Xiong *et al.* 2003; Tomita *et al.* 2004; Xiong and Steitz 2004; Yamashita and Tomita 2016). These interactions are with the sugar-phosphate backbone of the tRNA substrate and most prominently with the D and TΨC arms found together in the tertiary structure of tRNA (Fig. 1-1). Analysis of the structures of the regions of different tRNA-NTs that interact with the tRNA substrates revealed similar surface electrostatic potentials, shapes and sizes (Xiong *et al.* 2003; Xiong and Steitz 2004), suggesting that these domains play key roles in enzyme activity. The most recent crystal structure of *Thermotoga maritima* tRNA-NT complexed with tRNA (bearing a complete CCA sequence) revealed direct interaction between the tail domain of the enzyme and the phosphate backbone of the tRNA (Yamashita and Tomita 2016), showing that this region of the protein anchors the tRNA to prevent it from being dislodged during the course of the reaction, as first proposed by Toh *et al.* (2009). Yamashita and Tomita (2016) compared the crystal structures of *Thermotoga maritima* tRNA-NT with and without a bound tRNA substrate and noted that the tail of the enzyme moves around the tRNA to lock it in position. They also identified specific lysine, glycine and asparagine residues that generate an arm-like element responsible for anchoring the tRNA in place.

It seems reasonable to assume that a similar type of mechanism for tRNA positioning exists in other tRNA-NTs. In fact, more than 40 years ago, Zhu and Deutscher (cited in Zhu and Deutscher (1987)) first indicated that an *E. coli* tRNA-NT lacking its 21 C-terminal amino acids showed no activity. The more dramatic cleavage of 124 C-terminal amino acids from the Drosophila tRNA-NT reduced, but did not eliminate, its activity (Yang 2008). More recently, we showed that simply converting the C-terminal

KAKRQRIE sequence of the 605-residue *Arabidopsis thaliana* tRNA-NT to EAEEQEIE resulted in reduced tRNA binding (three-fold increase in K_D) and a reduction in enzyme activity (k_{cat} decreased by approximately 40%) (Leibovitch *et al.* 2013). Moreover, simply removing these nine amino acids resulted in a three-fold decrease in K_D and a 60% drop in k_{cat} as compared to the native enzyme (Leibovitch *et al.* 2013). As the tail domain of tRNA-NT has been implicated in tRNA binding and enzyme activity, we set out to perform a more detailed enzymatic analysis of the A[8] variant.

4.3.5 Kinetic Analysis and Possible Mechanisms of TRNT1 Alteration

With all combinations of tRNA transcripts ($tRNA^{Asp}$-N, $tRNA^{Asp}$-NC or $tRNA^{Asp}$-NCC) and nucleotides (ATP, CTP, or ATP and CTP), the A[8] variant showed the lowest level of NTP incorporation in end point assays of the three variants tested (Figs. 3-7 to 3-10). As these assays cannot distinguish between the role of substrate binding or catalysis in the reduced activities seen, we performed more detailed kinetic analyses.

These more detailed kinetic analyses revealed no real differences (all within a factor of two) in $K_{M,Apparent}$ for ATP, CTP (with a large experimental error) or $tRNA^{Asp}$-NCC binding (Tables 3-1 to 3-3), however, an 80- or 10-fold increase in $K_{M,Apparent}$ was seen for the $tRNA^{Asp}$-NC transcript (Table 3-4). In contrast, nearly the opposite was observed when turnover numbers were calculated for these reactions. The turnover number (k_{cat}) for the addition of AMP to the $tRNA^{Asp}$-NCC transcript was only 3-10% of that of the native enzyme, depending on whether ATP (Table 3-1) or $tRNA^{Asp}$-NCC (Table 3-3) concentrations were varied, while the k_{cat} for the addition of CMP to the $tRNA^{Asp}$-NC transcript remained within three-fold of that of the native enzyme, whether CTP (Table 3-2) or $tRNA^{Asp}$-NC (Table 3-4) were varied. This suggests that the changes at the C-terminus of the A[8] variant affect A- and C-additions differently. Similar decreases in k_{cat} were seen when the 10 (decreased five-fold) or 33 (decreased eight-fold) C-terminal amino acids were removed from TRNT1, although those deletions affected the $K_{M,Apparent}$ values for ATP and CTP differently (Leibovitch M., personal communication).

Given the results of our CD and fluorescence spectroscopy studies, which suggest no major changes in the secondary (Fig. S3) or tertiary (Fig. 3-6) structure of the protein, a lack of a change in $K_{M,Apparent}$ for ATP or CTP binding mediated by amino acids in the head and neck domains of the enzyme was as expected, given that the A[8] variant results in amino acid substitutions in the C-terminus far from the active site (Fig. 1-6). Likewise, an 80- or 10-fold increase in $K_{M,Apparent}$ for the $tRNA^{Asp}$-NC transcript also

was not unexpected as the tail domains of tRNA-NTs have been shown to be involved in tRNA binding (Shi *et al.* 1998; Yue *et al.* 1998; Tomita *et al.* 2004; Betat *et al.* 2004; Toh *et al.* 2009; Kuhn *et al.* 2015) and we saw a decrease in the amount of tRNA associated with the A[8] variant as compared to the native enzyme (Fig. 3-4) and an increase in higher molecular weight species, suggesting a change in organization of the C-terminus of the protein, as first proposed for the I326T variant (Leibovitch *et al.* 2019). What is more interesting is that this change in $K_{M,Apparent}$ was not seen for the $tRNA^{Asp}$-NCC transcript, yet AMP was incorporated into this transcript much less efficiently than was CMP into the $tRNA^{Asp}$-NC transcript.

4.3.5.1 Context of tRNA Binding and Orientation for CCA Addition

Given the size of TRNT1 (~48 kDa) and that of the $tRNA^{Asp}$-NC or -NCC transcript (~24 kDa), it is reasonable that multiple sites are involved in interactions with the tRNA (Betat *et al.* 2004; Yamashita *et al.* 2014; Kuhn *et al.* 2015; Yamashita and Tomita 2016). Changes in these interactions could lead to altered tRNA binding or orientation on the enzyme, which may affect different kinetic parameters. Previously, in the context of the I326T substitution in the body of TRNT1, we have argued that amino acid substitutions that modify the arrangement in space of the body domain of the protein may alter how tRNAs can bind and/or be presented as substrate, and therefore may affect enzyme activity in different ways (Leibovitch *et al.* 2019). Here, we propose that the replacement of the 17 C-terminal amino acids of TRNT1 with eight different amino acids (such that the protein loses its terminal α-helix and gains an overall positive charge in this region) results both in a decrease in the ability of this enzyme to bind and hold tRNA and to orient this tRNA properly for catalysis to occur.

Our earlier results with the Arabidopsis tRNA-NT (Leibovitch *et al.* 2013) have shown that if we substitute four negatively charged amino acids for positively charged amino acids within the last eight C-terminal amino acids of this protein, a 40% reduction in AMP incorporation into a $tRNA^{Asp}$-NCC transcript is observed. In contrast, if we simply remove nine C-terminal amino acids, a 60% reduction in enzyme activity results (Leibovitch *et al.* 2013). In both cases, there was no real effect on $K_{M,Apparent}$ (Table 1 in Leibovitch *et al.* (2013)). However, the K_D's were changed by approximately 10-fold when these two variants were compared, *i.e.*, stronger binding was evident in the deletion variant, while weaker binding was seen in the charge variant. In this case, we hypothesized that reducing the positive charge on this region of the protein reduced the potential for electrostatic interactions between the enzyme and the sugar-phosphate backbone of the tRNA substrate in the tail region of the protein such that binding was

less efficient. In the case of the A[8] variant discussed here, we retain three positively charged residues (and lose three negatively charged residues), but the relative positioning of the positive charges is altered as the variant protein is predicted to lose its secondary structural character in this region (Table 4-1). So, although the overall positive charge in this region of the protein is increased in the A[8] variant, we see a loss of tRNA associated with the enzyme (Fig. 3-4). This apparent reduced tRNA binding is reflected in the increased $K_{M,Apparent}$ for the $tRNA^{Asp}$-NC transcript (Table 3-4), but not the $tRNA^{Asp}$-NCC transcript (Table 3-3).

This suggests that, as with the Arabidopsis enzyme, this region of the protein is most important in binding tRNA prior to nucleotide incorporation and that as the tRNA is extended by cytidine, cytidine and adenosine, this region of the protein becomes less important in tRNA binding. However, it still must play a role in orienting the extending tRNA substrate appropriately for catalysis to continue. Fewer correct hydrogen-bonding or electrostatic interactions between the enzyme and the tRNA may alter this orientation. When the tRNA is modeled on the native enzyme or the A[8] variant (Fig. 3-21), a large difference in rotational position on the proteins is predicted (Fig. 3-21A). So while modeling suggests that if the tRNA binds to the A[8] variant, then its orientation is different from that of tRNA bound to the native enzyme. This model is supported by the observations that the $K_{M,Apparent}$'s for ATP, CTP and $tRNA^{Asp}$-NCC are close to those of the native enzyme (Tables 3-1 to 3-3), while the k_{cat} value for AMP incorporation into the $tRNA^{Asp}$-NCC transcript is reduced dramatically (Tables 3-1 and 3-3).

We propose that, in the native enzyme, the terminal α-helix (EKDELLSYIKKT) shows a positively charged face that can be involved in tRNA binding and organization. When that sequence is lost, as in the 10- or 33-amino acid deletion variants, or truncated by nine amino acids and replaced by the unstructured KWLPNGKR sequence of the A[8] variant, tRNA binding efficiency is reduced due to the loss of the positive charges and the α-helical structural motif. Furthermore, once the tRNA substrate is bound, this sequence may be responsible for anchoring the tRNA in position for subsequent cycles of C-, C- and A-addition. The separate roles that this sequence may play in tRNA binding and orientation may be reflected by the rearrangements that occur in the substrate and the conformational changes that the enzyme must undergo during the course of the reaction (Tomita *et al.* 2006; Toh *et al.* 2009; Yamashita *et al.* 2014; Yamashita and Tomita 2016), as well as product release (Wende *et al.* 2015; Yamashita and Tomita 2016).

Specifically, the tRNA-NT nucleotide binding pocket has different conformations for the incorporation of CMP and for AMP, and so has to undergo a conformational change after C-addition to allow for A-addition (Tomita *et al*. 2004; Toh *et al*. 2009; Yamashita *et al*. 2014; Ernst *et al*. 2015; Yamashita and Tomita 2016). We argue, due to the changes in the C-terminus of the A[8] variant, that once tRNA is bound, it is not oriented appropriately for C- and A-addition (approximated in Fig. 3-21A). Specifically, once the enzyme has undergone the conformational change from CTP binding to ATP binding, the active site is arranged to bind ATP efficiently (as evidenced by the $K_{M,Apparent}$ value close to that of the native enzyme), but the tRNA substrate is not appropriately oriented for the chemistry to happen (as evidenced by the drop in k_{cat}). This may result from a change in where the tRNA is bound on the enzyme, as the C-terminal sequences have been changed, or from the fact that the tRNA is not anchored strongly enough at the active site for the chemistry to happen (approximated in Fig. 3-21A). We saw similar characteristics in the I326T variant that we characterized previously, and Ernst *et al.* (2015) also proposed a similar explanation for a mutation in the neck domain of the protein, *i.e.*, although both substrates were bound to the enzyme, the distance and/or orientation of the substrates was altered such that the required nucleophilic attack did not occur efficiently. While these authors argue that this altered arrangement results from an amino acid substitution in the head and neck domain, we suggest that given the size of the tRNA substrate, the same type of altered organization of substrates could result from a modification in the C-terminal tail portion of the protein, reflecting primarily the positioning of the tRNA substrate.

4.3.5.2 Similar C-Terminal Variants

As the frame shift mutation altering the sequence and structure of TRNT1 starts at amino acid 418, it is interesting that there is a single point mutation that results in a protein with a K416E substitution in this region of the protein, which also results in SIFD (Chakraborty *et al.* 2014). Leibovitch (2016) showed that in the K416E variant, there was a small (less than four-fold) change in $K_{M,Apparent}$ for ATP or CTP (as we see here for the A[8] variant), but a seven-fold increase in $K_{M,Apparent}$ for $tRNA^{Asp}$-NCC (in contrast to the small change that we see here). Moreover, in terms of changes in k_{cat}, AMP addition to the $tRNA^{Asp}$-NCC transcript was only about 62% of that of the native enzyme as compared to the 10- to 30-fold reduction that we saw with the A[8] variant. Furthermore, the K416E variant showed an approximately 125-fold decrease in affinity for tRNA (Leibovitch 2016), which is consistent with the reduced tRNA binding that we saw with the A[8] variant (Fig. 3-4). Taken together, these data suggest that the K416E substitution, on its own, can reduce the binding of the tRNA substrate, but that once the tRNA is bound, the reaction

parameters that we measured were more similar to the native enzyme than to the more dramatic A[8] variant. This may suggest that the K416E substitution more dramatically affects tRNA binding than orientation during catalysis, although there is some effect on catalysis. One can imagine that K416 plays an early role in interacting directly with the negatively charged sugar-phosphate backbone of the tRNA during binding, or that this amino acid substitution alters the structure of this region of TRNT1 such that tRNA binding is reduced.

It also would be interesting to characterize the A[6] variant (DeLuca *et al.* 2016), which like the A[8] variant represents a frame shift mutation, but in this case resulting from the loss of a single adenine residue. This variant again begins at position 418, but results in the sequence VVTKWKKMNF such that the variant protein is seven amino acids shorter than the native enzyme but maintains three positively charged amino acids.

4.3.6 The A[8] Variant Is Associated With Systemic Phenotypes

The combined reduced $tRNA^{Asp}$-NC binding and A-adding activity that we saw *in vitro* may contribute to the phenotypes observed in the four human patients harboring the A[8] frame shift. The two brothers with the compound heterozygous A[8]/c.609-26T>C genotype exhibit a mild phenotype (Table 1-1), which is strikingly similar to that exhibited by the male patient with the compound heterozygous E43Δ/c.1246A[6] genotype (discussed in Section 4.2.9) (DeLuca *et al.* 2016). In fact, all three of these patients display the same symptoms – retinitis pigmentosa with erythrocytic microcytosis and anisocytosis with mild anemia. As in the case with the E43Δ variant (discussed in Section 4.2.9), a minor decrease in thermal stability of the A[8] variant (Fig. 3-5) may play a role in reduced protein levels in dermal fibroblasts and iPSC-derived retinal organoids particular to these two brothers and contribute to the retinitis pigmentosa phenotype (DeLuca *et al.* 2016; Sharma *et al.* 2017). Coupled with the weakened $tRNA^{Asp}$-NC binding and decreased A-adding activity, this altered stability may likewise induce in these retinal organoids high levels of oxidative stress, which generally are detrimental to photoreceptor cells (Sharma *et al.* 2017).

Moreover, the combination of the changes that were seen in the *in vitro* experiments with respect to thermal stability, tRNA binding and turnover number may play a role in red blood cell-linked abnormalities. These pathologies include microcytosis, anisocytosis and mild anemia exhibited by these two brothers (DeLuca *et al.* 2016), and sideroblastic anemia exhibited by the young child with the

compound heterozygous A[8]/I223T genotype (Chakraborty *et al.* 2014; Giannelou *et al.* 2018) and one patient with the compound heterozygous A[8]/K416E genotype (Giannelou *et al.* 2018) (Table 1-1). As with the E43Δ deletion, the A[8] frame shift in these patients might lead to an imbalanced synthesis of alpha or beta globin chains in hematopoietic cells (DeLuca *et al.* 2016) and detrimentally affect iron utilization (Taher *et al.* 2013).

Of course, one must also consider the partial LOF conferred by the other allele in each patient. In the case of the two brothers (A[8]/c.609-26T>C genotype), the c.609-26T>C intronic point mutation is unlikely to drastically alter the TRNT1 protein, as DeLuca *et al.* (2016) have shown by Western blot analysis that potentially alternatively spliced transcripts would simply not reach the protein translation stage, and therefore the phenotype presented would likely be due to the overall reduced levels of TRNT1 and the properties of the A[8] variant. This suggests that the effects of the A[8] variant, on their own, would not be severe enough to cause systemic and life-threatening conditions as the phenotypes exhibited by these two brothers are relatively mild (DeLuca *et al.* 2016). This also suggests that the more dramatic phenotype seen in the A[8]/I223T genotype (Giannelou *et al.* 2018), including SIFD (Chakraborty *et al.* 2014), must be driven primarily by the I223T substitution. Indeed, this makes sense as the I223T substitution has already been shown to be relatively severe from *in vitro* studies (Leibovitch *et al.* 2018). In the case of the A[8]/K416E genotype, the K416E substitution would also be an important contributor to the clinical manifestations observed (Giannelou *et al.* 2018), as hypogammaglobulinemia and developmental delay are systemic and the K416E variant, like the A[8] variant, demonstrates poor tRNA binding and a low specificity constant (Leibovitch 2016) and so is inefficient in generating mature tRNAs with 3' CCA-ends.

5.0 CONCLUSIONS AND FUTURE WORK

In this work, we set out to perform *in vitro* biophysical and biochemical characterizations of mutational variants of TRNT1, the human tRNA nucleotidyltransferase (tRNA-NT), in order to understand better the roles of specific amino acids and related structures of this protein in the context of protein stability, structure and function and, by extension, *TRNT1*-linked pathogenesis. The present work complements the studies of Leibovitch *et al.* (2018, 2019) by focusing on TRNT1 variants generated from the E43Δ deletion (DeLuca *et al.* 2016), R99W substitution (Aksentijevich *et al.* 2014; Hull *et al.* 2016; Frans *et al.* 2017; Kumaki *et al.* 2019) and A[8] frame shift (Chakraborty *et al.* 2014; DeLuca *et al.* 2016; Giannelou *et al.* 2018) – mapping to different regions of the resulting protein.

All three of these variants, regardless of type or location of modification, demonstrated major quantifiable decreases in AMP incorporation. The R99W variant showed a decrease in AMP incorporation likely based on reduced k_{cat} and decreased $K_{M,Apparent}$ for ATP binding (Sections 4.1.4 and 4.1.5), but led to relatively mild phenotypes in patients who are homozygous for R99W (Hull *et al.* 2016; Frans *et al.* 2017) as compared to those in patients bearing other mutations (Table 1-1). This suggests that the tremendous increase (~100-fold) in ATP binding to the R99W variant and lowered turnover number indicate that catalysis is compromised due to improper conformational changes either in the specificity switch toward ATP or in the catalysis of AMP incorporation itself. The E43Δ variant also showed a similar decrease in AMP incorporation, but likely based primarily on an increased $K_{M,Apparent}$ for ATP (Sections 4.2.4 and 4.2.5). This decreased affinity for ATP may have led to a phenotype confined primarily to the high-energy-requiring cells of the retina where ATP is used rapidly and continued protein synthesis is required, such that retinitis pigmentosa results (DeLuca *et al.* 2016; Sharma *et al.* 2017). Finally, the A[8] variant showed an almost 10-fold reduction in k_{cat} for AMP incorporation (Section 4.3.5) and also at least a 10-fold increase in $K_{M,Apparent}$ for $tRNA^{Asp}$-NC binding (Section 4.3.5.1). The combination of the weakening of both of these kinetic parameters may explain why this variant shows more severe phenotypes (Chakraborty *et al.* 2014; Giannelou *et al.* 2018).

In all three cases, effects on the incorporation of AMP seem to be the dominant factor leading to the phenotypes observed. Effects on the incorporation of CMP are not as pronounced as those of AMP and, in the case of the E43Δ variant, CMP incorporation seems even more efficient than in the native enzyme. Moreover, no major changes in thermal stability (always $\leq 3^{o}C$) were seen in any of the variants (Sections

4.1.3, 4.2.1 and 4.3.3). It is hence conceivable that as even small changes in the structure or stability of the R99W, E43Δ and A[8] variants are altered, different substructures, domains and motifs would be shifted in conformation such that AMP but not CMP incorporation is compromised. This may be linked to the inability to alter the conformation of the enzyme during the switch from CMP to AMP incorporation (Sections 4.1.5, 4.2.7, 4.2.8 and 4.3.5.1). Given the importance of ATP in the cell, it is not surprising that either a reduced ability to bind or to incorporate ATP would lead to a disease phenotype.

The T154I, M158V, L166S, R190I, I223T and I326T variants all also showed decreased AMP incorporation onto various tRNA transcripts (Leibovitch *et al.* 2018, 2019). For instance, the I326T variant showed a k_{cat} that was nine-fold lower than that of the native enzyme for AMP incorporation onto the $tRNA^{Asp}$-NCC transcript (Leibovitch *et al.* 2019), while the R190I variant showed reduced AMP incorporation onto a mitochondrial $tRNA^{Ser(AGY)}$ transcript as well as a mini-tRNA derivative from *B. subtilis* $tRNA^{Asp}$ (Leibovitch *et al.* 2018). Again, this suggests the importance of reduced AMP incorporation in the context of a disease phenotype. However, all of these variants showed a reduced thermal stability of ≥~5-7°C from that of the native enzyme (Leibovitch *et al.* 2018, 2019), suggesting a greater role of reduced thermal stability in these variants. It is intriguing that the R99W substitution near the active site shows a small decrease in thermal stability (<1°C), while all of the other active site substitutions characterized by Leibovitch *et al.* (2018, 2019) show the larger decrease in thermal stability.

An important limitation in the interpretation of this work, at the level of phenotype, is that eight out of the 12 patients described exhibit a compound heterozygous genotype. These are the R99W/D163V (Aksentijevich *et al.* 2014), R99W/R412X (Kumaki *et al.* 2019), E43Δ/A[6] (DeLuca *et al.* 2016), A[8]/c.609-26T>C (DeLuca *et al.* 2016), A[8]/I223T (Chakraborty *et al.* 2014; Giannelou *et al.* 2018) and A[8]/K416E (Giannelou *et al.* 2018) genotypes. In the case of the patients with the A[8]/c.609-26T>C genotype, any alternatively spliced transcripts resulting from the c.609-26T>C intronic point mutation are likely removed from the protein translation process and only the A[8] frame shift mutation likely influences the phenotype (DeLuca *et al.* 2016) (Section 4.3.6). In the cases of the patients with the A[8]/I223T and A[8]/K416E genotypes, the altered properties of the I223T and K416E variant proteins have been determined. The I223T variant binds CTP less well (Leibovitch *et al.* 2018) and the K416E variant binds tRNA less well (Leibovitch 2016). Therefore, an additive effect resulting from the combination of defects in the two partial LOF mutations in each of these patients may have led to the more severe phenotypes observed (Section 4.3.6).

Expressing each of these variant enzymes in *Saccharomyces cerevisiae* under the control of the native yeast *CCA1* promoter allowed for growth of a strain expressing the E43Δ variant, but not the R99W and A[8] variants, suggesting that *in vivo* the effects of the latter variants are more dramatic (Hanic P., personal communication). However, overexpression of these proteins from the *ScTDH3* promoter ensuring a higher level of gene expression allowed for growth with the E43Δ and R99W variants, but not the A[8] variant, suggesting that *in vivo* the A[8] variant is the most severely altered. This likely results from the combination of less efficient incorporation of AMP and reduced tRNA binding in this variant. These *in vivo* findings therefore support our claim that efficiency of AMP incorporation by these variants is a major criterion for cell survival, and that as the ability to incorporate AMP declines as in the case of the R99W, E43Δ and A[8] variant-expressing yeast strains, cell survival is adversely affected.

In this work, our data suggest that displacements of key residues within certain structures or motifs of TRNT1 due to structural shifts led to functional aberrations of these structures or motifs – triggering the decline in the overall ability of the enzyme to incorporate AMP. This is likely attributable to impairments of the disordered loop and the flexible loop for the R99W and E43Δ variants (Sections 4.1.5 and 4.2.7, respectively) and of motif C for the E43Δ variant (Section 4.2.7). Furthermore, as the spring function of motif C is possibly altered following the deletion of residue E43, multiple rounds of C-addition may occur yielding run-on transcription products with up to five C residues added to the 3'-ends of tRNAs in our *in vitro* assays (Section 4.2.8). We also suggest that the tail domain of the TRNT1 enzyme, in addition to binding tRNA prior to nucleotide incorporation, has a crucial role in orienting the extending tRNA so that all appropriate substrates are properly aligned at the active site of the enzyme for catalysis to occur (Section 4.3.5.1).

Future work aimed at elucidating additional functions of the tail domain of TRNT1 and confirming the findings made here for the A[8] variant may include the characterization of the A[6] variant, which is also shortened and retains three positively charged amino acids near its C-terminus (Section 4.3.5.2). It would be interesting to see if, for the A[6] variant, tRNA binding is similarly reduced or if catalytic properties are similar to those of the A[8] variant. Binding studies of this variant and of the R99W, E43Δ and A[8] variants with tRNA, either through fluorescence quenching (Shan *et al.* 2008) or gel filtration chromatography (Leibovitch *et al.* 2019), would reveal K_D values for tRNA and quantify tRNA binding affinity independent from that described by $K_{M,Apparent}$ values discussed in this work. This would allow more comprehensive comparisons in terms of tRNA binding with other TRNT1 substitution variants

already characterized (Leibovitch 2016; Leibovitch *et al.* 2019), given the disconnect we have seen between K_D and $K_{M,Apparent}$ values for other tRNA-NTs (Leibovitch *et al.* 2013, 2019; Leibovitch 2016).

Sideroblastic anemia, characterized by the presence of ring sideroblasts (red blood cell precursors marked by granular deposition of unincorporated iron in mitochondria forming a ring around the nucleus), is a mitochondrial disorder seen in multiple patients (Chakraborty *et al.* 2014) (Table 1-1). This disease likely results from reduced levels of functional TRNT1 in mitochondria leading to defects in mitochondrial protein synthesis. However, reduced functional TRNT1 in mitochondria may result from reduced stability, activity or amounts of the protein. In this work, the data from the characterized variants suggest reduced activity, but as yet we cannot exclude the possibility that there is actually less variant TRNT1 delivered to the mitochondrion. Given that the A[8] variant results in sideroblastic anemia, perhaps the change in stability and/or other physicochemical properties of the A[8] variant trigger(s) an altered distribution of this variant with respect to mitochondria localization. In addition, other disease phenotypes including sensorineural hearing loss associated with the R99W and A[8] mutations, and retinitis pigmentosa associated with the E43Δ mutation (Table 1-1), also involve tissues that have high energy demands and require efficient mitochondrial respiration. Therefore, *in vivo* localization studies may provide insight into the possible changes in subcellular localization of these altered TRNT1 proteins in human cells (*e.g.*, toward the cytosol, nucleus and/or mitochondria) in order to further place into context the biophysical and biochemical alterations of this essential enzyme. Indeed, Leibovitch *et al.* (2013) have shown that changes in stability in the body and tail domains of the *Arabidopsis* tRNA-NT, and not just the N-terminal transit peptide, influence the targeting of the tRNA-NT toward different organelles and a similar mechanism may be in place in human cells.

The results of this work reveal that, as opposed to our initial hypothesis based on the biophysical and biochemical characterization of the existing human TRNT1 variants (Leibovitch 2016; Leibovitch *et al.* 2018; Leibovitch *et al.* 2019), a change in thermal stability is not the primary defect leading to a disease phenotype in the E43Δ, R99W and A[8] variants. Instead, these variants suggest a role in ATP binding and incorporation. Even the A[8] variant, which as in other C-terminal variants (Leibovitch M., personal communication) showed reduced tRNA binding, also showed reduced AMP incorporation. This suggests that mutations lead to different types of defects in TRNT1 (affecting structure and/or function) that result in disease phenotypes. Given the absolute need for functional TRNT1, it will be interesting to see

how many different classes of partial LOF mutations will be discovered – in addition to those that alter the ability to use ATP as described here, or those that reduce thermal stability as described previously.

6.0 REFERENCES

Aebi M, Kirchner G, Chen J-Y, Vijayraghavan U, Jacobson A, Martin NC, Abelson J. 1990. Isolation of a temperature-sensitive mutant with an altered tRNA nucleotidyltransferase and cloning of the gene encoding tRNA nucleotidyltransferase in the yeast *Saccharomyces cerevisiae*. J Biol Chem. 265(27):16216–16220.

Aksentijevich I, Zhou Q, Giannelou A, Sediva A, Stone D, Rosenzweig S, Edwan J, Pelletier M, Monique S, Šrámková L, *et al.* 2014. TRNT1 missense mutations define an autoinflammatory disease characterized by recurrent fever, severe anemia, and B-cell immunodeficiency. Pediatr Rheumatol. 12(Suppl 1):O21.

Aravind L, Koonin EV. 1998. The HD domain defines a new superfamily of metal-dependent phosphohydrolases. Trends Biochem Sci. 23(12):469–472.

Aravind L, Koonin EV. 1999. DNA polymerase β-like nucleotidyltransferase superfamily: Identification of three new families, classification and evolutionary history. Nucleic Acids Res. 27(7):1609–1618.

Arts G-J, Kuersten S, Romby P, Ehresmann B, Mattaj IW. 1998. The role of exportin-t in selective nuclear export of mature tRNAs. EMBO J. 17(24):7430–7441.

Augustin MA, Reichert AS, Betat H, Huber R, Mörl M, Steegborn C. 2003. Crystal structure of the human CCA-adding enzyme: Insights into template-independent polymerization. J Mol Biol. 328(5):985–994.

Aurora R, Rose GD. 1998. Helix capping. Protein Sci. 7(1):21–38.

Ausubel M, Brent R, Kingston RE, Moore DD, Seidman JG, Smith JA, Struhl K, editors. 1989. Current protocols in molecular biology. 1st ed. Media, PA, USA: John Wiley & Sons.

Bader-Meunier B, Rieux-Laucat F, Touzot F, Frémond M-L, André-Schmutz I, Fraitag S, Bodemer C. 2018. Inherited immunodeficiency: A new association with early-onset childhood panniculitis. Pediatrics. 141(Supplement 5):S496–S500.

Betat H, Mede T, Tretbar S, Steiner L, Stadler PF, Mörl M, Prohaska SJ. 2015. The ancestor of modern Holozoa acquired the CCA-adding enzyme from Alphaproteobacteria by horizontal gene transfer. Nucleic Acids Res. 43(14):6739–6746.

Betat H, Mörl M. 2015. The CCA-adding enzyme: A central scrutinizer in tRNA quality control. BioEssays. 37(9):975–982.

Betat H, Rammelt C, Martin G, Mörl M. 2004. Exchange of regions between bacterial poly(A) polymerase and the CCA-adding enzyme generates altered specificities. Mol Cell. 15(3):389–398.

Betat H, Rammelt C, Mörl M. 2010. tRNA nucleotidyltransferases: Ancient catalysts with an unusual mechanism of polymerization. Cell Mol Life Sci. 67(9):1447–1463.

Bio-Rad protein assay. 2018a. [accessed 2018 Dec 9]. https://www.bio-rad.com/webroot/web/pdf/lsr/literature/LIT33.pdf.

Bradford MM. 1976. A rapid and sensitive method for the quantitation of microgram quantities of protein utilizing the principle of protein-dye binding. Anal Biochem. 72:248–254.

Chakraborty PK, Schmitz-Abe K, Kennedy EK, Mamady H, Naas T, Durie D, Campagna DR, Lau A, Sendamarai AK, Wiseman DH, *et al.* 2014. Mutations in TRNT1 cause congenital sideroblastic anemia with immunodeficiency, fevers, and developmental delay (SIFD). Blood. 124(18):2867–2871.

Chan CW, Chetnani B, Mondragón A. 2013. Structure and function of the T-loop structural motif in noncoding RNAs. Wiley Interdiscip Rev RNA. 4(5):507–522.

Cho HD, Oyelere AK, Strobel SA, Weiner AM. 2003. Use of nucleotide analogs by class I and class II CCA-adding enzymes (tRNA nucleotidyltransferase): Deciphering the basis for nucleotide selection. RNA. 9(8):970–981.

Cho HD, Verlinde CLMJ, Weiner AM. 2007. Reengineering CCA-adding enzymes to function as (U,G)- or dCdCdA-adding enzymes or poly(C,A) and poly(U,G) polymerases. Proc Natl Acad Sci. 104(1):54–59.

DeLuca AP, Whitmore SS, Barnes J, Sharma TP, Westfall TA, Scott CA, Weed MC, Wiley JS, Wiley LA, Johnston RM, *et al.* 2016. Hypomorphic mutations in *TRNT1* cause retinitis pigmentosa with erythrocytic microcytosis. Hum Mol Genet. 25(1):44–56.

Deutscher MP. 1983. tRNA nucleotidyltransferase and the -C-C-A terminus of transfer RNA. In: Jacob ST, editor. Enzymes of nucleic acid synthesis and modification. Vol. 2. 1st ed. Boca Raton, Florida, USA: CRC Press. (CRC series in the biochemistry and molecular biology of the cell nucleus). p. 159.

Deutscher MP. 1990. Transfer RNA nucleotidyltransferase. Methods Enzymol. 181:434–439.

Engelman DM, Steitz TA, Goldman A. 1986. Identifying nonpolar transbilayer helices in amino acid sequences of membrane proteins. Annu Rev Biophys Biophys Chem. 15:321–353.

Ernst FGM, Rickert C, Bluschke A, Betat H, Steinhoff H-J, Mörl M. 2015. Domain movements during CCA-addition: A new function for motif C in the catalytic core of the human tRNA nucleotidyltransferases. RNA Biol. 12(4):435–446.

Frans G, Moens L, Schaballie H, Wuyts G, Liston A, Poesen K, Janssens A, Rice GI, Crow YJ, Meyts I, *et al.* 2017. Homozygous N-terminal missense mutation in *TRNT1* leads to progressive B-cell immunodeficiency in adulthood. J Allergy Clin Immunol. 139(1):360-363.e6.

Giaever G, Chu AM, Ni L, Connelly C, Riles L, Véronneau S, Dow S, Lucau-Danila A, Anderson K, André B, *et al.* 2002. Functional profiling of the *Saccharomyces cerevisiae* genome. Nature. 418:387–391.

Giannelou A, Wang H, Zhou Q, Park YH, Abu-Asab MS, Ylaya K, Stone DL, Sediva A, Sleiman R, Sramkova L, *et al.* 2018. Aberrant tRNA processing causes an autoinflammatory syndrome responsive to TNF inhibitors. Ann Rheum Dis. 77(4):612–619.

Giegé R, Jühling F, Pütz J, Stadler P, Sauter C, Florentz C. 2012. Structure of transfer RNAs: Similarity and variability. Wiley Interdiscip Rev RNA. 3(1):37–61.

Goring ME, Leibovitch M, Gea-Mallorqui E, Karls S, Richard F, Hanic-Joyce PJ, Joyce PBM. 2013. The ability of an arginine to tryptophan substitution in *Saccharomyces cerevisiae* tRNA nucleotidyltransferase to alleviate a temperature-sensitive phenotype suggests a role for motif C in active site organization. Biochim Biophys Acta BBA - Proteins Proteomics. 1834(10):2097–2106.

Gorodetsky C, Morel CF, Tein I. 2018. Expanding the phenotype of *TRNT1* mutations to include Leigh syndrome. Can J Neurol Sci. Suppl. 2(S51):P.133.

Green CJ, Stewart GC, Hollis MA, Vold BS, Bott KF. 1985. Nucleotide sequence of the *Bacillus subtilis* ribosomal RNA operon, *rrnB*. Gene. 37(1–3):261–266.

Green R, Noller HF. 1997. Ribosomes and translation. Annu Rev Biochem. 66:679–716.

Hendrickson TL. 2001. Recognizing the D-loop of transfer RNAs. Proc Natl Acad Sci. 98(24):13473–13475.

Hoffmeier A, Betat H, Bluschke A, Günther R, Junghanns S, Hofmann H-J, Mörl M. 2010. Unusual evolution of a catalytic core element in CCA-adding enzymes. Nucleic Acids Res. 38(13):4436–4447.

Holm L, Sander C. 1995. DNA polymerase β belongs to an ancient nucleotidyltransferase superfamily. Trends Biochem Sci. 20(9):345–347.

Hull S, Malik ANJ, Arno G, Mackay DS, Plagnol V, Michaelides M, Mansour S, Albanese A, Brown KT, Holder GE, *et al.* 2016. Expanding the phenotype of *TRNT1*-related immunodeficiency to include childhood cataract and inner retinal dysfunction. JAMA Ophthalmol. 134(9):1049.

Jakubowski H. 2012. Quality control in tRNA charging. Wiley Interdiscip Rev RNA. 3(3):295–310.

Juhling F, Morl M, Hartmann RK, Sprinzl M, Stadler PF, Putz J. 2009. tRNAdb 2009: Compilation of tRNA sequences and tRNA genes. Nucleic Acids Res. 37(Database):D159–D162.

Just A, Butter F, Trenkmann M, Heitkam T, Morl M, Betat H. 2008. A comparative analysis of two conserved motifs in bacterial poly(A) polymerase and CCA-adding enzyme. Nucleic Acids Res. 36(16):5212–5220.

Kim DE, Chivian D, Baker D. 2004. Protein structure prediction and analysis using the Robetta server. Nucleic Acids Res. 32(Web Server):W526–W531.

Kim DF, Green R. 1999. Base-pairing between 23S rRNA and tRNA in the ribosomal A site. Mol Cell. 4(5):859–864.

Kim S, Liu C, Halkidis K, Gamper HB, Hou Y-M. 2009. Distinct kinetic determinants for the stepwise CCA addition to tRNA. RNA. 15(10):1827–1836.

Kim SH, Quigley GJ, Suddath FL, McPherson A, Sneden D, Kim JJ, Weinzierl J, Rich A. 1973. Three-dimensional structure of yeast phenylalanine transfer RNA: Folding of the polynucleotide chain. Science. 179(4070):285–288.

de Korte D, Haverkort WA, van Gennip AH, Roos D. 1985. Nucleotide profiles of normal human blood cells determined by high-performance liquid chromatography. Anal Biochem. 147(1):197–209.

Kuhn C-D, Wilusz JE, Zheng Y, Beal PA, Joshua-Tor L. 2015. On-enzyme refolding permits small RNA and tRNA surveillance by the CCA-adding enzyme. Cell. 160(4):644–658.

Kumaki E, Tanaka K, Imai K, Aoki-Nogami Y, Ishiguro A, Okada S, Kanegane H, Ishikawa F, Morio T. 2019. Atypical SIFD with novel *TRNT1* mutations: A case study on the pathogenesis of B-cell deficiency. Int J Hematol. [accessed 2019 Feb 17].

Kutay U, Lipowsky G, Izaurralde E, Bischoff FR, Schwarzmaier P, Hartmann E, Görlich D. 1998. Identification of a tRNA-specific nuclear export receptor. Mol Cell. 1(3):359–369.

Leatherbarrow RJ. 2009. GraFit. Horley, U.K.: Erithacus Software Ltd.

Leibovitch M. 2016. Exploring the interplay of structure, stability, activity and localization in tRNA nucleotidyltransferase function. [Montreal, Quebec, Canada]: Concordia University.

Leibovitch M, Bublak D, Hanic-Joyce PJ, Tillmann B, Flinner N, Amsel D, Scharf K-D, Mirus O, Joyce PBM, Schleiff E. 2013. The folding capacity of the mature domain of the dual-targeted plant tRNA nucleotidyltransferase influences organelle selection. Biochem J. 453(3):401–412.

Leibovitch M, Hanic-Joyce PJ, Joyce PBM. 2018. *In vitro* studies of disease-linked variants of human tRNA nucleotidyltransferase reveal decreased thermal stability and altered catalytic activity. Biochim Biophys Acta BBA - Proteins Proteomics. 1866(4):527–540.

Leibovitch M, Reid NE, Victoria J, Hanic-Joyce PJ, Joyce PBM. 2019. Analysis of the pathogenic I326T variant of human tRNA nucleotidyltransferase reveals reduced catalytic activity and thermal stability *in vitro* linked to a conformational change. Biochim Biophys Acta BBA - Proteins Proteomics. 1867(6):616–626.

Li F, Xiong Y, Wang J, Cho HD, Tomita K, Weiner AM, Steitz TA. 2002. Crystal structures of the *Bacillus stearothermophilus* CCA-adding enzyme and its complexes with ATP or CTP. Cell. 111(6):815–824.

Lipowsky G, Bischoff FR, Izaurralde E, Kutay U, Schäfer S, Gross HJ, Beier H, Görlich D. 1999. Coordination of tRNA nuclear export with processing of tRNA. RNA. 5(4):539–549.

Liu JC-H, Liu M, Horowitz J. 1998. Recognition of the universally conserved 3'-CCA end of tRNA by elongation factor EF-Tu. RNA. 4(6):639–646.

Lizano E, Scheibe M, Rammelt C, Betat H, Mörl M. 2008. A comparative analysis of CCA-adding enzymes from human and *E. coli*: Differences in CCA addition and tRNA 3'-end repair. Biochimie. 90(5):762–772.

Lougaris V, Chou J, Baronio M, Gazzurelli L, Lorenzini T, Soresina A, Moratto D, Badolato R, Seleman M, Bellettato M, *et al.* 2018. Novel biallelic *TRNT1* mutations resulting in sideroblastic anemia, combined B and T cell defects, hypogammaglobulinemia, recurrent infections, hypertrophic cardiomyopathy and developmental delay. Clin Immunol. 188:20–22.

Makhatadze GI. 2005. Thermodynamics of α-helix formation. Adv Protein Chem. 72:199–226.

Martin G, Keller W. 2007. RNA-specific ribonucleotidyl transferases. RNA. 13(11):1834–1849.

McGann RG, Deutscher MP. 1980. Purification and characterization of a mutant tRNA nucleotidyltransferase. Eur J Biochem. 106:321–328.

Mucocutaneous features of congenital sideroblastic anemia associated with B cell immunodeficiency, periodic fevers, and developmental delay (SIFD). 2019. [accessed 2019 Mar 14]. http://rgdoi.net/10.13140/RG.2.2.17007.69286.

Neuenfeldt A, Just A, Betat H, Morl M. 2008. Evolution of tRNA nucleotidyltransferases: A small deletion generated CC-adding enzymes. Proc Natl Acad Sci. 105(23):7953–7958.

Nissen P, Hansen J, Ban N, Moore PB, Steitz TA. 2000. The structural basis of ribosome activity in peptide bond synthesis. Science. 289:920–930.

Oh B-K, Pace NR. 1994. Interaction of the 3'-end of tRNA with ribonuclease P RNA. Nucleic Acids Res. 22(20):4087–4094.

Pagani R, Tabucchi A, Carlucci F, Leoncini R, Consolmagno E, Molinelli M, Valerio P. 1991. Some aspects of purine nucleotide metabolism in human lymphocytes before and after infection with HIV-1 virus: Nucleotide content. Adv Exp Med Biol. 309B:43–46.

Pearson WR, Lipman DJ. 1988. Improved tools for biological sequence comparison. Proc Natl Acad Sci. 85(8):2444–2448.

Phizicky EM, Hopper AK. 2010. tRNA biology charges to the front. Genes Dev. 24(17):1832–1860.

Popenda M, Szachniuk M, Antczak M, Purzycka KJ, Lukasiak P, Bartol N, Blazewicz J, Adamiak RW. 2012. Automated 3D structure composition for large RNAs. Nucleic Acids Res. 40(14):e112–e112.

QuikChange II site-directed mutagenesis kit. 2015. [accessed 2018 Nov 29]. https://www.agilent.com/cs/library/usermanuals/public/200523.pdf.

Rahman MS. 2017. Biophysical and biochemical characterization of yeast tRNA nucleotidyltransferase variants. [Montreal, Quebec, Canada]: Concordia University.

Rasband WS. 2018. ImageJ. Bethesda, Maryland, USA: National Institutes of Health.

Remmert M, Biegert A, Hauser A, Söding J. 2012. HHblits: Lightning-fast iterative protein sequence searching by HMM-HMM alignment. Nat Methods. 9(2):173–175.

Rosset R, Monier R. 1963. On the instability of transfer-RNA terminal nucleotide sequence in yeast. Biochem Biophys Res Commun. 10(2):195–199.

Rubin GM. 1973. The nucleotide sequence of *Saccharomyces cerevisiae* 5.8 S ribosomal ribonucleic acid. J Biol Chem. 248(11):3860–3875.

Sambrook J, Maniatis T, Fritsch EF. 1989. Molecular cloning. 2nd ed. Cold Spring Harbor Laboratory Press.

Sarin PS, Zamecnik PC. 1964. On the stability of aminoacyl-s-RNA to nucleophilic catalysis. Biochim Biophys Acta. 91(4):653–655.

Sasarman F, Thiffault I, Weraarpachai W, Salomon S, Maftei C, Gauthier J, Ellazam B, Webb N, Antonicka H, Janer A, *et al.* 2015. The 3′ addition of CCA to mitochondrial $tRNA^{Ser(AGY)}$ is specifically impaired in patients with mutations in the tRNA nucleotidyl transferase *TRNT1*. Hum Mol Genet. 24(10):2841–2847.

Shan X, Russell TA, Paul SM, Kushner DB, Joyce PBM. 2008. Characterization of a temperature-sensitive mutation that impairs the function of yeast tRNA nucleotidyltransferase. Yeast. 25(3):219–233.

Sharma TP, Wiley LA, Whitmore SS, Anfinson KR, Cranston CM, Oppedal DJ, Daggett HT, Mullins RF, Tucker BA, Stone EM. 2017. Patient-specific induced pluripotent stem cells to evaluate the pathophysiology of *TRNT1*-associated retinitis pigmentosa. Stem Cell Res. 21:58–70.

Shi P-Y, Maizels N, Weiner AM. 1998. CCA addition by tRNA nucleotidyltransferase: Polymerization without translocation? EMBO J. 17(11):3197–3206.

Simonovic M, Steitz TA. 2008. Peptidyl-CCA deacylation on the ribosome promoted by induced fit and the O3′-hydroxyl group of A76 of the unacylated A-site tRNA. RNA. 14(11):2372–2378.

Simpson RJ, Adams PD, Golemis EA. 2009. Basic methods in protein purification and analysis. 1st ed. Cold Spring Harbor Laboratory Press.

Soukup GA, Breaker RR. 1999. Relationship between internucleotide linkage geometry and the stability of RNA. RNA. 5(10):1308–1325.

Sprinzl M, Cramer F. 1979. The -C-C-A end of tRNA and its role in protein biosynthesis. Prog Nucleic Acid Res Mol Biol. 22:1–69.

Steitz T, Smerdon S, Jager J, Joyce C. 1994. A unified polymerase mechanism for nonhomologous DNA and RNA polymerases. Science. 266:2022–2025.

Steitz TA. 1998. A mechanism for all polymerases. Nature. 391:231–232.

Taher AT, Viprakasit V, Musallam KM, Cappellini MD. 2013. Treating iron overload in patients with non-transfusion-dependent thalassemia. Am J Hematol. 88(5):409–415.

Tamura K, Hasegawa T. 1997. Role of the CCA end of tRNA and its vicinity in aminoacylation. Nucleic Acids Symp Ser. 37:133–134.

The PyMOL molecular graphics system. 2018b. Schrödinger.

Thompson JE, Venegas FD, Raines RT. 1994. Energetics of catalysis by ribonucleases: Fate of the 2',3'-cyclic phosphodiester intermediate. Biochemistry. 33(23):7408–7414.

Toh Y, Takeshita D, Numata T, Fukai S, Nureki O, Tomita K. 2009. Mechanism for the definition of elongation and termination by the class II CCA-adding enzyme. EMBO J. 28(21):3353–3365.

Tomita K, Fukai S, Ishitani R, Ueda T, Takeuchi N, Vassylyev DG, Nureki O. 2004. Structural basis for template-independent RNA polymerization. Nature. 430:700–704.

Tomita K, Ishitani R, Fukai S, Nureki O. 2006. Complete crystallographic analysis of the dynamics of CCA sequence addition. Nature. 443:956–960.

Torrance JD, Whittaker D. 1979. Distribution of erythrocyte nucleotides in pyrimidine 5'-nucleotidase deficiency. Br J Haematol. 43(3):423–434.

Tretbar S, Neuenfeldt A, Betat H, Morl M. 2011. An inhibitory C-terminal region dictates the specificity of A-adding enzymes. Proc Natl Acad Sci. 108(52):21040–21045.

Wangsa-Wirawan ND. 2003. Retinal oxygen: Fundamental and clinical aspects. Arch Ophthalmol. 121:547–557.

Wedatilake Y, Niazi R, Fassone E, Powell CA, Pearce S, Plagnol V, Saldanha JW, Kleta R, Chong WK, Footitt E, *et al.* 2016. TRNT1 deficiency: Clinical, biochemical and molecular genetic features. Orphanet J Rare Dis. 11(90).

Weiner AM. 2004. tRNA maturation: RNA polymerization without a nucleic acid template. Curr Biol. 14(20):R883–R885.

Weinger JS, Parnell KM, Dorner S, Green R, Strobel SA. 2004. Substrate-assisted catalysis of peptide bond formation by the ribosome. Nat Struct Mol Biol. 11(11):1101–1106.

Wellner K, Betat H, Mörl M. 2018. A tRNA's fate is decided at its 3' end: Collaborative actions of CCA-adding enzyme and RNases involved in tRNA processing and degradation. Biochim Biophys Acta BBA - Gene Regul Mech. 1861(4):433–441.

Wende S, Bonin S, Gotze O, Betat H, Morl M. 2015. The identity of the discriminator base has an impact on CCA addition. Nucleic Acids Res. 43(11):5617–5629.

Werner A, Siems W, Schmidt H, Rapoport I, Gerber G, Toguzov RT, Tikhonov YV, Pimenov AM. 1987. Determination of nucleotides, nucleosides and nucleobases in cells of different complexity by reversed-phase and ion-pair high-performance liquid chromatography. J Chromatogr B Biomed Sci App. 421:257–265.

Wilusz JE, Whipple JM, Phizicky EM, Sharp PA. 2011. tRNAs marked with CCACCA are targeted for degradation. Science. 334(6057):817–821.

Wiseman DH, May A, Jolles S, Connor P, Powell C, Heeney MM, Giardina PJ, Klaassen RJ, Chakraborty P, Geraghty MT, *et al.* 2013. A novel syndrome of congenital sideroblastic anemia, B-cell immunodeficiency, periodic fevers, and developmental delay (SIFD). Blood. 122(1):112–123.

Wong C, Sridhara S, Bardwell JCA, Jakob U. 2000. Heating greatly speeds Coomassie Blue staining and destaining. BioTechniques. 28(3):426, 428, 430, 432.

Wu X-Q, Gross HJ. 1993. The long extra arms of human $tRNA^{(Ser)Sec}$ and $tRNA^{Ser}$ function as major identity elements for serylation in an orientation-dependent, but not sequence-specific manner. Nucleic Acids Res. 21(24):5589–5594.

Xiong Y, Li F, Wang J, Weiner AM, Steitz TA. 2003. Crystal structures of an archaeal class I CCA-adding enzyme and its nucleotide complexes. Mol Cell. 12(5):1165–1172.

Xiong Y, Steitz TA. 2004. Mechanism of transfer RNA maturation by CCA-adding enzyme without using an oligonucleotide template. Nature. 430:640–645.

Yakunin AF, Proudfoot M, Kuznetsova E, Savchenko A, Brown G, Arrowsmith CH, Edwards AM. 2004. The HD domain of the *Escherichia coli* tRNA nucleotidyltransferase has 2′,3′-cyclic phosphodiesterase, 2′-nucleotidase, and phosphatase activities. J Biol Chem. 279(35):36819–36827.

Yamashita S, Takeshita D, Tomita K. 2014. Translocation and rotation of tRNA during template-independent RNA polymerization by tRNA nucleotidyltransferase. Structure. 22(2):315–325.

Yamashita S, Tomita K. 2016. Mechanism of 3′-matured tRNA discrimination from 3′-immature tRNA by class-II CCA-adding enzyme. Structure. 24(6):918–925.

Yan Y, Zhang D, Zhou P, Li B, Huang S-Y. 2017. HDOCK: A web server for protein–protein and protein–DNA/RNA docking based on a hybrid strategy. Nucleic Acids Res. 45(W1):W365–W373.

Yang N. 2008. ATP: CTP nucleotidyltransferase: Interaction with tRNA and functional roles of conserved arginine residues, the C-terminus, the tRNA T-loop, and metal ions. [Worcester, Massachusetts, USA]: Clark University.

Yue D, Maizels N, Weiner AM. 1996. CCA-adding enzymes and poly(A) polymerases are all members of the same nucleotidyltransferase superfamily: Characterization of the CCA-adding enzyme from the archaeal hyperthermophile *Sulfolobus shibatae*. RNA. 2:895–908.

Yue D, Weiner AM, Maizels N. 1998. The CCA-adding enzyme has a single active site. J Biol Chem. 273(45):29693–29700.

Yumada Y, Ohki M, Ishikura H. 1983. The nucleotide sequence of *Bacillus subtilis* tRNA genes. Nucleic Acids Res. 11(10):3037–3045.

Zhu L, Cudny H, Deutscher MP. 1986. A mutation in *Escherichia coli* tRNA nucleotidyltransferase that affects only AMP incorporation is in a sequence often associated with nucleotide-binding proteins. J Biol Chem. 261(32):14875–14877.

Zhu L, Deutscher MP. 1987. tRNA nucleotidyltransferase is not essential for *Escherichia coli* viability. EMBO J. 6(8):2473–2477.

7.0 APPENDIX

Table S0: Chemicals, Reagents and Enzymes Used in This Study

Chemical / Reagent / Enzyme	Grade	Supplier
Acrylamide	Ultra Pure	BioShop
Acetic acid	ACS Grade	Caledon
Adenosine triphospate (ATP), [α-^{32}P] *(10 µCi/µL, 3000 Ci/mmol)*		PerkinElmer
Agar	Bacteriological Grade II	BioShop
Agarose	Electrophoresis Grade	BioShop
Ammonium acetate	ACS Grade	Omega
Ammonium persulfate (APS)		BioShop
Ampicillin (Amp)		Goldbio
β-mercaptoethanol		ICN
Baker's yeast tRNA	Crude	Roche
Bbs I (restriction enzyme)		New England Biolabs
Bio-tryptone	Bacteriological Grade	BioShop
Bis -acrylamide	BioUltra Pure	BioShop
Boric acid	Biotechnology Grade	BioShop
Bromophenol blue	Electrophoresis Grade	Bio-Rad
cOmplete, EDTA-free Protease Inhibitor Cocktail Tablets		Roche Diagnostics
Coomassie Brilliant Blue R-250		BioShop
Deoxynucleoside triphosphates (dNTPs)		Bio Basic
Distilled water (dH_2O)	DNase/RNase/Protease-Free, Sterile-Filtered	BioShop
Dpn I (restriction enzyme)		New England Biolabs
EcoLite(+) Liquid Scintillation Cocktail		MP Biomedicals
EDTA (disodium salt)	Biotechnology Grade	BioShop
Ethanol		Commercial Alcohols
Ethyl ether (BHT stabilized)	ACS Grade	Fisher Scientific
Fok I (restriction enzyme)		New England Biolabs
Fluo-DNA/RNA Gel Staining Solution		ZmTech Scientific
Gel Loading Dye, Purple *(6X)*		New England Biolabs
GeneJET Plasmid Miniprep Kit		Thermo Scientific
GeneRuler 1-kb Plus DNA Ladder		Thermo Scientific
Glycerol	Molecular Biology Grade	Fisher Scientific
Glycine	Biotechnology Grade	BioShop
Guanidine hydrochloride (Gdn-HCl)	Biotechnology Grade	BioShop
Hydrochloric acid (HCl)	ACS Grade	Caledon

Chemical / Reagent / Enzyme	Grade	Supplier
Imidazole	Biotechnology Grade	BioShop
Isopropanol		Fisher Scientific
Isopropyl-β-D-thiogalactopyranoside (IPTG)		Goldbio
Magnesium acetate	ACS Grade	Anachemia
Magnesium chloride hexahydrate	Biotechnology Grade	BioShop
NEBuffer 2 *(10X)*		New England Biolabs
NEBuffer 4 *(10X)*		New England Biolabs
Ni-NTA agarose		QIAGEN
Nickel sulfate hexahydrate		???
Nucleoside triphosphates (NTPs)		Thermo Scientific
Phenol	Molecular Biology Grade	Fisher Scientific
Phusion HF Buffer *(5X)*		Thermo Scientific
Phusion HF DNA Polymerase		New England Biolabs
Potassium chloride (KCl)		BDH
Potassium phosphate (monobasic)	ACS Grade	BioShop
Protein Assay Dye Reagent Concentrate		Bio-Rad
RNase A (Pancreatic)		BioShop
RNAsecure Reagent		Ambion
Snake Venom Phosphodiesterase I, Type VI (from *Crotalus adamanteus*)		Sigma-Aldrich
Sodium acetate	Enzyme Grade	Fisher Scientific
Sodium chloride (NaCl)	ACS Grade	Fisher Scientific
Sodium dodecyl sulfate (SDS)	Ultra Pure	BioShop
Sodium phosphate (dibasic) heptahydrate	ACS Grade	BioShop
Tetramethylethylenediamine (TEMED)	Ultra Pure	Bio Basic
T7 RNA Polymerase		Thermo Scientific
Transciption Buffer *(5X)*		Thermo Scientific
Tris	BioUltra Pure	BioShop
Unstained Protein Molecular Weight Marker		Thermo Scientific
Urea	BioUltra Pure, Molecular Biology Grade	BioShop
Xylene cyanol	Electrophoresis Grade	Fisher Scientific
Yeast Extract		BioShop

Table S1: Total Concentrations, Amounts and Purities of Native and Variant TRNT1 Proteins

TRNT1 Variant	Total Protein Concentration *(ng/uL)*	Total Protein Isolated *(mg)*	Enzyme Purity *(%)*
Native	1171	8.78	91.6
R99W	473	3.55	100.0
E43Δ	300	2.25	100.0
A[8]	617	4.63	83.9

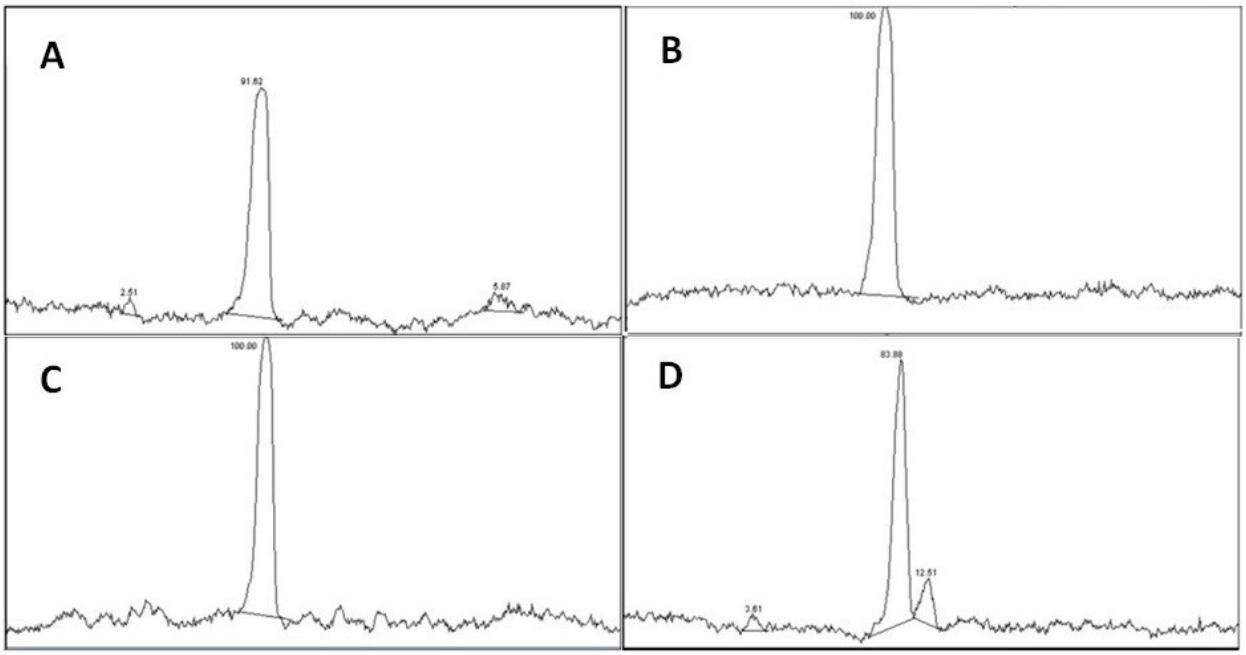

Figure S1: Densitometry Analysis of SDS-PAGE of Native and Variant TRNT1 Proteins

Intensity peaks representing the protein species separated per gel lane by SDS-PAGE **(Figure 3-1)**. Each spectrum displays peaks from left to right in order of descending molecular weight. **(A)** Native, **(B)** R99W, **(C)** E43Δ, **(D)** A[8].

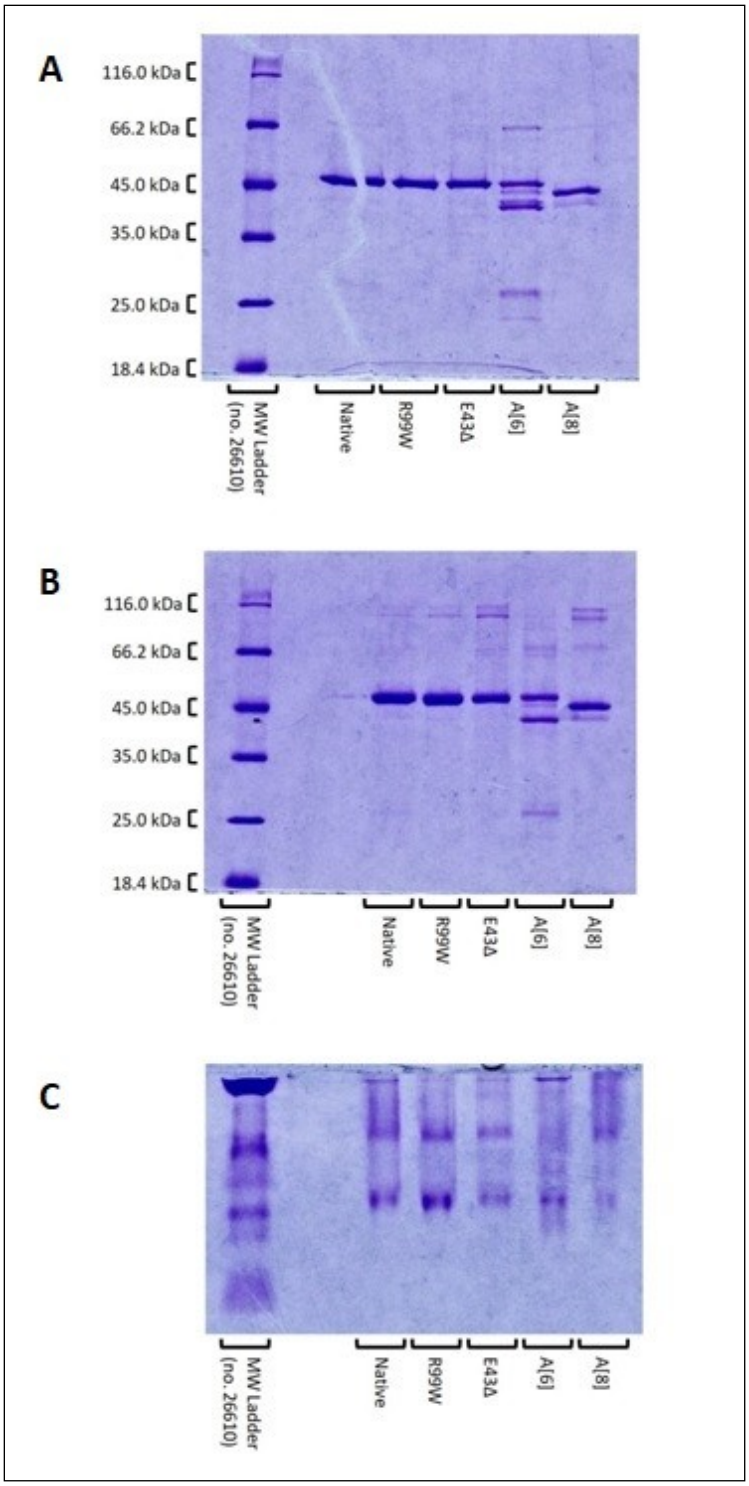

Figure S2: SDS-PAGE, Non-Reducing SDS-PAGE and Native PAGE of Native and Variant TRNT1 Proteins. Original gels include the A[6] variant (not discussed in this thesis).

(A) SDS-PAGE – for legend, refer to **Figure 3-1**.
(B) Non-reducing SDS-PAGE – for legend, refer to **Figure 3-2**.
(C) Native PAGE – for legend, refer to **Figure 3-3**.

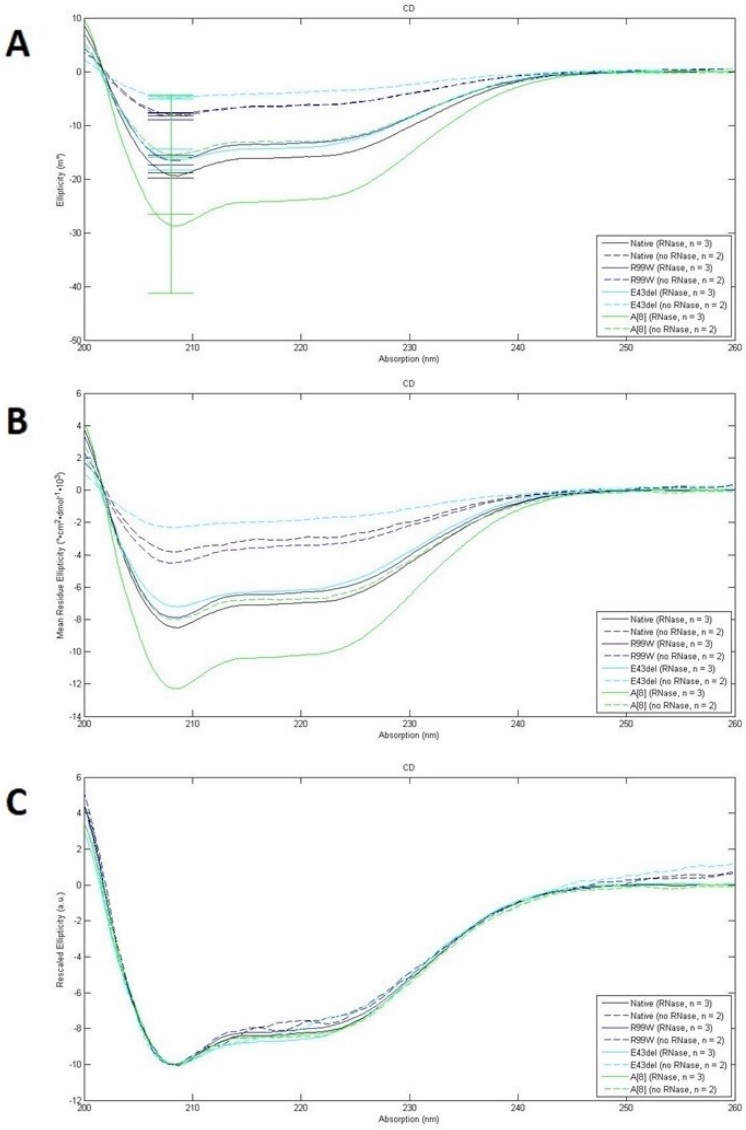

Figure S3: CD Spectra of Native and Variant TRNT1 Proteins

Signal traces are displayed for native (black), R99W (blue), E43Δ (cyan) and A[8] (green). Traces for RNase-treated and non-RNase-treated aliquots are displayed as solid lines and dashed lines, respectively. For each trace, the number of experimental replicates is denoted in parentheses. Each error bar above or below a data point represents one SEM. All traces are representative of a mixed α-helix/β-strand character.

(A) Traces are shown with ellipticity *(m°)* as a function of absorption *(nm)*. These correspond to the raw data and reflect the unequal protein concentrations of the aliquots.
(B) Traces are shown with mean residue ellipticity (MRW) *(°•cm^2•dmol^{-1}•10^3)* as a function of absorption *(nm)*. $[\vartheta]_{MRW} = 100 \bullet \vartheta / (C \bullet N \bullet L)$; where ϑ = ellipticity *(m°)*, *C* = concentration *(M)*, *N* = number of amino acids in the protein and *L* = cuvette pathlength *(cm)* = 0.2 cm (Kelly et al. 2005).
(C) Traces are shown with ellipticity rescaled as arbitrary units *(a.u.)* as a function of absorption *(nm)*. Each trace is rescaled such that 208 nm corresponds to -10 a.u.

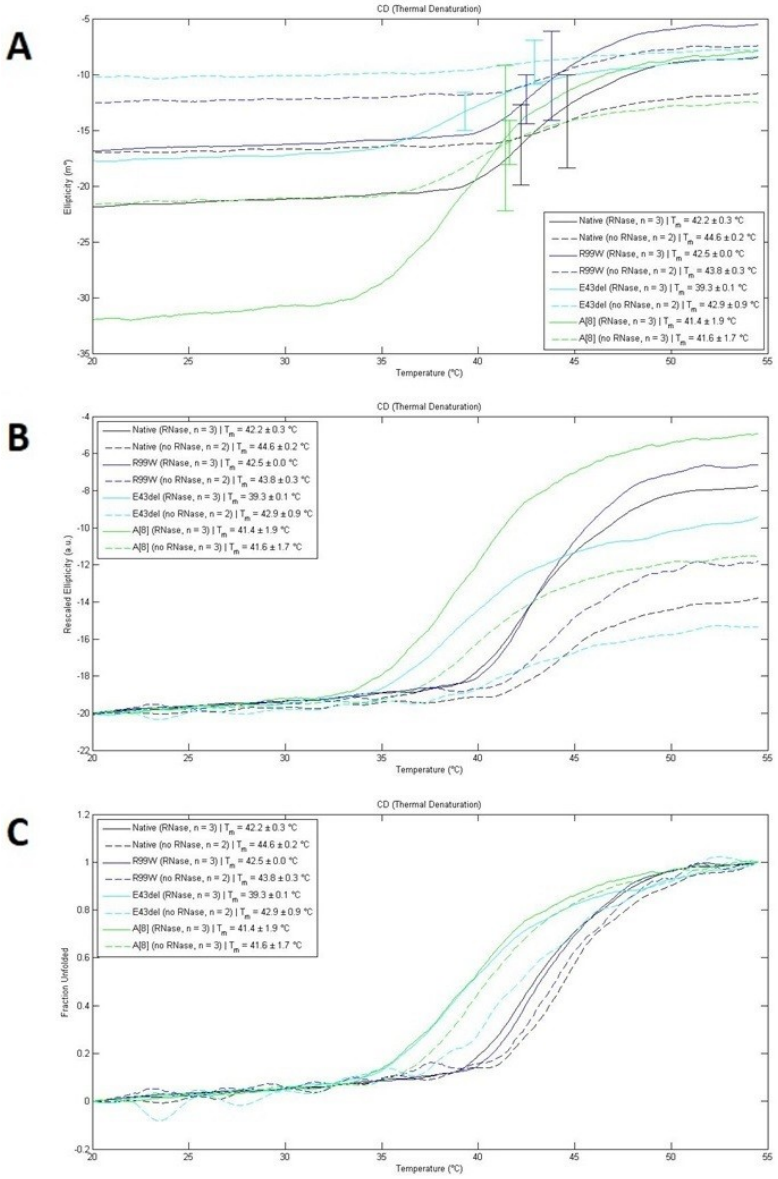

Figure S4: Thermal Denaturation Curves of Native and Variant TRNT1 Proteins

Denaturation curves are displayed for native (black), R99W (blue), E43Δ (cyan) and A[8] (green). Curves for RNase-treated and non-RNase-treated aliquots are displayed as solid lines and dashed lines, respectively. For each curve and corresponding T_m, the number of experimental replicates is denoted in parentheses. Each error bar above or below a T_m data point represents one SEM.

(A) Curves are shown with ellipticity *(m°)* as a function of temperature *(°C)*. These correspond to the raw data and reflect the unequal protein concentrations of the aliquots.
(B) Curves are shown with ellipticity rescaled as arbitrary units *(a.u.)* as a function of temperature *(°C)*. Each trace is rescaled such that 20 °C corresponds to -20 a.u.
(C) Curves are shown with fraction unfolded (F) as a function of temperature *(°C)*. $F = (\vartheta - \vartheta_i) / (\vartheta_f - \vartheta_i)$; where ϑ = ellipticity *(m°)*, ϑ_i = initial ellipticity *(m°)* at 20 °C and ϑ_f = final ellipticity *(m°)* at 54.5 °C (Leibovitch et al. 2018).

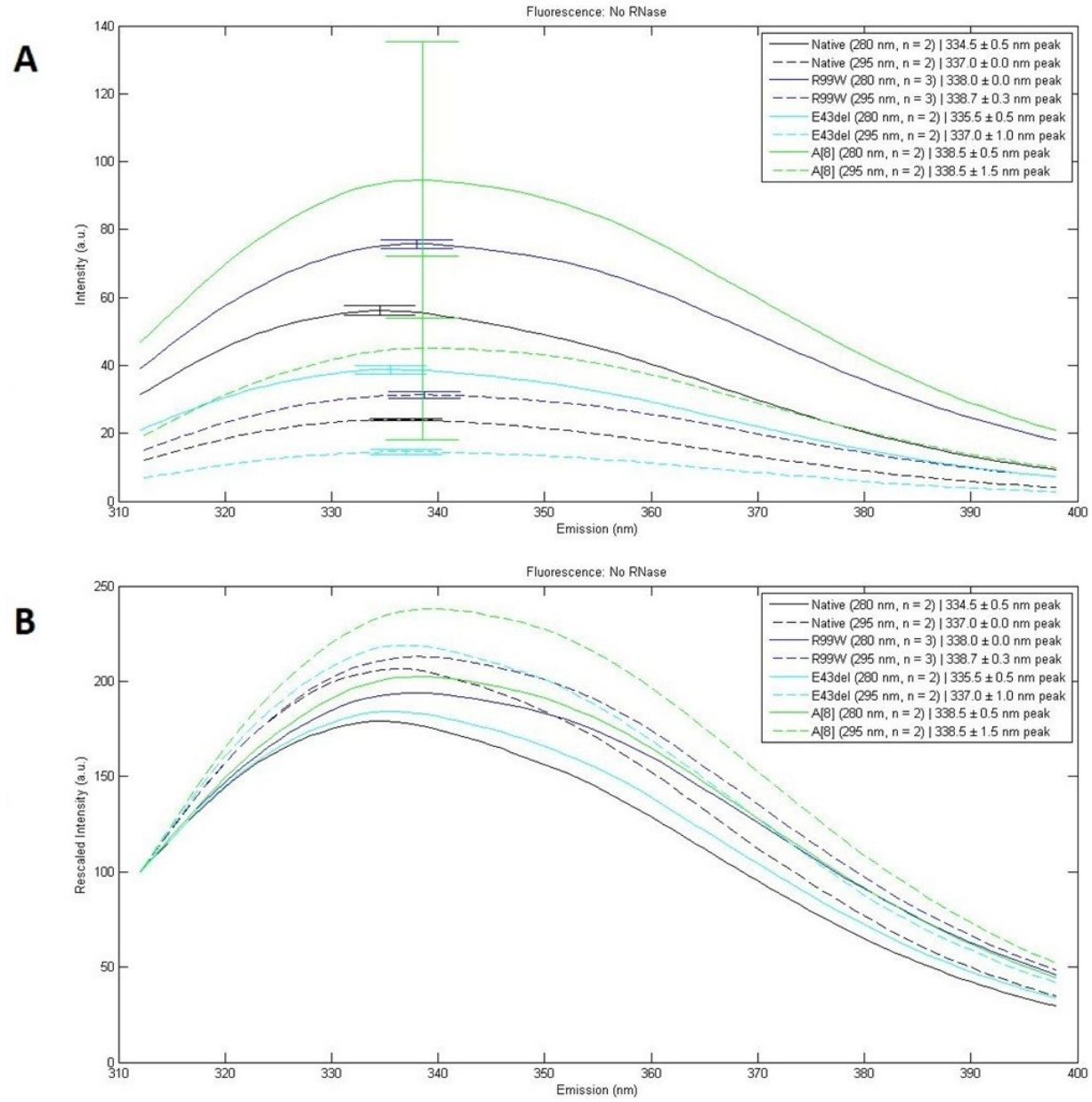

Figure S5: Fluorescence Emission Spectra of Native and TRNT1 Variant Proteins (Non-RNase-Treated)

Emission traces are displayed for non-RNase-treated aliquots of native (black), R99W (blue), E43Δ (cyan) and A[8] (green). Traces from 280-nm and 295-nm excitations are displayed as solid lines and dashed lines, respectively. For each trace and corresponding maximum, the number of experimental replicates is denoted in parentheses. Each error bar above or below a maximum represents one SEM.

(A) Traces are shown with intensity *(arbitrary units, a.u.)* as a function of emission *(nm)*. These correspond to the raw data and reflect the unequal protein concentrations of the aliquots.
(B) Traces are shown with rescaled intensity *(a.u.)* as a function of emission *(nm)*. Each trace is rescaled such that 312 nm corresponds to 100 a.u.

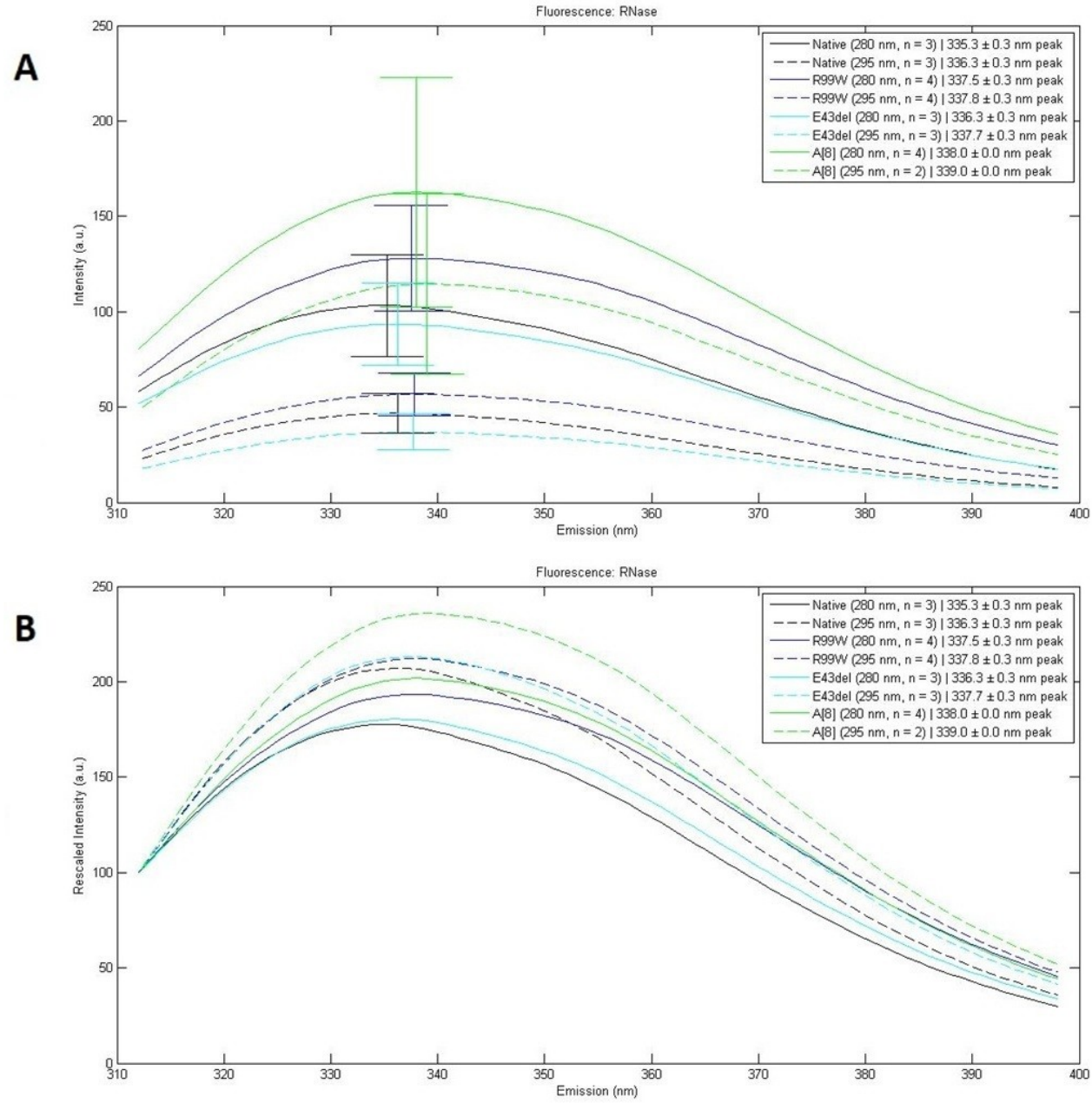

Figure S6: Fluorescence Emission Spectra of Native and TRNT1 Variant Proteins (RNase-Treated)

Emission traces are displayed for RNase-treated aliquots of native (black), R99W (blue), E43Δ (cyan) and A[8] (green). Traces from 280-nm and 295-nm excitations are displayed as solid lines and dashed lines, respectively. For each trace and corresponding maximum, the number of experimental replicates is denoted in parentheses. Each error bar above or below a maximum represents one SEM.

(A) Traces are shown with intensity *(arbitrary units, a.u.)* as a function of emission *(nm)*. These correspond to the raw data and reflect the unequal protein concentrations of the aliquots.
(B) Traces are shown with rescaled intensity *(a.u.)* as a function of emission *(nm)*. Each trace is rescaled such that 312 nm corresponds to 100 a.u.

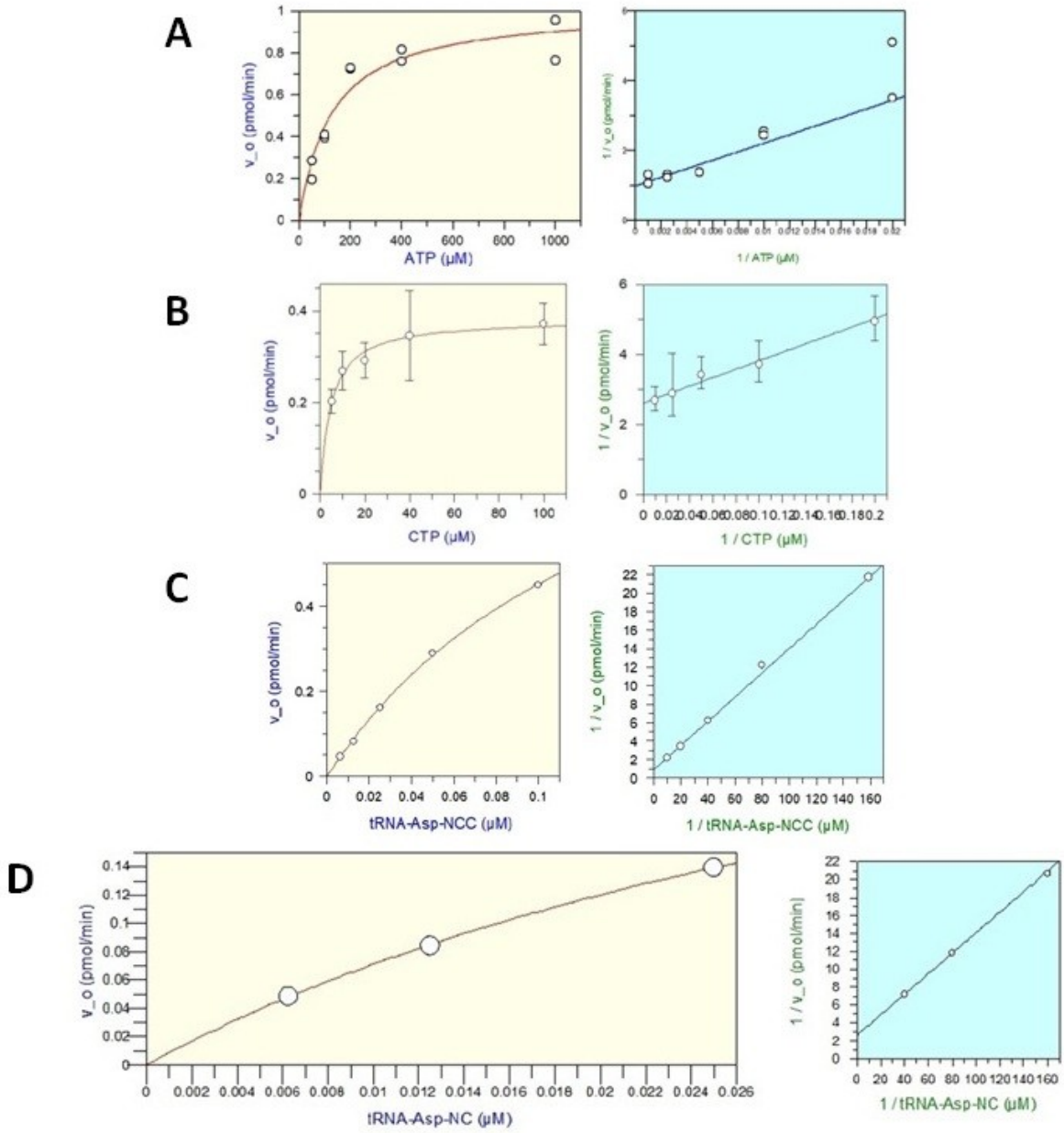

Figure S7: Sample Kinetic Assay Plots for Native TRNT1 Enzyme

Displayed on the left-hand side are representative kinetic assay plots for native TRNT1 fitted to the Michaelis-Menten model using nonlinear regression via GraFit 7 (Leatherbarrow 2009). Displayed on the right-hand side are Lineweaver-Burk plots corresponding to the former. Each error bar above or below a data point represents one SEM.

(A) Varying ATP and fixed $tRNA^{Asp}$-NCC as substrates; 4.82 ng of enzyme per reaction.
(B) Varying CTP and fixed $tRNA^{Asp}$-NC as substrates; 1.83 ng of enzyme per reaction.
(C) Varying $tRNA^{Asp}$-NCC and fixed ATP as substrates; 0.23 ng of enzyme per reaction.
(D) Varying $tRNA^{Asp}$-NC and fixed CTP as substrates; 0.23 ng of enzyme per reaction.

7.1 Appendix References

Kelly SM, Jess TJ, Price NC. 2005. How to study proteins by circular dichroism. Biochim Biophys Acta BBA - Proteins Proteomics. 1751(2):119–139.

Leatherbarrow RJ. 2009. GraFit. Horley, U.K.: Erithacus Software Ltd.

Leibovitch M, Hanic-Joyce PJ, Joyce PBM. 2018. *In vitro* studies of disease-linked variants of human tRNA nucleotidyltransferase reveal decreased thermal stability and altered catalytic activity. Biochim Biophys Acta BBA - Proteins Proteomics. 1866(4):527–540.